VNIVERSITAT DE VALÈNCIA

ESTIMATION OF KEY BIOPHYSICAL PARAMETERS RELATED TO CROP STRESS THROUGH NEW REMOTE SENSORS AND MULTI-CROP *IN SITU* DATA

NIEVES PASQUALOTTO VICENTE

Directores:

Jesús Delegido Gómez
Shari Van Wittenberghe
José Moreno Méndez

Doctorado en Teledetección
Febrero 2020

UNIVERSITAT DE VALÈNCIA

Facultat de Física
Departament de Física de la Terra i Termodinàmica

Estimation of key biophysical parameters related to crop stress through new remote sensors and multi-crop *in situ* data

Doctorado en Teledetección
PhD Thesis
January 2020

NIEVES PASQUALOTTO VICENTE

PhD advisors:

Jesús Delegido Gómez
Shari Van Wittenberghe
José Moreno Méndez

JESÚS DELEGIDO GÓMEZ, Profesor Titular en el departamento de Física de la Tierra y Termodinámica de la Facultad de Física, Universidad de Valencia.

SHARI VAN WITTENBERGHE, Investigadora postdoctoral en el Laboratorio de Procesamiento de Imágenes, Universidad de Valencia.

JOSÉ MORENO MÉNDEZ, Catedrático en el departamento de Física de la Tierra y Termodinámica de la Facultad de Física, Universidad de Valencia.

CERTIFICAN:

Que la tesis doctoral "Estimation of key biophysical parameters related to crop stress through new remote sensors and multi-crop in situ data", presentada por Nieves Pasqualotto Vicente ha sido realizada bajo su dirección y es favorable para optar a grado de Doctora por la Universidad de Valencia en el programa de doctorado en Teledetección.

Y para que así conste, firman el presente certificado en Burjassot, a 14 de febrero de 2020.

Fdo.: Jesús Delegido Gómez 

Fdo.: Shari Van Wittenberghe 

Fdo.: José Moreno Méndez 

Este trabajo ha sido posible gracias a la financiación económica recibida por parte de:

La beca predoctoral Vali+d (ACIF/2016/378) financiada por la Generalitat Valenciana.

El Proyecto AVANFLEX - Productos avanzados para la misión FLEX (ESP2016-79503-C2-1-P) financiado por el Ministerio de Economía y Competitividad.

Otros proyectos y contratos científicos en los que he colaborado y han financiado diversas actividades científicas como participación a congresos:

El Proyecto HYPERCITY - Hyperspectral biomonitoring: air quality and the city (SR/00/303) financiado por BELSPO - Belgium Federal Science Policy Office.

El Proyecto SENSAGRI - Sentinels Synergy for Agriculture (H2020-EO-2016-730074) financiado por la Comisión Europea.

El Contrato Aplicaciones de Copernicus y utilización de datos de satélites Sentinels para la Dirección General del Agua (OTR 2017/17773 FORMA) financiado por el Ministerio de Agricultura y Pesca, Alimentación y Medio Ambiente.

El Contrato Framework Partnership Agreement on Copernicus User Uptake. Courses, workshops and seminars in Europe and Latin America (FPA 275/G/GRO/COPE/17/10042) financiado por la Comisión Europea.

A la resiliencia de las mujeres, en todas sus expresiones. Y, especialmente, a mi madre.

AGRADECIMIENTOS

Entre tantas horas de frustración, trabajo duro y de días enteros para escribir un párrafo que acabarás borrando, supongo que hay un momento mínimo de lucidez en el que decides escribir este trocito, pequeño pero indispensable, de la tesis. Dedicado a dar las gracias.

Todo empezó sin quererlo, cuando mi tutor del trabajo final del máster y uno de los directores de esta tesis, Jesús, me sugirió pedir las becas predoctorales. Por esa época hacer doctorado era de mis últimos planes, pero puedo asegurar que, una vez casi acabada, lo pienso y sé que fue una decisión acertada. No solo por los conocimientos y habilidades adquiridas en este tiempo, sino, sobre todo, por todas aquellas personas que he conocido en el proceso. Y no solo personas, también por los momentos y aventuras vividas. Que al final es lo más importante. Las personas y las aventuras que te aportan.

Empiezo por Jesús, no podía ser de otra forma, el culpable de toda esta historia. Quién me animó no solo a iniciarla, sino en mis peores momentos a lo largo de la misma. Gracias por todos esos viajes, risas y, sobre todo, por enseñarme a quitarle importancia a las cosas. Tampoco podía faltar Shari, gracias por aceptar ser mi directora, contarme tus inquietudes y comprobar que ambas tenemos muchísimo en común. Y gracias finalmente a mi otro director, Pepe, por acogerme en tu grupo y abrirme las puertas al mundo científico.

Gracias a Alejandro y a Cristina, mi pequeña familia argentina, por esas campañas de campo juntos, por esas comilonas, pero también por hacerme recorrer en coche casi 1000 km para enseñarme un trocito de ese maravilloso país.

No podían faltar los compis de Valladolid. Gracias a Vanessa, David, Vicente y demás compañeros del ITACyL, habéis sido prácticamente mi segunda casa en este doctorado.

Grazie ai miei piccoli napoletani, a Guido per essere stato il mio tutore durante il mio soggiorno e per avermi insegnato così tanto. Grazie a tutti gli ARIESPACE, in particolare Salvatore, Oscar, Marco e Luigi, per il loro aiuto, le loro conversazioni così assurde a pranzo e per i loro (tanti) caffè napoletani. Ma non posso

dimenticarmi nemmeno di Daniela! Grazie, grazie e ancora grazie per avermi fatto conoscere i tuoi amici e per le grandi chiacchierate sulla vita in spagnolo/italiano/inglese! Ahahah, spero che la nostra amicizia rimanga sempre forte nel tempo com'è ora. Grazie a tutti voi. Porto via con me un ricordo stupendo di quella città, così incasinata quanto unica. Non avrei potuto davvero scegliere un posto migliore per la mia esperienza all'estero.

Bueno, bueno, bueno. El turno de mis compis PhD. Si pienso en el IPL, directamente mi mente piensa en Anna y Gonzalo por los pasillos, me encantáis y habéis hecho que trabajar aquí mole tantísimo. Gracias a Emiliano, Daniel, Emmanuel, Roberto, Diego, Jose, Dan, Valero y Adrián (shht pasáis por PhD students), por nuestras cenas épicas. ¡Es que este grupo mola!

Gracias al grupo LEO y todas las personitas que lo integran, gracias a Adrián, MaPi, Luis, Luca, Jochem, Santi, Charlotte, Jose, Pablo, Helena y gracias también a Neus y Jorge, que, aunque no estéis ahora, siempre estáis presente en el grupo. Gracias a Antonio, a la juventud que desprendes y a tus mil historias. Gracias a la última incorporación, Xavi, por esos vinos y por esas risas. También gracias a Juan Carlos y a Drazen, por picarnos tanto por los pasillos.

Especialmente gracias a ellas. A Carol y al nuevo miembro de la banda, a Eatidal con sus rompetodo, a Marcela, mi hermana mayor, e…indispensable, a Patri, necesitaría una página entera, no solo por los mapas y por los programas, que también, sino por tantísimos consejos de vida, vocabulario nuevo, risas y por algún que otro lloro. A pesar del aire acondicionado, no podría tener una compi de despacho, de vida, mejor.

Sin duda gracias a mi familia, especialmente a mis padres, porque como en cualquier tesis, ellos tienen más ganas de que se acabe esta etapa que nosotros mismos, gracias por apoyarme. Gracias a mi hermano Angelo, porque, aunque nos pasemos la vida separados, eres una de las personitas que más quiero en el mundo.

Gracias a todas esas personas que están ahí cuando salgo del trabajo. A mis amigos de toda la vida, a Luis, Isa, Cortellet, Roseta, Salinas, Fredy, Angela, Gabri. Especialmente gracias a Marc, por todo lo que hemos vivido y porque sé que puedo contar contigo siempre, significa mucho. Gracias a Panda por todas esas birras, nachos y conversaciones que me salvaban el día. Gracias a Lore porque somos copias y por comprenderme tantísimo. Gracias a Jesús, hace poco que

coincidimos gracias a Steph, pero contigo es imposible aburrirse. Gracias a esos amigos que encontré por casualidad pero que ahora son tan importantes, gracias a Matt, Vicent y Jordi. ¡Estáis fatal y me encanta! También dar gracias a mis compis del Máster, sobre todo gracias a Julia, Laura y Juanjo, porque aprendí mucho más de vosotros que en cualquier clase. Gracias a los Popus, a esas personas que me llevé de la carrera de ambientales, especialmente a Nuri, Sandra, Inma, Dani, Ursu y Steph. Por ser tan diferentes a los demás.

Y, finalmente, gracias a Amanda, por vivir conmigo mis mejores momentos. Y los que nos quedan.

Que suerte he tenido.

Gracias. Gracias. Gracias.

NOTA INTRODUCTORIA

Esta Tesis doctoral se presenta para obtener el título de Doctorado en Teledetección de la Universidad de Valencia, con mención de Doctorado Internacional.

Según el Reglamento vigente sobre depósito, evaluación y defensa de la Tesis doctoral de la Universidad de Valencia, la Tesis doctoral puede ser presentada de dos formas: 1) Tesis tradicional o 2) Tesis por compendio de publicaciones. En este caso, la Tesis presentada está elaborada por compendio de publicaciones. La Tesis de acuerdo con esta opción, tiene que cumplir los siguientes requisitos:

1. Se deben presentar un mínimo de tres artículos, ya publicados o aceptados en revistas indexadas en algún índice internacional como JCR (WoS) y/o SJR (Scopus) y ser el autor de la tesis el primer firmante de cada uno de ellos.
2. La Tesis debe presentar un resumen global de la temática, de los principales resultados y de las conclusiones.
3. La Tesis debe incluir una copia completa de los trabajos publicados o admitidos para publicación.

Concretamente, esta Tesis doctoral está compuesta de las siguientes publicaciones:

1. **Pasqualotto, N.**; Delegido, J.; Van Wittenberghe, S.; Verrelst, J.; Rivera, J.; Moreno, J., 2018. Retrieval of canopy water content of different crop types with two new hyperspectral indices: Water Absorption Area Index and Depth Water Index. *International Journal of Applied Earth Observation and Geoinformation*, 67, 69–78.
2. **Pasqualotto, N.**; Delegido, J.; Van Wittenberghe, S.; Rinaldi, M.; Moreno, J., 2019. Multi-crop green LAI estimation with a new simple Sentinel-2 LAI Index (SeLI). *Sensors*, 19(4), 904.
3. **Pasqualotto, N.**; D'Urso, G.; Bolognesi, S.F.; Belfiore, O.R.; Van Wittenberghe, S.; Delegido, J.; Pezzola, A.; Winschel, C.; Moreno, J., 2019. Retrieval of evapotranspiration from Sentinel-2: Comparison of vegetation indices, semi-empirical models and SNAP Biophysical Processor approach. *Agronomy*, 9(10), 663.

Por otra parte, como se pretende optar a Tesis con mención internacional, siguiendo el Artículo 9 del Reglamento sobre depósito, evaluación y defensa de la tesis doctoral, al menos el resumen y las conclusiones de la Tesis doctoral deben estar redactados en inglés. Por este motivo, a continuación, se presenta el Abstract y el capítulo final de Conclusiones en inglés.

CONTENIDO

ACRÓNIMOS Y ABREVIACIONES

ANN Artificial Neural Network

AVIRIS Airborne Visible/Infrared Imaging Spectrometer

CCC Canopy Chlorophyll Content

$CI_{red\text{-}edge}$ Red-Edge Chlorophyll Index

CLAIR Clevers Leaf Area Index by Reflectance

CWC Canopy Water Content

DWI Depth Water Index

EnMAP Environmental Mapping and Analysis Program

ESA European Space Agency

ET Evapotranspiration

ET_o Reference Evapotranspiration

ET_c Crop Potential Evapotranspiration

FAO Food and Agriculture Organization

FLEX Fluorescence Explorer

FVC Fractional Vegetation Cover

HyMap Hyperspectral Mapper

K_c Crop Coefficient

LAI Leaf Area Index

LCC Leaf Chlorophyll Content

LWC Leaf Water Content

MSI Multi-Spectral Imager

NIR Near-Infrared

PRISMA PRecursore IperSpettrale della Missione Applicativa

RTM Radiative Transfer Model

S2 Sentinel-2

S2A Sentinel-2A

S2B Sentinel-2B

SAIL Scattering from Arbitrarily Inclined Leaves

SeLI Sentinel-2 LAI_{green} Index

SNAP Sentinel Application Platform

SPARC03 Spectra bARax Campaign

SWIR Shortwave-Infrared

VI Vegetation Indices

VIS Visible

WAAI Water Absorption Area Index

ABSTRACT

Evidence suggests that human-induced greenhouse gases emissions have altered our climate at a relatively rapid rate, rising the global temperatures and inducing drastic changes in precipitation patterns to water-limited environments and agricultural areas, restricting crop yield, production rates and food availability. Biophysical parameters, such as leaf water content (LWC), leaf area index (LAI) or leaf chlorophyll content (LCC), are considered important indicators of health, growth and productivity of crops. As they define the status of the vegetation, they provide important inputs to models quantifying the exchange of energy and matter between the land surface and the atmosphere. Also, knowledge of their spatial and temporal distribution is highly useful for regional or global-scale applications related to crop monitoring, weather prediction and climate change studies.

The direct field measurements of biophysical parameters require continuous updates and can be extremely time-consuming and expensive, therefore, an alternative estimation methodology is necessary. Remote sensing from satellite and airborne sensors has become a commonly used technique for monitoring agricultural areas due to its ability to acquire synoptic information at different times and spatial scales. For an optimal agricultural monitoring by remote sensing, the spatial resolution should be at least 20 m and, preferably, 10 m, and a temporal resolution of less than a week, in order to follow-up acute changes in the crop condition and provide a timely response in management practices.

In this context, the Sentinel-2 (S2) missions from the European Space Agency (ESA) Copernicus program respond to such operational requirements. S2 is a constellation of satellites, with currently the Sentinel-2A (S2A) and Sentinel-2B (S2B) satellites in orbit. Together, they provide a 5-day nominal revisit, at the Equator, of the Earth's land surfaces with a 10, 20 and 60 m of pixel size. S2A and S2B carry on-board a virtually identical sensor, the Multi-Spectral Imager (MSI), covering a spectral range from 443 to 2190 nm through 13 bands located in the visible (VIS, 440 – 690 nm), the near-infrared (NIR, 750 – 1300 nm) and the shortwave-infrared (SWIR, 1300 – 2500 nm) spectral regions. With the narrow band configurations specifically located for vegetation monitoring, the S2 missions

improve the temporal, spatial and spectral resolution of remote sensing data, compared to other multi-spectral missions, such as Landsat, and offers great opportunities for agricultural monitoring. The mission's main objective is providing quality information for agricultural and forestry practices and, hence, helping management and food security applications. In addition, ESA has incorporated a user-friendly Biophysical Processor toolbox within the SNAP (Sentinel Application Platform) program, for the straightforward delivering of biophysical parameter products, such as LAI and canopy chlorophyll content (CCC). These parameters are automatic products, associated with a quality indicator, produced through an artificial neural network (ANN) which has been trained with simulated spectra generated from well-known radiative transfer models (RTMs), i.e., physically-based models that describe the absorption and scattering of light throughout the leaf, canopy and atmosphere. Only eight bands are used (B3, B4, B5, B6, B7, B8a, B11 and B12) for the biophysical parameter products estimation. This way, the values of biophysical parameters can be obtained in any study area with available S2 images, being very useful in operational agronomic studies.

On the other hand, hyperspectral sensors are becoming more and more relevant, which will be available by satellites such as the future EnMAP (Environmental Mapping and Analysis Program) mission or the recently launched PRISMA (PRecursore IperSpettrale della Missione Applicativa) satellite, or through airplanes punctually over the corresponding study area, such as AVIRIS (Airborne Visible/Infrared Imaging Spectrometer) and HyMap (Hyperspectral Mapper) sensors. This type of sensors allows to identify and to discriminate with great precision the surface, thanks to its high spectral resolution, allowing the detection of anomalies with precision. The future FLEX (Fluorescence Explorer) mission should also be specially highlighted, of which ESA is currently carrying out scientific development. The main objective of FLEX mission is to observe the vegetation functioning from space, based on the emitted fluorescence signal. The fluorescence measurement provides direct information of the photosynthesis process, constituting a novel tool for the rapid detection of vegetation stress, before damage is irreversible. In this context, all the methodologies developed to estimate biophysical parameters that are physiological state indicators are, therefore, fundamental to understand the behaviour of terrestrial vegetation at the global scale.

In general, there are three approaches for estimating biophysical parameters from remotely sensed data, i.e., (1) empirical retrieval methods, which consist of relating the biophysical parameter of interest against spectral data by means of simple relations (e.g., vegetation indices—VIs), (2) statistical methods, which define complex regression functions according to information from remote sensing data (e.g., artificial neural network—ANN) and (3) physically-based retrieval methods, which typically refers to the inversion of RTMs.

There are numerous scientific contributions related to the biophysical parameters estimation through remote sensing, but most of these studies focus on a single or a small number of crop types. The challenge arises when these remote sensing techniques are applied in a general context, i.e. for a high diversity in crop types. This is important as agricultural areas are often composed of multi-crop types but also because the retrieval algorithms should be robust on a global scale. This Thesis attempts to achieve techniques to assess the general character of three important vegetation health indicators for crop monitoring: canopy water content (CWC), LAI and CCC. The methodologies finally proposed aim to present a physical basis for applied crop monitoring and produce accurate results for a wide range of crop types.

The **starting point** (Pasqualotto et al., 2018a) of this Thesis has been the proposal of a methodology defined for the estimation of CWC. For this purpose, the SPARC03 (Spectra bARax Campaign) dataset has been used. This field data was obtained in July 2003 in Albacete (Spain) and is composed of CWC destructive values of six different crop types, as well as the spectral information obtained from the hyperspectral HyMap airborne sensor. This sensor has a wavelength range between 430 nm and 2490 nm and, for this campaign specifically, images with a spatial resolution of 5 m were obtained. Using the multi-crop SPARC03 dataset, commonly used water content index formulations were analysed and validated for the variety of crops, indicating possibilities for improvement. Instead of using specific band combinations, influenced by other parameters such as chlorophyll content and LAI, a more physically based approach was employed. After a study of the HyMap sensor spectra and the modelled spectra simulated with PROSAIL, it was observed that, with simulations assuming no water content in the leaves, the spectrum presented a straight-line shape in the range of water absorption between 800 and 1200 nm. The slope and the magnitude of this reflectance line depended mainly on LAI. This line was used as a reference to define the Water

Absorption Area Index (WAAI), which consists in determining the difference between the area under the null water content reference line and the area under the measured reflectance in the range 911 – 1271 nm, where the influence of water content is maximal. The WAAI is an area index essentially developed for high spectral resolution data. However, since hardly any of the currently operational satellite sensors are equipped with such a high spectral resolution, the so-called Depth Water Index (DWI) is proposed as a possible guide for the configuration of future optical superspectral sensors. The DWI is a simplified four-band index based on the spectral depths produced by the water absorption at 970 and 1200 nm and two reference bands. Hence, in this study two new CWC estimation indices were defined, by means of which the CWC of multi-crop areas can be estimated, obtaining more promising results ($R^2 > 0.7$) than the conventional indices ($R^2 < 0.6$).

Secondly (Pasqualotto et al., 2019a), in the same context of improving remote biophysical parameter retrieval of important crop growth parameters, a simple and operative methodology for the estimation of the LAI was developed. The LAI is fundamental both for its function as an indicator of the plant physiological state and for its essential role in scaling the leaf-based measurable parameters water and chlorophyll content at canopy level. LAI can be distinguished in two types. There is the LAI_{green}, representing the leaves which are photosynthetically active, being the most common type of LAI and the one studied in this Thesis, and, on the other hand, there is the LAI_{brown}, representing the leaf area normalized which is senescent and losing photosynthetic function. Two large field campaigns were conducted that resulted in two independent datasets, composed of LAI *in situ* values ranging from 0 to 4.5 m^2/m^2, obtained at test sites in Valencia (Spain) and Foggia (Italy). The Valencia dataset is composed of LAI *in situ* values of 13 different crop types from the *Huerta de Valencia* and Foggia's dataset is composed of information from 3 crop types. Simultaneous satellite data from S2 overpasses was analysed for the two test sites. The first analysis consisted in applying the indices commonly used in the literature to estimate LAI for the Valencia dataset, obtaining statistics that can be improved given a saturation process of the method for high LAI values (≥ 3). Subsequently, an analysis was performed to verify better band combinations for the estimation of LAI in multi-crop zones, minimizing the effects of the saturation process. A physically meaningful combination of bands was chosen for the normalized index $(R_{865} - R_{705})/(R_{865} + R_{705})$, with the 705 nm band

located in the red-edge region, a spectral area which balances the influence of strong chlorophyll absorption and minimal scattering at moderate-high LAI values, and the 865 nm band located in the NIR region, as a reference band. Improved statistics were obtained by applying this index for a partial dataset, with a linear adjustment. The new index proposed, the Sentinel-2 LAI_{green} Index (SeLI), avoids saturation of the LAI estimation, allowing an improved LAI retrieval for different crop types.

The **third study** (Pasqualotto et al., 2019b) of this Thesis consisted in the analysis of the different existing methodologies for LAI and CCC retrieval, two key parameters for the estimation and monitoring of evapotranspiration (ET) of vegetation. In particular, this study performed a comparative analysis of empirical VIs, semi-empirical approaches (CLAIR - Clevers Leaf Area Index by Reflectance model with fixed and calibrated extinction coefficient) and artificial neural network S2 products (ANN S2 products) to analyse the most optimal approach for LAI and CCC estimation, from a statistical and operational point of view, using concomitant S2 band information. The main objective of this analysis was to verify how the method used for the estimation of these input parameters influences the final result of crop growth models, here using the Penman-Monteith model, widely applied for the estimation of ET. One of the main strengths of this third study is that in order to carry out the comparative analysis of the different estimation methods, four datasets composed of *in situ* LAI and CCC values from different crop types and different plot sizes were used, allowing to obtain robust results. The datasets collected in Italy (Caserta and Tarquinia), Argentina (Bahía Blanca) and Spain (Valencia) covered *in situ* data with a LAI range of 0 to 5, and a CCC range of 0 to 5.4 g/m^2. SeLI is the index that presents good statistics in each dataset ($R^2 > 0.71$, RMSE < 0.78) for LAI parameter and for the CCC, the $CI_{red\text{-}edge}$ ($R^2 > 0.67$, RMSE < 0.62 g/m^2). Both indices use bands located in the red-edge region, highlighting the importance of this spectral region. The biggest problem with VIs was that the SeLI index produced saturation with LAI values > 3. On the other hand, the LAI CLAIR model estimated with fixed extinction values (α*) of 0.41 for herbaceous crops and 0.30 for tree species obtained good statistics ($R^2 >$ 0.63, RMSE < 1.47) and the CLAIR model optimizing the parameter α* ($CLAIR_{opt}$) for each of the study areas only slightly improved the RMSE in the two Italian datasets (RMSE ≈ 0.70). ANN S2 products produced statistics very similar to the VIs, but without producing saturation at high LAI values. It should be mentioned

that with the Valencia area dataset, all the methodologies produce improvable results ($R^2 < 0.5$, RMSE > 0.7 for LAI; $R^2 < 0.4$, RMSE > 1.0 g/m² for CCC), due to the high soil influence in this area and the small size of the plots (< 1 ha). Finally, the influence of the LAI parameter on the Penman-Monteith ET model adapted to remote sensing was analysed, which derives the reference (ET_o) and potential (ET_c) crop ET. During recent years, there has been a consistent effort to estimate vegetation parameters from remotely sensed data, allowing to adapt the Penman-Monteith equation for direct use with remote sensing data, minimizing time and cost. To evaluate ET_c throughout the season, the dataset from the Tarquinia test site with available temporal *in situ* LAI data of two crop types, wheat and tomato, was used. Due to the absence of independent reference ET data, the estimated ET_c with the LAI *in situ* values were considered as the proxy of the ground-truth. Also, the results were compared with ET_c estimated as the product of the reference evapotranspiration (ET_o) and the crop specific coefficient (K_c) derived from FAO (Food and Agriculture Organization) table values, according to the methods commonly used in operational studies. As a result, it was obtained that the ET_c values obtained with the LAI estimated with SeLI index were the closest to the truth-terrain in the case of wheat, while for tomato the best correlation was obtained with the ET_c estimated with the ANN S2 LAI product. Therefore, with all the above, it can be concluded that VIs produce the best statistics for low LAI values, but the ANN S2 products are the only ones that do not produce saturation towards higher values, both for the direct estimation of the LAI and CCC parameters and the derived estimation of ET. It demonstrates the great potential of ANN S2 products for operational use in the monitoring of agricultural areas.

The influence of soil can compromise the retrieval results of all the different methodologies defined in this Thesis when the fractional vegetation cover is low (FVC < 30 %). Future work should consider the soil reflectance in order to improve the general retrieval of vegetation biophysical properties.

The studies presented in this Doctoral Thesis demonstrate the high value of current operational high spatial resolution S2 satellites for the monitoring of biophysical crop parameters in the context of an increasing demand to secure optimal growth and food production. The availability of high spatial and temporal resolution of multispectral band sensors allow the application of biophysical

parameters for water and pigment content at an unprecedented spatial and temporal detail. Combined with growth or evapotranspiration models, these biophysical parameters allow even further the remote scaling of biophysical processes at the agricultural unit scale. This was demonstrated by integrating the S2-derived LAI in the adapted Penman-Monteith equation for evapotranspiration modelling. Future hyperspectral missions will even allow a further improved retrieval of biophysical parameters, as demonstrated in the study on the Water Absorption Area Index. Application of such spectrally detailed monitoring will further allow to improve the monitoring of crop growth and functioning at different scales.

RESUMEN EXTENSO

1. Contexto

1.1 Parámetros biofísicos claves de la vegetación

Las emisiones de gases de efecto invernado inducidas por actividades humanas han alterado nuestro clima a un ritmo relativamente rápido (IPCC, 2019), con la consecuencia de que el aumento de las temperaturas y los cambios en el patrón de precipitaciones exponen drásticamente los ecosistemas limitados por el agua, como son los ecosistemas agrícolas, restringiendo el rendimiento de los cultivos, la productividad y la disponibilidad de alimentos (McKersie, 2015). El seguimiento de los cultivos a lo largo de toda la etapa de crecimiento es esencial para detectar anomalías y optimizar los costes y recursos del sector agrícola (Brisco et al., 1998). Los parámetros biofísicos de la vegetación, principalmente el contenido en agua de las hojas, el índice de área foliar o el contenido en clorofila, están considerados indicadores importantes de la salud, crecimiento y productividad de los cultivos (Gitelson et al., 2003). El conocimiento espacial de las mismas es determinante para la toma de decisiones relativas principalmente a la planificación del riego (Jackson et al., 2004) y para la estimación de la productividad (Peñuelas et al., 1993; Zhang et al., 2010).

Concretamente, el índice de área foliar (LAI - *leaf area index*) se define como la superficie foliar por unidad de superficie de suelo (m^2 de hoja/m^2 de suelo o adimensional); el contenido en agua a nivel de cubierta (CWC - *canopy water content*) como la cantidad de agua en la vegetación por unidad de superficie (g de agua/m^2 de suelo) y suele ser estimada como el producto del contenido de agua a nivel de hoja (g de agua/m^2 de hoja) por el parámetro LAI; y el contenido en clorofila a nivel de cubierta (CCC - *canopy chlorophyll content*) como la cantidad de pigmentos verdes de la hoja por superficie de suelo (g de clorofila/m^2 de suelo), parámetro estimado comúnmente multiplicando la clorofila a nivel de hoja (g de clorofila/m^2 de hoja) por el LAI.

Estos parámetros biofísicos no solo son importantes por proporcionar información por sí mismos del estado fisiológico de la vegetación, sino también porque son

parámetros clave de entrada en importantes modelos de crecimiento de cultivo. A modo de ejemplo, el LAI es un parámetro de entrada en el modelo adaptado Penman-Monteith de la FAO - *Food and Agriculture Organization* (Allen et al., 1998), el cual deriva la evapotranspiración de referencia y potencial de los cultivos.

1.2 Nuevos sensores remotos

La medida directa de estos parámetros biofísicos sobre el terreno requiere elevados recursos económicos y de tiempo (Bréda, 2003), por lo que es necesaria una metodología de estimación alternativa. La detección remota a través de satélites y sensores aerotransportados se ha convertido en una técnica comúnmente utilizada para el seguimiento de los cultivos debido a su capacidad de adquirir información a diferentes escalas, tanto espaciales como temporales (Campos-Taberner et al., 2016; Yao et al., 2017). Para una óptima monitorización de la agricultura a través de teledetección, la resolución espacial debe ser al menos de 20 m y, preferiblemente, de 10 m, con el fin de hacer posible la gestión de áreas específicas. En cuanto a la resolución temporal, es necesaria una resolución menor a una semana para detectar cambios en las condiciones de los cultivos y proporcionar una respuesta eficaz (Mulla, 2013).

Actualmente está cobrando especial importancia en los estudios agronómicos la serie de satélites Sentinel-2 (S2) del programa Copernicus, de la Agencia Espacial Europea (ESA - *European Space Agency*) (Drusch et al., 2012). S2 es una constelación de satélites, de los cuales actualmente están en órbita los satélites Sentinel-2A (S2A) y Sentinel-2B (S2B), lanzados por la ESA el 23 de junio de 2015 y el 7 de marzo de 2017, respectivamente. Ocupan la misma órbita a una altitud de ~786 km, pero separados por 180°. Juntos proporcionan un periodo de revisita de 5 días, en el Ecuador, de la superficie de la Tierra con un tamaño de píxeles de 10, 20 y 60 m. S2A y S2B llevan a bordo un sensor idéntico, denominado *Multi-Spectral Imager* (MSI), que abarca la región del espectro comprendida entre 443 nm y 2190 nm mediante 13 bandas localizadas en las regiones espectrales del visible (VIS, 440 – 690 nm), del infrarrojo cercano (NIR - *Near-Infrared*, 750 – 1300 nm) y del infrarrojo de onda corta (SWIR - *Shortwave-Infrared*, 1300 – 2500 nm). La región espectral entre el VIS y el NIR, es decir, entre 690 y 750 nm, se denomina zona del *red-edge*

y es la zona entre el máximo de absorción de la clorofila en el rojo y el máximo de reflectividad en el NIR. Numerosos estudios con datos espectrales reales (Delegido et al., 2008; Herrmann et al., 2011) y simulados (Delegido et al., 2011; Liu et al., 2004) han evidenciado la fuerte relación de esta zona espectral con parámetros biofísicos como la clorofila y el LAI, ya que esta zona minimiza la saturación que suele producirse en la región del rojo a altos valores de LAI. Además, la señal en esta región es alta y con poca presencia de ruido. S2 incorpora nuevas bandas estrechas (ancho de banda de 20 nm aproximadamente) localizadas en esta región, concretamente centradas a 705 nm y 740 nm. Por lo tanto, la misión S2 mejora la resolución temporal, espacial y espectral de los datos de teledetección, en comparación con otras misiones operativas multiespectrales anteriores, como Landsat, ofreciendo grandes oportunidades para la monitorización agrícola. El principal objetivo de la misión es proporcionar información de calidad para el seguimiento agrícola y forestal y, por tanto, ayudar a gestionar la seguridad alimentaria. Además, actualmente la ESA ha incorporado, en las imágenes de S2 corregidas atmosféricamente (Nivel 2A), productos de parámetros biofísicos, como el LAI y el CCC, proporcionados a través de la herramienta *Biophysical Processor* del programa SNAP (*Sentinel Application Platform*). Estos parámetros son productos automáticos obtenidos a través de una red neuronal artificial (ANN - *Artificial Neural Network),* calibrada con bases de datos simuladas generadas a través de modelos de transferencia radiativa (RTMs - *Radiative Transfer Models*, modelos de base física que describen la absorción y dispersión de la luz a través de la hoja, cubierta y atmósfera), principalmente a través del modelo SAIL – *Scattering from Arbitrarily Inclined Leaves* (Weiss and Baret, 2016). Para la estimación de dichos parámetros biofísicos, tan solo se utiliza la información espectral de ocho bandas de Sentinel-2: B3, B4, B5, B6, B7, B8a, B11 and B12. De esta manera, se pueden obtener parámetros biofísicos de cualquier zona de estudio que disponga de imágenes de S2, siendo muy útil en el contexto de estudios agronómicos operativos. Hay que mencionar que tanto las imágenes proporcionadas por la serie de satélites S2 como el programa SNAP son totalmente gratuitos, y en un futuro no solo van a seguir proporcionándose este tipo de imágenes y productos, sino que está prevista su continua mejora.

Por otro lado, también están cobrando especial importancia los sensores hiperespectrales, que serán transportados por satélites como la futura misión EnMAP - *Environmental Mapping and Analysis Program* (Guanter et al., 2015) o la recientemente lanzada PRISMA - *PRecursore IperSpettrale della Missione Applicativa* (Candela et al., 2016), o aerotransportados a través de aviones de manera puntual sobre la zona de estudio correspondiente, como AVIRIS - *Airborne Visible/Infrared Imaging Spectrometer* (Vane, 1987) y HyMap – *Hyperespectral Mapper* (Cocks et al., 1998). Este tipo de sensores permiten identificar y discriminar con gran precisión la superficie terrestre, gracias a su alta resolución espectral, permitiendo la detección de anomalías con alta precisión.

Hay que destacar especialmente la futura misión hiperespectral FLEX – *Fluorescence Explorer*, de la cual la ESA está realizando el desarrollo científico actualmente (posible lanzamiento hacia 2024) (Coppo et al., 2017). Esta misión presenta como principal objetivo la observación del funcionamiento de la vegetación desde el espacio, basado en la señal de emisión de la fluorescencia. La medida de la fluorescencia proporciona información directa del proceso de fotosíntesis, constituyendo una novedosa herramienta para la rápida detección del estrés en la vegetación, antes de que el daño sea irreversible. En este contexto, todas las metodologías desarrolladas para estimar parámetros biofísicos indicadores del estado fisiológico de la vegetación son, por tanto, fundamentales para entender el comportamiento de la vegetación terrestre a escala global.

1.3 Metodologías de estimación basadas en información remota

Cada parámetro biofísico presenta su influencia máxima en una zona del espectro, como se ha comentado previamente con la región del *red-edge* y los parámetros clorofila y LAI. Gracias a esta relación, se pueden estimar los parámetros biofísicos a través de técnicas de teledetección.

De manera general, existen tres tipos de metodologías para estimar los parámetros biofísicos a partir de datos obtenidos por teledetección: (1) métodos empíricos, que consisten en relacionar el parámetro biofísico de interés con la información

espectral a través de relaciones simples (p.ej. índices de vegetación – VIs), (2) métodos estadísticos, los cuales definen funciones de regresión más complejas a través de la información espectral (p.ej. ANN), y (3) métodos físicos, que se refieren a la inversión de RTMs.

Los enfoques empíricos proporcionan un nivel de precisión aceptable en la estimación de parámetros biofísicos y pueden calcularse sin grandes exigencias computacionales, pero debido a la sensibilidad de las VIs al tipo de vegetación y características del sensor, se requieren mediciones *in situ* fiables para la calibración del modelo. Además, los VIs se ven muy afectados por los parámetros que afectan a la reflectividad, como son la estructura del dosel, la orientación y distribución espacial de las hojas, las propiedades ópticas de las hojas y del suelo y la geometría del sensor (Sakamoto et al., 2012). Asimismo, los VIs se basan generalmente en una combinación de pocas bandas espectrales y en una observación de un solo ángulo, lo que lleva a una subexplotación de todo el rango espectral y direccional disponible en los sensores de nueva generación. Debe ser mencionado que la mayoría de los VIs dejan de ser sensibles cuando parámetros como el LAI superan un cierto límite, comúnmente 2 o 3 (Haboudane et al., 2004). Esta saturación a altos valores de LAI se produce en el rango del rojo (600 – 700 nm) debido a la gran absorción que produce la clorofila en este rango (Kira et al., 2016). Para evitar esta saturación se utilizan bandas localizadas en la zona del *red-edge* (690 – 750 nm), ya que se encuentra entre el máximo de absorción de la clorofila en el rojo y la máxima reflectividad producida en el NIR debido a la estructura celular (LAI) (Guyot et al., 1992). Además, hay modelos basados en VIs que han sido mejorados incluyendo factores de corrección, como es el caso del modelo CLAIR (*Clevers Leaf Area Index by Reflectance)* (Clevers, 1989), que incluye un factor correctivo de la influencia del suelo.

Los métodos estadísticos pueden ser paramétricos o no-paramétricos (Lázaro-Gredilla et al., 2013). Los modelos paramétricos se basan en el conocimiento físico del problema y construyen expresiones parametrizadas explícitas, asumiendo un conjunto finito de parámetros. Por lo tanto, la complejidad del modelo está limitada incluso cuando la cantidad de datos es ilimitada. Esto les hace bastante inflexibles. Alternativamente, los modelos no-paramétricos se ajustan para predecir un modelo empírico utilizando un conjunto de datos (pares de datos entrada-salida), construyendo un modelo de regresión no lineal utilizando los

parámetros observados como entradas y sin tener en cuenta las restricciones físicas. Esto les proporciona un carácter más flexible.

Por otro lado, los modelos físicos consideran la arquitectura del cultivo, la iluminación, la influencia del suelo y las geometrías de iluminación y de visualización, haciéndolos útiles en múltiples aplicaciones operativas para la estimación de parámetros biofísicos del cultivo (Bacour et al., 2006). Sin embargo, presentan otras restricciones, como el riesgo intrínseco de simplificar excesivamente la arquitectura del dosel (Casa et al., 2010). Generalmente, los modelos físicos realizan una descripción simple de la arquitectura del dosel que puede no representar la real, particularmente en las superficies vegetales más dispersas o arboladas. Además, en los modelos de base física, las incertidumbres de las mediciones radiométricas deben añadirse a las simulaciones cuando se elaboran las bases de datos de calibración (Frederic and Buis, 2008). Otra restricción es lo que se denomina el problema *ill-posed*, cuando diferentes combinaciones de parámetros proporcionan una firma espectral idéntica, lo que produce incertidumbres significativas en la estimación de parámetros, por lo que se debe realizar un proceso de regulación de los resultados que considere tan solo las respuestas cercanas a la realidad (Atzberger, 2004).

2. Aportación de la tesis y organización

Existen numerosos estudios científicos de estimación de parámetros biofísicos a través de sensores remotos. Pero la gran mayoría de estas aportaciones están enfocadas a un solo tipo o a un número reducido de tipos de cultivo. El reto surge cuando se quieren utilizar estas técnicas de teledetección en un contexto general, es decir, aplicables a numerosos tipos de cultivos. Esto es realmente importante ya que las zonas agrícolas suelen presentar heterogeneidad de cultivos. Esta tesis intenta conseguir técnicas con ese carácter general, analizando, en primer lugar, las metodologías existentes y su comportamiento ante bases de datos *in situ* de diversos tipos de cultivos y, posteriormente, definir nuevas técnicas de estimación de tres indicadores importantes del estado de la vegetación: contenido en agua (CWC), índice de área foliar (LAI) y contenido en clorofila (CCC). Concretamente, el esquema de trabajo seguido es el representado en la Figura 1, mediante el cual se quieren conseguir los objetivos específicos siguientes:

- Toma de medidas *in situ* de los tres parámetros clave en diferentes tipos de cultivo y entornos agrícolas.
- Asociación de las medidas *in situ* con la información espectral de la nueva misión S2 y el sensor hiperespectral HyMap.
- Definición de las regiones del espectro donde la influencia de cada una de los parámetros es máxima, mediante información *in situ* y espectros simulados.
- Análisis de las técnicas preexistentes para la estimación de los parámetros CWC, LAI y CCC con teledetección, desde el punto de vista de aplicabilidad a diversidad de cultivos.
- Definición de nuevas metodologías con base física, que puedan ser aplicadas a diversos tipos de cultivo.
- Comparación de las nuevas metodologías con las existentes y seleccionar finalmente la más óptima, desde el punto de vista estadístico, físico y aplicabilidad a zonas heterogéneas.
- Análisis de cómo el método de estimación de estos indicadores afecta al resultado final de modelos agronómicos que utilizan estos parámetros como valores de entrada.

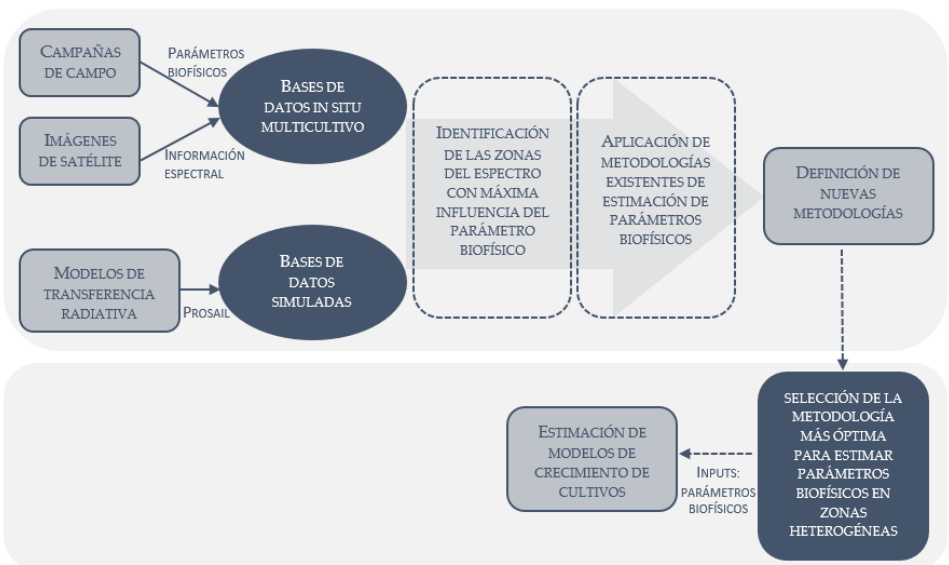

Figura 1. Esquema general de trabajo seguido en esta tesis.

3. Resultados

Los resultados de esta tesis se refieren a los tres artículos de los que está compuesta, anexados al final de este documento. En primer lugar, el Artículo 1 (Pasqualotto et al., 2018a), se basa en la estimación del contenido en agua a nivel de cubierta a través del sensor hiperespectral HyMap. El Artículo 2 (Pasqualotto et al., 2019a) se enfoca en la estimación del índice de área foliar con el satélite operativo S2 y, finalmente, el Artículo 3 (Pasqualotto et al., 2019b) realiza un análisis comparativo de diferentes metodologías, basadas en S2, de estimación de los parámetros LAI y CCC, además de analizar la influencia del parámetro de entrada LAI en un modelo agronómico de estimación de evapotranspiración. En esta sección se van a describir las principales aportaciones de cada uno de los artículos, pudiéndose consultar la metodología y resultados completos en los artículos señalados.

3.1 Artículo 1. Estimación del contenido en agua de cubierta de diferentes tipos de cultivos con dos nuevos índices hiperespectrales: Water Absorption Area Index y Depth Water Index

Basado en el artículo (Pasqualotto et al., 2018a) y congresos (Pasqualotto et al., 2017, 2018b) realizados durante el periodo doctoral:

Pasqualotto, N., Delegido, J., Van Wittenberghe, S., Verrelst, J., Rivera, J.P., Moreno, J., 2018a. Retrieval of canopy water content of different crop types with two new hyperspectral indices: Water Absorption Area Index and Depth Water Index. *International Journal of Applied Earth Observation and Geoinformation*, 67, 69–78.

Pasqualotto, N., Delegido, J., Van Wittenberghe, S., Verrelst, J., Moreno, J., 2017. Estimación del contenido en agua de la cubierta vegetal de diversos cultivos mediante teledetección hiperespectral. *XVII Congreso de la Asociación Española de Teledetección*. 3-7 octubre, 2017. Murcia, España.

Pasqualotto, N., Delegido, J., Van Wittenberghe, S., Verrelst, J., Rivera, J.P., Moreno, J., 2018b. Remote estimation of canopy water content in different crop types with new hyperspectral indices. *International Geoscience and Remote Sensing Symposium, IGARSS.* 20-27 julio, 2018. Valencia, España.

El punto de partida de esta tesis ha sido la estimación del parámetro contenido en agua a nivel de cubierta (CWC), un indicador esencial del estado fisiológico de los cultivos. A lo largo de los años, se han elaborado multitud de índices de vegetación para la estimación de este parámetro, definidos la mayoría de ellos para uno o unos pocos tipos de cultivos, por lo que no pueden ser aplicados de manera universal. Este estudio se basa en la definición de nuevos índices de estimación de CWC aplicables a una gran variedad de tipos de cultivos. Para ello, se ha utilizado la base de datos SPARC03 – *Spectra bARax Campaign* (Delegido et al., 2013), que se obtuvo en julio de 2003 en Albacete (España), compuesta por valores destructivos de CWC tomada en seis tipos de cultivos diferentes, así como por la información espectral obtenida por el sensor hiperespectral aerotransportado HyMap. Este sensor presenta un rango de longitud de onda entre 430 nm y 2490 nm, con 125 bandas espectrales con un ancho de banda espectral entre 11 y 21 nm y, en esta campaña, una resolución espacial de 5 m.

En primer lugar, se determinaron las áreas del espectro donde la influencia del contenido en agua es máxima. Este estudio se realizó produciendo diferentes modelizaciones con el modelo de transferencia radiativa PROSAIL y analizando los espectros obtenidos en campo con HyMap. El agua presenta mayor influencia en la zona del NIR y del SWIR, presentando picos principalmente en 970, 1200, 1450, 1940 y 2500 nm, pero finalmente se decidió basar este estudio tan solo en la región del NIR (750-1300 nm) debido a que en esta área del espectro la sensibilidad al contenido de agua líquida es mayor y, además, la señal producida en el SWIR está muy contaminada por la celulosa y otros materiales que componen la hoja.

Utilizando esta base de datos, se probaron los principales índices de vegetación utilizados para estimar CWC con las bandas establecidas por los autores originales, obteniendo que todos los índices producían estadísticos mejorables cuando se aplican a diversos tipos de cultivos. Posteriormente, se procedió a

realizar todas las combinaciones de bandas posibles con las estructuras de los índices comúnmente utilizados para estimar CWC junto a otros índices definidos por la bibliografía para estimar otros parámetros biofísicos. Este análisis se realizó para determinar si algún índice ya establecido podría utilizarse para una gran diversidad de cultivos cambiando simplemente la combinación de bandas. Al probar todas las combinaciones se obtuvieron correlaciones muy altas ($R^2 > 0,8$), pero al analizar las bandas seleccionadas para obtener tan alta correlación se observó que no presentaba sentido directo desde el punto de vista físico debido a que muchas bandas utilizadas no solo estaban influenciadas por el contenido en agua sino también por otros parámetros como la clorofila y el LAI. A partir de este punto, se procedió a definir dos nuevos índices que produjeran buenos estadísticos, pero también que presentaran sentido físico, que estuvieran basados en zonas donde la influencia del contenido en agua fuese máxima.

Tras el estudio de los espectros reales y de las modelizaciones generadas con PROSAIL, se observó que, con contenidos de agua nulos, el espectro presentaba forma de línea recta entre 800 y 1200 nm, variando la pendiente de la línea y el nivel de reflectividad tan solo con el parámetro LAI. Esta línea se tomó como referencia para definir el *Water Absorption Area Index* (WAAI), el cual consiste en la diferencia entre el área debajo de la línea de referencia y el área debajo de la curva de reflectividad entre los límites 911 y 1271 nm. Estos límites fueron los que proporcionaban los mejores resultados, lo cual puede ser debido a que a 911 nm comienza el primer pico de absorción del contenido en agua y a 1271 nm termina la máxima influencia de este parámetro. El índice WAAI requiere una gran resolución espectral y la mayoría de los sensores actuales no la presentan, por lo que en este estudio se propone otro índice que utiliza menos bandas y, por tanto, más aplicable a los sensores convencionales. El *Depth Water Index* (DWI) es un índice de cuatro bandas basado en las profundidades espectrales producidas por la absorción del contenido en agua a 970 y 1200 nm y dos bandas de referencia.

Por tanto, en este estudio se definen dos nuevos índices de estimación de CWC, mediante los cuales se puede estimar el CWC de zonas heterogéneas obteniendo incluso estadísticos mejores que con los índices convencionales. El índice WAAI presenta mejores estadísticos que el DWI. Esto puede ser debido a que el índice WAAI explota un rango continuo del espectro, demostrándose

en numerosos estudios previos la potencialidad de utilizar un mayor número de bandas. A pesar de esto, los índices propuestos presentan problemas con cultivos cuya fracción de cobertura vegetal (FVC) es menor al 30 %, como es el caso del ajo y la cebolla. Estos cultivos suelen presentar gran cantidad de agua en sus hojas, pero al extrapolar a la cubierta, esta cantidad de agua se subestima debido a la poca cobertura aérea que presentan, dejando al suelo un papel predominante. Una posible solución futura, es introducir en estos nuevos índices el parámetro FVC, para no subestimar el contenido en agua en cultivos influidos por el suelo de fondo.

3.2 Artículo 2. Estimación de LAI verde de múltiples tipos de cultivo mediante un nuevo índice simple basado en Sentinel-2 (SeLI)

Basado en el artículo (Pasqualotto et al., 2019a) y congresos (Amin et al., 2018; Pasqualotto et al., 2018c, 2018d) realizados durante el periodo doctoral:

Pasqualotto, N., Delegido, J., Van Wittenberghe, S., Rinaldi, M., Moreno, J., 2019a. Multi-crop green LAI estimation with a new simple Sentinel-2 LAI Index (SeLI). *Sensors,* 19(4), 904.

Pasqualotto, N., Delegido, J., Amin, E., Cisneros, A., Van Wittenberghe, S., Verrelst, J., Paredes Gómez, V., Moreno, J., 2018c. Estimación del índice de área foliar verde y marrón de diferentes cultivos con Sentinel-2. *XVIII Congreso Nacional de Tecnologías de la Información Geográfica.* 20-22 junio, 2018. Valencia, España.

Amin-Darei, E., Verrelst, J., Rivera-Caicedo, J.P., **Pasqualotto, N.**, Delegido, J., Ruiz-Verdú, A., Moreno, J., 2018. The SENSAGRI Sentinel-2 LAI green and brown product: from algorithm development towards operational mapping. *International Geoscience and Remote Sensing Symposium, IGARSS.* 20-27 julio, 2018. Valencia, España.

Pasqualotto, N., Delegido, J., Van Wittenberghe, S., Rinaldi, M., Moreno, J., 2018d. Estimación de LAI verde de diversos cultivos mediante el nuevo índice SeLI para Sentinel-2. *XVIII Simposio Internacional en Percepción Remota*

y Sistemas de Información Geográfica (SELPER). 6-9 noviembre, 2018. La Habana, Cuba.

En segundo lugar, en el contexto de esta tesis se quiso estudiar cual era la mejor metodología para estimar el índice de área foliar (LAI), ya que es un parámetro fundamental tanto por su función indicadora del estado fisiológico de la planta como por su papel esencial para escalar los parámetros contenido en agua y clorofila a nivel de cubierta. Existen dos tipos de LAI, el LAI_{verde} que representa las hojas que están fotosintéticamente activas, siendo el tipo de LAI más común y el que se estudia a lo largo de esta Tesis, y el $LAI_{marrón}$, que representa las hojas en estado senescente y que han perdido la función fotosintética. Debido a la importancia creciente de la misión S2 por la idoneidad de sus características para el seguimiento de zonas agrícolas, el objetivo de este segundo artículo era definir un índice sencillo y operativo basado en la información espectral de S2 y en las zonas del espectro con mayor influencia del parámetro LAI, para la estimación del mismo en zonas heterogéneas.

El punto de partida de este estudio fue la realización de campañas de campo de las que se obtuvieron dos amplias bases de datos independientes, compuestas por valores *in situ* de LAI tomados en Valencia (España) y Foggia (Italia), de varios tipos de cultivo, en un rango de valores de 0 a 4,5 m^2/m^2. La base de datos de Valencia está compuesta por información de 13 cultivos diferentes de la Huerta, los cuales están cultivados en parcelas de pequeño tamaño (< 1 ha), y se utilizó como calibración del futuro índice. La base de datos de Foggia está compuesta por información de 3 tipos de cultivo y se utilizó para validar el nuevo índice. Las campañas de campo se realizaron próximas al paso de satélite S2, por lo que las bases de datos se completaron con la información espectral correspondiente.

El primer análisis consistió en aplicar los índices comúnmente utilizados en la literatura para estimar LAI a la base de datos de Valencia, para comprobar su comportamiento al ser aplicados a diversos tipos de cultivos. Se obtuvo un coeficiente de correlación entre 0,1 y 0,6 con diferentes tipos de ajuste, así como un proceso de saturación con valores altos de LAI (≥ 3). Esto puede ser debido a que la mayoría de estos índices utilizan bandas localizadas en la zona del espectro correspondiente al rojo (B4 = 665 nm), comprobándose en este estudio

con espectros reales de S2 que esa zona del espectro produce saturación con altos valores de LAI, mientras que las bandas localizadas en la zona del *red-edge* no producen tal saturación. Al descartar la utilidad de estos índices para su uso en zonas heterogéneas, se pasó a realizar un análisis para identificar qué bandas de S2 están más correlacionadas con el parámetro LAI. Este análisis consistió en realizar todas las combinaciones de bandas utilizando la estructura tanto de los índices utilizados para estimar LAI como otros índices comúnmente utilizados para estimar otros parámetros biofísicos. Como resultado se obtuvieron unos estadísticos mejores, pero al observar las bandas utilizadas para obtener tales estadísticos, en general 1610 nm o 2190 nm, estaban localizadas en zonas del espectro influidas principalmente por otros parámetros como son la lignina o el contenido en agua, por lo que no presenta sentido físico. El único caso que presentaba sentido físico, era la combinación de bandas dada para el índice normalizado de tipo NDVI (R_{865} - R_{705})/(R_{865} + R_{705}) ya que la banda de 705 nm es una banda localizada en la región del *red-edge* y la banda de 865 nm se encuentra en la región del NIR, ambas regiones influidas principalmente por el parámetro LAI.

Al aplicar este índice a la base de datos de Foggia, se obtuvieron aún mejores estadísticos con un ajuste lineal, por lo que se decidió seleccionar este índice finalmente. Este nuevo índice se denominó *Sentinel-2 LAI_{green} Index* (SeLI), el cual produce buenos estadísticos sin producir saturación en un rango de LAI de 0 a 4,5 m^2/m^2, presentando sentido físico al estar basado en las zonas del espectro donde la influencia del parámetro LAI es máxima. Además, es aplicable a zonas heterogéneas, incluso cuando las parcelas son de pequeño tamaño como es el caso de la zona de Valencia, en la que por primera vez en esta zona la distinción de cambios dentro de la parcela es posible por teledetección operativa. A pesar de esto, el índice agrícola SeLI debe ser validado con valores de LAI superiores a 5 para determinar su comportamiento y posible saturación, así como determinar si con estos altos valores de LAI se sigue manteniendo el ajuste lineal o son necesarios modelos no lineales.

3.3 Artículo 3. Estimación de la evapotranspiración con Sentinel-2: Comparación entre índices de vegetación, modelos semi-empíricos y la herramienta Biophysical Processor de SNAP

Basado en el artículo (Pasqualotto et al., 2019b) y congresos (Pasqualotto et al., 2019c, 2019d) realizados durante el periodo doctoral:

Pasqualotto, N., D'Urso, G., Bolognesi, S.F., Belfiore, O.R., Van Wittenberghe, S., Delegido, J., Pezzola, A., Winschel, C., Moreno, J., 2019b. Retrieval of Evapotranspiration from Sentinel-2: Comparison of Vegetation Indices, Semi-Empirical Models and SNAP Biophysical Processor Approach. *Agronomy*, 9(10), 663.

Pasqualotto, N., Delegido, J., Pezzola, A., Winschel, C., Moreno, J., 2019c. Estimación del contenido de clorofila a nivel de cubierta (CCC) en cultivos: Comparativa de índices de vegetación y el producto de nivel 2A de Sentinel-2. *XVIII Congreso de la Asociación Española de Teledetección*. 24-27 septiembre, 2019. Valladolid, España.

Pasqualotto, N.; Bolognesi, S.F.; Belfiore, O.R.; Delegido, J.; D'Urso, G.; Moreno, J., 2019d. Canopy chlorophyll content and LAI estimation from Sentinel-2: vegetation indices and Sentinel-2 Level-2A automatic products comparison. *IEEE International Workshop on Metrology for Agriculture and Forestry*. 24-26 octubre, 2019. Portici, Italia.

El tercer estudio consistió en realizar un análisis de las diferentes metodologías existentes para la estimación de LAI y contenido en clorofila a nivel de cubierta (CCC), dos parámetros clave para la estimación de la evapotranspiración (ET). El objetivo principal de este análisis era comprobar cómo el método utilizado para la estimación de estos parámetros influye en el resultado final de los modelos agronómicos, como es el caso del modelo Penman-Monteith (Allen et al., 1998) ampliamente utilizado para la estimación de la ET. Concretamente, este estudio analiza métodos empíricos (VIs), semi-empíricos (modelo CLAIR) y los productos automáticos de redes neuronales de S2 para comprobar cuál es el más óptimo para

la estimación de los parámetros LAI y CCC, desde un punto de vista estadístico, físico y operativo, utilizando la información espectral de S2.

Una de las principales fortalezas de este tercer estudio es que para llevar a cabo el análisis comparativo de los diferentes métodos de estimación de los parámetros LAI y CCC, se han utilizado cuatro bases de datos *in situ* totalmente independientes: dos provenientes de Italia (Caserta y Tarquinia), una de Argentina (Bahía Blanca) y otra de España (Valencia). La base de datos de Caserta está compuesta por información de 3 tipos de cultivo diferente, cultivados en parcelas > 100 m de lado. La base de datos de Tarquinia está formada por valores de 2 tipos de cultivo, cultivados en parcelas < 100 m de lado. La tomada en Bahía Blanca está compuesta por información de 7 tipos de cultivo, cultivados en parcelas > 300 m de lado y, la base de datos de Valencia, está formada por valores tomados en 12 cultivos diferentes, cultivados en parcelas de 40-100 m de lado. Todas estas bases de datos se completaron con la información espectral de las imágenes de S2 más próximas a la toma de la información de campo. Las bases de datos abarcan un rango de LAI de 0 a 5, y de CCC un rango de 0 a 5,4 g/m^2.

En primer lugar, a cada base de datos se aplicaron los índices más comúnmente utilizados para estimar CCC y LAI, incluido el nuevo índice SeLI; el modelo CLAIR, con valores del coeficiente de extinción (α*) fijos y calibrados; y los productos automáticos que proporcionan las imágenes de S2 a través de la herramienta SNAP. Como resultado se obtuvo que el índice de estimación de LAI que producía mejores estadísticos en cada una de las bases de datos era SeLI (R^2 > 0,71, RMSE < 0,78) y para estimar el parámetro CCC era el $CI_{red\text{-}edge}$ (R^2 > 0,67, RMSE < 0,62 g/m^2). Ambos índices utilizan bandas localizadas en la región del *red-edge*, destacando la importancia de esta zona espectral. El mayor problema con los índices de vegetación fue que el índice SeLI producía saturación con valores de LAI > 3. En cuanto al modelo CLAIR, el modelo producía para el parámetro LAI en cada una de las bases de datos un R^2 > 0,63 y un RMSE < 1,47 utilizando valores fijos de α* (0,41 para las especies herbáceas y 0,30 para las arbóreas) y calibrando este coeficiente, solo mejoraba el RMSE en dos zonas de estudio (RMSE ≈ 0,70). Los productos automáticos de S2 presentaron buenos estadísticos tanto para el parámetro LAI (R^2 > 0,70, RMSE < 0,86) como para el CCC (R^2 > 0,75, RMSE < 0,68 g/m^2) cuando se compararon con los valores de campo de cada una de las bases de datos, sin producir saturación para valores altos de LAI. En general todos los modelos obtuvieron buenos estadísticos en cada una de las bases de datos, excepto

para el caso de Valencia. En esta zona los modelos no producían buenos resultados seguramente debido a que la base de datos está compuesta por cultivos en los que su cobertura es dispersa y escasa, como es el caso de los cultivos de cebolla y naranjos.

En segundo lugar, se analizó la influencia del parámetro LAI en la estimación de la ET. En este estudio se utilizó el modelo adaptado de Penman-Monteith de la FAO-56, el cual estima la evapotranspiración de referencia (ET_o) y la potencial (ET_c) de los cultivos. Durante los últimos años, se ha realizado un esfuerzo constante para estimar los parámetros biofísicos a partir de la teledetección, lo que ha permitido adaptar la ecuación de Penman-Monteith de tal forma que se puede calcular directamente con información espectral de satélites (D'Urso, 2010), reduciendo al mínimo el tiempo y el coste económico. Concretamente en este estudio se estimó la ET_c en la zona de estudio de Tarquinia, debido a que en esta zona se tienen datos temporales *in situ* de LAI de 2 tipos de cultivo: tomate y trigo. Debido a la ausencia de datos *in situ* de ET, se tomó la ET_c estimada con el LAI *in situ* como la verdad-terreno, comparando con estos datos la ET_c estimada con el LAI obtenido con las diferentes metodologías. Además, se realizó una comparación con la ET_c estimada como el producto de ET_o por los correspondientes coeficientes de cultivo (K_c) derivados de las tablas tabuladas de la FAO, método comúnmente utilizado en estudios operativos. Como resultado se obtuvo que los valores de ET_c obtenidos con el LAI estimado con el índice SeLI eran los más próximos a la verdad-terreno en el caso del trigo, mientras que para el tomate la mejor correlación se obtenía con la ET_c estimada con el producto automático de LAI de S2.

En definitiva, este estudio muestra como los VIs producen los mejores estadísticos tanto para la estimación directa de los parámetros LAI y CCC, como para la estimación final de la ET. Sin embargo, los productos automáticos de S2 de LAI y CCC producen buenos estadísticos y es la única metodología que no produce saturación a altos valores de LAI, por lo que se concluye que es la metodología más óptima para estimar estos parámetros biofísicos claves y el producto final de ET_c, desde el punto de vista operativo. En un futuro se quiere validar el producto automático de S2 de cobertura vegetal (FVC), para incorporarlo a los modelos que se aplican a zonas con cultivos con FVC < 50 %, como es el caso de la Huerta de Valencia.

4. Conclusions

The main conclusions drawn from the different analysis carried out in this Doctoral Thesis about key biophysical parameters retrieval using remote sensing data are summarized as follow:

- Commonly used canopy water content (CWC) and leaf area index (LAI) indices applied to multi-crop *in situ* datasets produce a R^2 lower than 0.6, using linear, exponential and polynomial fitting.

- Common LAI indices are affected by a saturation process when values are higher than 2 or 3. This is mainly because these indices use bands located in the red spectral range (600 – 700 nm), where high chlorophyll absorption occurs.

- When systematically deducing the vegetation indices (VIs) from best band combinations, the optimal bands produce good statistics but sometimes lack a direct physical meaning for the corresponding biophysical parameter.

- The Water Absorption Area Index (WAAI) defined as the difference between the area under the null water content of reflectance (reference line, depending on the LAI parameter) simulated with PROSAIL and the area under measured reflectance using hyperspectral HyMap sensor between 911 and 1271 nm is proposed as a new hyperspectral CWC retrieval method. The Depth Water Index (DWI) is also proposed, a simplified four-band index based on the spectral depths produced by the water absorption at 970 and 1200 nm and two reference bands. The DWI was formulated as a simpler and thus more applicable index to conventional sensors with less spectral band information.

- Both the WAAI and DWI outperform established indices in predicting CWC when applied to heterogeneous croplands, using an exponential fit.

- The use of more bands influenced by CWC improves the correlation with the *in situ* values; the WAAI leads to better results than the four-bands DWI.

- The new Sentinel-2 LAI_{green} Index (SeLI) is defined, based on a calibration and validation with two independent *in situ* datasets, obtaining good statistics with a linear fitting. SeLI is a normalized index that uses the new Sentinel-2 (S2) narrow B5-band located at the beginning of the red-edge region (705 nm), a spectral area which balances the influence of strong chlorophyll absorption and minimal scattering at moderate-high LAI values, and a NIR band (865 nm) influenced by leaf scattering, as a reference band.

- Using S2 spectral information and four independent *in situ* LAI and canopy chlorophyll content (CCC) datasets, a comparative analysis of empirical (VIs), semi-empirical (CLAIR model with fixed and calibrated extinction coefficient) and artificial neural network S2 products derived from the Sentinel Application Platform Software (SNAP) Biophysical Processor (ANN S2 products) approaches is performed for the estimation of LAI and CCC. It is concluded that:

  - SeLI is the index that presents good statistics in each dataset ($R^2 > 0.71$, RMSE < 0.78) for LAI and for the CCC, the ratio red-edge chlorophyll index ($CI_{red\text{-}edge}$) performs best ($R^2 > 0.67$, RMSE < 0.62 g/m^2).
  - The LAI CLAIR model estimated with fixed extinction values (α*) of 0.41 for herbaceous crops and 0.30 for tree species obtained good statistics ($R^2 > 0.63$, RMSE < 1.47) and the CLAIR model optimizing the parameter α* ($CLAIR_{opt}$) for each of the study areas only slightly improved the RMSE in two datasets (RMSE ≈ 0.70).
  - The ANN S2 products present good statistics for LAI ($R^2 > 0.70$, RMSE < 0.86) and CCC ($R^2 > 0.75$, RMSE < 0.68 g/m^2) retrievals.

- The influence of the LAI input parameter on the FAO-56 Penman-Monteith evapotranspiration model adapted to remote sensing was analysed. This analysis showed that the crop potential evapotranspiration (ET_c) values obtained with the LAI estimated with the SeLI index were the

closest to the truth-terrain (ET_c estimated with LAI *in situ*) in the case of wheat, while for tomato the best correlation was obtained with the ET_c estimated with the ANN S2 LAI product.

- VIs are an easy applicable methodology that produces the best statistics for LAI and CCC estimation for lower values, but the ANN S2 products are the only ones that do not produce saturation at higher LAI values, demonstrating the great potential of ANN S2 products for operational use in the monitoring of agricultural areas.

- The saturation produced by the VIs, including the new SeLI index, which use bands located in the red-edge spectral region, indicates that the location of the S2 red-edge bands should be improved in future satellites.

- The influence of soil can compromise the retrieval results when the fractional vegetation cover is low (FVC < 30 %). Future work should consider the soil reflectance in order to improve the general retrieval of vegetation biophysical properties.

- The studies presented in this Doctoral Thesis demonstrate the relevance of current high spatial resolution S2 satellites for the monitoring of biophysical crop parameters, allowing the remote scaling of biophysical processes at the agricultural management unit scale. Future hyperspectral missions will allow improved retrievals for crop growth and functioning at different scales, considering the specific band locations used in each new index defined. The presented analyses and results in this Thesis are therefore of relevance to the spectral configuration of future operational superspectral sensors for biophysical parameter retrieval.

BIBLIOGRAFÍA

Allen, R.G., Pereira, L.S., Raes, D., Smith, M., 1998. Crop evapotranspiration - Guidelines for computing crop water requirements, FAO Irrigation and Drainage Paper.

Amin, E., Verrelst, J., Rivera-Caicedo, J., Pasqualotto, N., Delegido, J., Ruiz Verdú, A., Moreno, J., 2018. The Sensagri Sentinel-2 LAI green and brown product: From algorithm development towards operational mapping, in: International Geoscience and Remote Sensing Symposium (IGARSS). Valencia, Spain, pp. 1822–1825. https://doi.org/10.1109/IGARSS.2018.8518938

Atzberger, C., 2004. Object-based retrieval of biophysical canopy variables using artificial neural nets and radiative transfer models. Remote Sens. Environ. 93, 53–67. https://doi.org/10.1016/j.rse.2004.06.016

Bacour, C., Baret, F., Béal, D., Weiss, M., Pavageau, K., 2006. Neural network estimation of LAI, fAPAR, fCover and LAI×Cab, from top of canopy MERIS reflectance data: Principles and validation. Remote Sens. Environ. 105, 313–325. https://doi.org/10.1016/j.rse.2006.07.014

Bréda, N.J.J., 2003. Ground-based measurements of leaf area index: A review of methods, instruments and current controversies. J. Exp. Bot. 54, 2403–2417. https://doi.org/10.1093/jxb/erg263

Brisco, B., Brown, R.J., Hirose, T., McNairn, H., Staenz, K., 1998. Precision agriculture and the role of remote sensing: A review. Can. J. Remote Sens. 24, 315–327. https://doi.org/10.1080/07038992.1998.10855254

Campos-Taberner, M., García-Haro, F.J., Camps-Valls, G., Grau-Muedra, G., Nutini, F., Crema, A., Boschetti, M., 2016. Multitemporal and multiresolution leaf area index retrieval for operational local rice crop monitoring. Remote Sens. Environ. 187, 102–118. https://doi.org/10.1016/j.rse.2016.10.009

Candela, L., Formaro, R., Guarini, R., Loizzo, R., Longo, F., Varacalli, G., 2016. The PRISMA mission, in: International Geoscience and Remote Sensing Symposium (IGARSS). pp. 253–256. https://doi.org/10.1109/IGARSS.2016.7729057

Casa, R., Baret, F., Buis, S., Lopez-Lozano, R., Pascucci, S., Palombo, A., Jones,

H.G., 2010. Estimation of maize canopy properties from remote sensing by inversion of 1-D and 4-D models. Precis. Agric. 11, 319–334. https://doi.org/10.1007/s11119-010-9162-9

Clevers, J.G.P.W., 1989. The application of a weighted infrared-red vegetation index for estimating leaf area index by correcting for soil moisture. Remote Sens. Environ. 29, 25–37.

Cocks, T., Jenssen, R., Stewart, A., Wilson, I., Shields, T., 1998. The HyMap airborne hyperspectral sensor: The system, calibration and performance, in: EARSeL Workshop on Imaging Spectroscopy. pp. 37–42.

Coppo, P., Taiti, A., Pettinato, L., Francois, M., Taccola, M., Drusch, M., 2017. Fluorescence imaging spectrometer (FLORIS) for ESA FLEX mission. Remote Sens. 9, 649. https://doi.org/10.3390/rs9070649

D'Urso, G., 2010. Current status and perspectives for the estimation of crop water requirements from earth observation. Ital. J. Agron. 5, 107–120. https://doi.org/10.4081/ija.2010.107

Delegido, J., Fernandez, G., Gandia, S., Moreno, J., 2008. Retrieval of chlorophyll content and LAI of crops using hyperspectral techniques: Application to PROBA/CHRIS data. Int. J. Remote Sens. 29, 7107–7127. https://doi.org/10.1080/01431160802238401

Delegido, J., Verrelst, J., Alonso, L., Moreno, J., 2011. Evaluation of sentinel-2 red-edge bands for empirical estimation of green LAI and chlorophyll content. Sensors 11, 7063–7081. https://doi.org/10.3390/s110707063

Delegido, J., Verrelst, J., Meza, C.M., Rivera, J.P., Alonso, L., Moreno, J., 2013. A red-edge spectral index for remote sensing estimation of green LAI over agroecosystems. Eur. J. Agron. 46, 42–52. https://doi.org/10.1016/j.eja.2012.12.001

Drusch, M., Del Bello, U., Carlier, S., Colin, O., Fernandez, V., Gascon, F., Hoersch, B., Isola, C., Laberinti, P., Martimort, P., Meygret, A., Spoto, F., Sy, O., Marchese, F., Bargellini, P., 2012. Sentinel-2: ESA's optical high-resolution mission for GMES operational services. Remote Sens. Environ. 120, 25–36. https://doi.org/10.1016/j.rse.2011.11.026

Frederic, B., Buis, S., 2008. Estimating canopy characteristics from remote sensing observations: Review of methods and associated problems, in: Advances in Land Remote Sensing. Berlin, Germany, pp. 173–201.

https://doi.org/10.1007/978-1-4020-6450-0

Gitelson, A.A., Viña, A., Arkebauer, T.J., Rundquist, D.C., Keydan, G., Leavitt, B., 2003. Remote estimation of leaf area index and green leaf biomass in maize canopies. Geophys. Res. Lett. 30. https://doi.org/10.1029/2002GL016450

Guanter, L., Kaufmann, H., Segl, K., Foerster, S., Rogass, C., Chabrillat, S., Kuester, T., Hollstein, A., Rossner, G., Chlebek, C., Straif, C., Fischer, S., Schrader, S., Storch, T., Heiden, U., Mueller, A., Bachmann, M., Mühle, H., Müller, R., Habermeyer, M., Ohndorf, A., Hill, J., Buddenbaum, H., Hostert, P., Van Der Linden, S., Leitão, P.J., Rabe, A., Doerffer, R., Krasemann, H., Xi, H., Mauser, W., Hank, T., Locherer, M., Rast, M., Staenz, K., Sang, B., 2015. The EnMAP spaceborne imaging spectroscopy mission for earth observation. Remote Sens. 7, 8830–8857. https://doi.org/10.3390/rs70708830

Guyot, G., Baret, F., Jacquemond, S., 1992. Imaging spectroscopy for vegetation studies. Imaging Spectrosc. Fundam. Prospect. Appl. 2, 145–165.

Haboudane, D., Miller, J.R., Pattey, E., Zarco-Tejada, P.J., Strachan, I.B., 2004. Hyperspectral vegetation indices and novel algorithms for predicting green LAI of crop canopies: Modeling and validation in the context of precision agriculture. Remote Sens. Environ. 90, 337–352. https://doi.org/10.1016/j.rse.2003.12.013

Herrmann, I., Pimstein, A., Karnieli, A., Cohen, Y., Alchanatis, V., Bonfil, D.J., 2011. LAI assessment of wheat and potato crops by VENμS and Sentinel-2 bands. Remote Sens. Environ. 115, 2141–2151. https://doi.org/10.1016/j.rse.2011.04.018

IPCC, 2019. Summary for Policymakers. In: Climate Change and Land: an IPCC special report on climate change, desertification, land degradation, sustainable land management, food security, and greenhouse gas fluxes in terrestrial ecosystems [P.R. Shukla, J. Skea, E. Calvo Buendia, V. Masson-Delmotte, H.- O. Pörtner, D. C. Roberts, P. Zhai, R. Slade, S. Connors, R. van Diemen, M. Ferrat, E. Haughey, S. Luz, S. Neogi, M. Pathak, J. Petzold, J. Portugal Pereira, P. Vyas, E. Huntley, K. Kissick, M. Belkacemi, J. Malley, (eds.)]. In press.

Jackson, T.J., Chen, D., Cosh, M., Li, F., Anderson, M., Walthall, C., Doriaswamy, P., Hunt, E.R., 2004. Vegetation water content mapping using Landsat data derived normalized difference water index for corn and soybeans. Remote Sens. Environ. 92, 475–482. https://doi.org/10.1016/j.rse.2003.10.021

Kira, O., Nguy-Robertson, A.L., Arkebauer, T.J., Linker, R., Gitelson, A.A., 2016. Informative spectral bands for remote green LAI estimation in C3 and C4 crops. Agric. For. Meteorol. 218–219, 243–249. https://doi.org/10.1016/j.agrformet.2015.12.064

Lázaro-Gredilla, M., Titsias, M.K., Verrelst, J., Camps-valls, G., Member, S., 2013. Retrieval of biophysical parameters with heteroscedastic gaussian processes. IEEE Geosci. Remote Sens. Lett. 11, 838–842.

Liu, J., Miller, J.R., Haboudane, D., Pattey, E., 2004. Exploring the relationship between red edge parameters and crop variables for precision agriculture. IGARSS 2004. 2004 IEEE Int. Geosci. Remote Sens. Symp. 2, 1276–1279. https://doi.org/10.1109/IGARSS.2004.1368649

McKersie, B., 2015. Planning for food security in a changing climate. J. Exp. Bot. 66, 3435–3450. https://doi.org/10.1093/jxb/eru547

Mulla, D.J., 2013. Twenty five years of remote sensing in precision agriculture: Key advances and remaining knowledge gaps. Biosyst. Eng. 114, 358–371. https://doi.org/10.1016/j.biosystemseng.2012.08.009

Pasqualotto, N., Delegido, J., Van Wittenberghe, S., Verrelst, J., Moreno, J., 2017. Estimación del contenido en agua de la cubierta vegetal de diversos cultivos mediante teledetección hiperespectral, in: XVII Congreso de La Asociación Española de Teledetección. Murcia, Spain.

Pasqualotto, N., Delegido, J., Van Wittenberghe, S., Verrelst, J., Rivera, J., Moreno, J., 2018a. Retrieval of canopy water content of different crop types with two new hyperspectral indices: Water Absorption Area Index and Depth Water Index. Int. J. Appl. Earth Obs. Geoinf. 67, 69–78. https://doi.org/10.1016/j.jag.2018.01.002

Pasqualotto, N., Delegido, J., Van Wittenberghe, S., Verrelst, J., Rivera, J., Moreno, J., 2018b. Remote estimation of canopy water content in different crop types with new hyperspectral indices, in: International Geoscience and Remote Sensing Symposium (IGARSS). Valencia, Spain, pp. 3812–3815. https://doi.org/10.1109/IGARSS.2018.8517523

Pasqualotto, N., Delegido, J., Amin, E., Cisneros, A., Van Wittenberghe, S., Verrelst, J., Paredes-Gómez, V., Moreno, J., 2018c. Estimación del índice de área foliar verde y marrón de diferentes cultivos con Sentinel-2, in: XVIII Congreso Nacional de Tecnologías de La Información Geográfica. Valencia,

Spain.

Pasqualotto, N., Delegido, J., Van Wittenberghe, S., Rinaldi, M., Moreno, J., 2018d. Estimación de LAI verde de diversos cultivos mediante el nuevo índice SeLI para Sentinel-2, in: XVIII Simposio Internacional En Percepción Remota y Sistemas de Información Geográfica (SELPER). La Habana, Cuba.

Pasqualotto, N., Delegido, J., Van Wittenberghe, S., Rinaldi, M., Moreno, J., 2019a. Multi-crop green LAI estimation with a new simple Sentinel-2 LAI Index (SeLI). Sensors 19, 904. https://doi.org/10.3390/s19040904

Pasqualotto, N., D'Urso, G., Bolognesi, S.F., Belfiore, O.R., Van Wittenberghe, S., Delegido, J., Pezzola, A., Winschel, C., Moreno, J., 2019b. Retrieval of evapotranspiration from Sentinel-2: Comparison of vegetation indices, semi-empirical models and SNAP Biophysical Processor approach. Agronomy 9, 663.

Pasqualotto, N., Delegido, J., Pezzola, A., Winschel, C., Moreno, J., 2019c. Estimación del contenido de clorofila a nivel de cubierta (CCC) en cultivos: Comparativa de índices de vegetación y el producto de nivel 2A de Sentinel-2, in: XVIII Congreso de La Asociación Española de Teledetección. Valladolid, Spain, pp. 24–27.

Pasqualotto, N., Bolognesi, S.F., Belfiore, O.R., Delegido, J., D'Urso, G., Moreno, J., 2019d. Canopy chlorophyll content and LAI estimation from Sentinel-2: vegetation indices and Sentinel-2 Level-2A automatic products comparison, in: IEEE International Workshop on Metrology for Agriculture and Forestry. Portici, Italy.

Peñuelas, J., Filella, I., Biel, C., Serrano, L., Savé, R., 1993. The reflectance at the 950–970 nm region as an indicator of plant water status. Int. J. Remote Sens. https://doi.org/10.1080/01431169308954010

Sakamoto, T., Gitelson, A., Nguy-Robertson, A., Arkebauer, T., Wardlow, B., SuykerA., Verma, S., Shibayama, M., 2012. An alternative method using digital cameras for continuous monitoring of crop status. Agric. For. Meteorol. 154, 113–126. https://doi.org/10.1016/j.agrformet.2011.10.014

Vane, G., 1987. Airborne Visible/lnfrared Imaging Spectrometer (AVIRIS). A description of the sensor, ground data processing facility, laboratory calibration, and first results.

Weiss, M., Baret, F., 2016. S2ToolBox Level 2 products: LAI, FAPAR, FCOVER

[WWW Document]. URL http://step.esa.int/docs/extra/ATBD_S2ToolBox_L2B_V1.1.pdf (accessed 7.29.19).

Yao, X., Wang, N., Liu, Y., Cheng, T., Tian, Y., Chen, Q., Zhu, Y., 2017. Estimation of wheat LAI at middle to high levels using unmanned aerial vehicle narrowband multispectral imagery. Remote Sens. 9, 1304. https://doi.org/10.3390/rs9121304

Zhang, J., Xu, Y., Yao, F., Wang, P., Guo, W., Li, L., Yang, L., 2010. Advances in estimation methods of vegetation water content based on optical remote sensing techniques. Sci. China Technol. Sci. 53, 1159–1167. https://doi.org/10.1007/s11431-010-0131-3

LISTA DE PUBLICACIONES

ARTÍCULO 1

"Retrieval of canopy water content of different crop types with two new hyperspectral indices: Water Absorption Area Index and Depth Water Index"

This article was published in "International Journal of Applied Earth Observation and Geoinformation" in 2018. This journal had in 2018 an impact factor of 4.846 and the position of 5/30 (Q1) in Remote Sensing category.

Int J Appl Earth Obs Geoinformation 67 (2018) 69–78

Contents lists available at ScienceDirect

Int J Appl Earth Obs Geoinformation

journal homepage: www.elsevier.com/locate/jag

Retrieval of canopy water content of different crop types with two new hyperspectral indices: Water Absorption Area Index and Depth Water Index

Nieves Pasqualotto[a,*], Jesús Delegido[a], Shari Van Wittenberghe[a], Jochem Verrelst[a], Juan Pablo Rivera[b], José Moreno[a]

[a] Image Processing Laboratory (IPL), University of Valencia, C/Catedrático José Beltrán 2, 46980, Paterna, Valencia, Spain
[b] CONACYT-UAN, Secretariat of Research and Postgraduate, C/3, 63173, Tepic, Mexico

ARTICLE INFO

Keywords:
HyMap
Hyperspectral
Canopy water content
Vegetation indices

ABSTRACT

Crop canopy water content (CWC) is an essential indicator of the crop's physiological state. While a diverse range of vegetation indices have earlier been developed for the remote estimation of CWC, most of them are defined for specific crop types and areas, making them less universally applicable. We propose two new water content indices applicable to a wide variety of crop types, allowing to derive CWC maps at a large spatial scale. These indices were developed based on PROSAIL simulations and then optimized with an experimental dataset (SPARC03; Barrax, Spain). This dataset consists of water content and other biophysical variables for five common crop types (lucerne, corn, potato, sugar beet and onion) and corresponding top-of-canopy (TOC) reflectance spectra acquired by the hyperspectral HyMap airborne sensor. First, commonly used water content index formulations were analysed and validated for the variety of crops, overall resulting in a R^2 lower than 0.6. In an attempt to move towards more generically applicable indices, the two new CWC indices exploit the principal water absorption features in the near-infrared by using multiple bands sensitive to water content. We propose the Water Absorption Area Index (WAAI) as the difference between the area under the null water content of TOC reflectance (reference line) simulated with PROSAIL and the area under measured TOC reflectance between 911 and 1271 nm. We also propose the Depth Water Index (DWI), a simplified four-band index based on the spectral depths produced by the water absorption at 970 and 1200 nm and two reference bands. Both the WAAI and DWI outperform established indices in predicting CWC when applied to heterogeneous croplands, with a R^2 of 0.8 and 0.7, respectively, using an exponential fit. However, these indices did not perform well for species with a low fractional vegetation cover (<~ 30%). HyMap CWC maps calculated with both indices are shown for the Barrax region. The results confirmed the potential of using generically applicable indices for calculating CWC over a great variety of crops.

1. Introduction

Water is the most abundant molecule in leaves and its availability in leaf tissues is essential for cell enlargement, and, hence, plant growth. The knowledge of leaf water content (LWC) is important for assessing the physiological state, especially for detecting drought stress of the plant. Shortage in water content can produce not only environmental impacts such as an increase in fire risk, but moreover social and economic negative effects caused by food production decrease (Carlson and Burgan, 2003; Chuvieco et al., 2004; Riaño et al., 2005; Stimson et al., 2005). In agriculture fields, crop water content provides vital information for making correct decisions regarding irrigation planning (Jackson et al., 2004) and is used for productivity estimation (Peñuelas et al., 1993; Zhang et al., 2010). What is more, the success of sustainable agriculture, mainly in arid and semi-arid regions of the world, depends entirely on water availability (Alderfasi and Nielsen, 2001). Because the quantity of water in leaf tissues is a critical factor in plant survival (Kumar, 2007), assessing water stress symptoms accurately using spectral reflectance measurements has been an important goal for remote sensing research during the past decades. Remote sensing can play a unique and essential role because of its ability to acquire synoptic information at different time and space scales (Jackson, 1986; Oppelt and Mauser, 2004; Peñuelas et al., 1993).

Vegetation biophysical variables, such as chlorophyll (Chl), leaf area index (LAI) and water content, are considered to be the most important indicators of vegetation health, growth and productivity

* Corresponding author.
E-mail addresses: m.nieve.pasqualotto@uv.es (N. Pasqualotto), Jesus.Delegido@uv.es (J. Delegido), Shari.Wittenberghe@uv.es (S. Van Wittenberghe), Jochem.Verrelst@uv.es (J. Verrelst), jprivera@conacyt.mx (J.P. Rivera), Jose.Moreno@uv.es (J. Moreno).

https://doi.org/10.1016/j.jag.2018.01.002
Received 3 October 2017; Received in revised form 8 January 2018; Accepted 8 January 2018

(Gitelson et al., 2003). At leaf level, LWC is usually calculated by the weight difference of freshly harvested leaves and their weight after a drying process, i.e. a time-consuming procedure, especially for large-scale study areas. At this large spatial scale, canopy water content (CWC), defined as the amount of water in the vegetation per surface unit (g/m^2 ground surface), is a physiological variable of high interest which can be estimated multiplying the leaf water content (LWC, g/cm^2 of leaf) with the LAI (m^2 leaf per m^2 surface or dimensionless) to obtain CWC. Therefore, alternative non-destructive methods have been developed by means of linking water content with optical remote sensing data (Pu et al., 2003). The rationale for doing so is as follows. Water absorbs light energy along the entire spectrum, but in the near-infrared (NIR, 750–1300 nm), and short-wave infrared (SWIR, 1300–2500 nm) regions, water produces maximum absorptions features concretely at 970, 1200, 1450, 1940 and 2500 nm (Carter, 1991; Knipling, 1970; Tucker, 1980). Thus, with the understanding of the water absorption spectra, spectroradiometers provide the opportunity to quantify CWC through non-destructive methods (Inoue et al., 1993).

At the same time, an important process to consider in the study of CWC is the atmospheric correction because atmospheric water vapour (WV) absorption effects in the air column affect the reflected radiance in the 900–1000 nm region measured at the remote sensor, at the aircraft or satellite platform (Datt, 1999; Gao and Goetz, 1990; Goetz and Boardman, 1995). The atmospheric correction process aims to retrieve top-of-canopy (TOC) reflectance by removing the atmospheric effects. This correction is one of the critical steps to obtain good information related to the surface properties. Thus, the overall accuracy of CWC retrieval will strongly depend on the accuracy achieved by the atmospheric correction process (Sabater et al., 2014; Vicent et al., 2015, 2017).

Statistical methods are most widely used to identify sensitive wavelength bands from atmospherically corrected TOC reflectance data for the development of simple vegetation indices (VIs), which relate the biophysical variable of interest to an arithmetic formulation of bands (Verrelst et al., 2015a). These indices are defined in a way that enhance the spectral characteristics associated with a given vegetation property (Glenn et al., 2008). The potential of VIs for the biophysical variables determination has been widely demonstrated in numerous studies: they are intuitive, simple and fast (Broge and Leblanc, 2000; Colombo et al., 2003; Gitelson et al., 2005). Over the last several decades, some authors have proposed indices for LWC or CWC estimation, generally used for monitoring different aspects of vegetation health, such as fire risk assessment (Peñuelas et al., 1997) or disease monitoring (Pu et al., 2003). These indices typically use an insensitive band to water absorption (e.g., 820 and 900 nm) and a sensitive band to change in this variable (e.g., 970 and 1600 nm). Some of them have been defined in order to provide LWC (e.g., Datt, 1999; Hunt et al., 1987; Peñuelas et al., 1993; Pu et al., 2003). These authors have proposed LWC indices for the study of a specific plant species. For example, Datt (1999) proposed two normalized indices to determinate water content of various species of Eucalyptus, and Pu et al. (2003) established two ratio indices in order to calculate LWC of oak leaves. On the other hand, several authors established indices to calculate CWC (e.g., Hardisky et al., 1983; Hunt and Rock, 1989; Rollin and Milton, 1998; Wang and Qu, 2007). Some of these CWC indices are derived from indices developed at the leaf scale, such as the Water Index proposed by Peñuelas et al. (1997) being a modification of the Water Band Index (Peñuelas et al., 1993) used for calculating LWC.

Despite the positive aspects of VIs, their major weakness is the lack of a generally applicable index for multiple vegetation types. A universal relationship between a biophysical variable and a spectral signature cannot be expected since the reflected signal depends on complex interrelationships between internal and external physical factors, which can involve significant variation in time, space, and between one type of crop and another (Colombo et al., 2003). The best way to find efficient and robust indices is to use large and diverse field datasets, with a large variety in canopy structures (Glenn et al., 2008; le Maire et al., 2008). This applies as well for different crop development stages, representing instraspecies variability in canopy structure and biophysical variables. Moreover, VIs have been traditionally developed for sensors configured with only a few spectral bands. Several studies have confirmed that applying indices composed of a few bands to hyperspectral data is suboptimal and not recommended (Kira et al., 2016; Verrelst et al., 2015b). It is more optimal to use a larger number of bands, thereby always taking into account multiple sensitive bands along the spectral range (Verrelst et al., 2016). Accordingly, several authors have shown that exploiting a contiguous reflectance curve instead of using a few single bands sensitive to biophysical variables tend to be more promising to obtain good parameter retrieval results (Delegido et al., 2010; Malenovský et al., 2006; Mutanga et al., 2005; Oppelt and Mauser, 2004). This thus suggests that there is a need for the development of VIs not just based on a few bands as is commonly done, but rather based on multiple bands along the spectral range.

When aiming to develop generically applicable CWC indices, an ideal tool for studying general relationships between biophysical variables and VIs are Radiative Transfer Models (RTMs). RTMs are physically-based models that describe the absorption and scattering of light throughout the leaf, canopy and atmosphere. In several studies, RTMs have been used to develop optimized indices sensitive to water content at leaf and canopy scales (Clevers et al., 2010; Haboudane et al., 2002; Malenovský et al., 2006). One of the most popular leaf RTMs is PROSPECT (Jacquemoud et al., 1996; Jacquemoud and Baret, 1990), which considers the leaf as a succession of absorption layers. And one of the most popular canopy RTMs is SAIL (Verhoef, 1984), which describes the canopy as a homogenous and horizontal turbid-medium. The coupling of PROSPECT and SAIL, also known as PROSAIL (Jacquemoud et al., 2009), has been widely used to study canopy directional reflectance and their relationships with biophysical variables, including CWC (Clevers et al., 2010).

The main goal of this study is to develop generically applicable CWC indices, which are capable of providing CWC in heterogeneous crop types areas, based on remote sensing measurements of the leaf spectral behaviour when varying water content. For this purpose, PROSAIL simulations and a large field dataset are used to tackle the following two objectives. The first objective is to identify the spectral bands that present the highest correlation (R^2) for the estimation of CWC, tested with commonly used VIs by the scientific community. Based on this analysis and on a subsequent spectral sensitivity study of the multiple crop types in response to changes in CWC, a second objective is to develop and validate two new CWC indices, i.e. respectively applicable to data with high and low spectral resolution. The performances of the newly developed indices and established VIs sensitive to CWC are evaluated and CWC maps are generated.

2. Materials and methods

2.1. SPARC03 experimental dataset

The used dataset is based on the Spectra Barrax Campaign (SPARC03) (Delegido et al., 2013). This campaign took place between 12th and 14th of July (2003) in Barrax, La Mancha, Spain (coordinates 39°3′ N, 2°6′ W, 700 m a.s.l., *Datum* ETRS89). The SPARC03 dataset has been earlier used in various studies because it covers multiple crop types, growth phases, canopy geometries and soil conditions. Specifically, field data of lucerne (*Medicago sativa*), corn (*Zea mays*), potato (*Solanum tuberosum*), sugar beet (*Beta vulgaris*), garlic (*Allium sativum*) and onion (*Allium cepa*) were collected. Table 1 describes the biophysical and structural variables for each crop, indicating low structural and biophysical differences between the different elementary samplings units (ESUs) for each crop. The considered crops were in different development stage at the moment of flight overpass. Lucerne was in the pre-bloom phase, bud stage, in addition to being sparse with ray grass.

Table 1
Mean values and standard deviation of the obtained variables for each crop species used in the SPARC03 campaign.

Crop species	N° of ESUs	Growth phase	Chl (μg/cm²)	FVC (%)	LAI (m²/m²)	LWC (g/m² leaf)	CWC (g/m² surface)
Luceme	18	Bud stage	48.51 ± 0.98	60 ± 17	2.71 ± 0.75	137 ± 8	368 ± 102
Corn	14	Swelling ear	51.02 ± 0.74	65 ± 6	3.4 ± 0.42	180 ± 10	612 ± 75
Potato	12	Tuber bulking	35.51 ± 0.59	96 ± 1	5.29 ± 0.37	223 ± 15	1165 ± 90
Sugar beet	22	Maturity	44.09 ± 1.72	94 ± 1	4.05 ± 0.51	448 ± 11	1805 ± 225
Garlic	14	Maturity	14.51 ± 1.94	12 ± 3	0.58 ± 0.11	595 ± 15	344 ± 60
Onion	10	Maturity	20.38 ± 1.47	64 ± 1	1.96 ± 0.46	681 ± 14	1334 ± 316

During the campaign (12th–14th of July), airborne hyperspectral HyMap flight-lines were.

Corn crop was beginning to produce ears. Potato and sugar beet were dense and well developed, ready to be harvested. Garlic crop was in a maturity stage, but this crop type was in poor state and very sparse. And, finally, onion was in a maturity stage, with mature bulbs.

Regarding the variables used, chlorophyll content (Chl), fraction of green vegetation cover (FVC), effective LAI (green LAI) and leaf water content (LWC) were measured for a total of 100 ESUs of 20 × 20 m. Each ESU was assigned a Chl value, measured using a CCM-200 Chlorophyll Content Meter and calibrated through laboratory analysis of specific samples (Gandia et al., 2004); a FVC value, which was estimated through hemispherical photographs; a LAI value with LicorLAI-2000 digital analyser (Welles and Norman, 1991), which uses a fish-eye lens with an hemispheric field view (± 148°) to calculate the interception of blue light (320–490 nm); and a LWC value, obtained through a drying and weighing method, collecting three leaves at the top level, due to this is the part of the plant observed by the sensor. For CWC estimation, leaf area was obtained by digital photographs of each leaf over squared grid paper. From the two masses and the known sampled area, LWC was calculated. LWC multiplied with LAI values (m^2 leaf/m^2 surface) provided CWC in g/m^2 of ground surface.

During the campaign (12th–14th of July), airborne hyperspectral HyMap flight-lines were acquired for the study site, obtaining the TOC reflectance value for each of the ESUs. HyMap is a hyperspectral sensor that spans the 430–2490 nm wavelength range with 125 usable bands. Spectral bandwidth varied between 11 and 21 nm and the pixel size at overpass was 5 m. The ESU TOC reflectance was computed as the mean value of the central pixel and all adjacent pixels. The images obtained were geometrically corrected (Alonso and Moreno, 2005) and then atmospherically corrected by the ATCOR4-r (Atmospheric and Topographic Correction – rugged terrain) method at the German Aerospace Center (DLR), according to Guanter et al. (2005).

The total field and airborne dataset consisted of 100 CWC values and their corresponding radiometric hyperspectral information, covering multiple crop types, i.e., 18 lucernes, 14 corns, 12 potatoes, 22 sugar beets, 14 garlics, 10 onions and 10 bare soils, in which LAI and CWC values were zero.

2.2. Analysis of generic vegetation indices

The systematic analysis of the predicted power of VIs was mainly conducted by using the Automated Radiative Transfer Models Operator (ARTMO) scientific software package (Verrelst et al., 2012). ARTMO consists of RTMs (e.g., PROSAIL) and several retrieval toolboxes that enable the development and optimization of retrieval algorithms to convert optical images into maps of vegetation properties. The spectral indices assessment toolbox (Rivera et al., 2014) was used to calibrate and validate established and generic indices by providing all the possible band combinations in the NIR region (750–1300 nm).

Based on established CWC indices in the literature, a series of VIs was introduced into the toolbox together with the multi-crop TOC reflectance data. The indices introduced in ARTMO were a series of generic indices, i.e. formulas in which the specific bands to be used are not defined, whose formulation was based on commonly used CWC indices (Table 2, in shading), among other VIs typically used to estimate various biophysical variables (mainly Chl).

The first analysis was to test with different types of fitting functions (linear, exponential and polynomial) the performance of commonly used CWC indices, with their specific bands as defined by the original authors, given the SPARC03 field TOC reflectance dataset acquired over a variety of crops.

Secondly, for each generic CWC index introduced (Table 2), all band combinations were analysed, resulting in a best performing combination of bands. Only the NIR region was evaluated because of its high sensitivity to mainly liquid water, whereas the signal from the SWIR region is additionally heavily influenced by cellulose (Delegido et al., 2015). A cross-validation method was used to ensure more robust results. To cross-validate each index with the SPARC03 dataset, the *k*-fold method was used (Snee, 1977; Yang and Huang, 2014). This method divides the available data into *k* subsets. From these *k* sub-datasets, *k*-1 sub-datasets are selected as a calibration dataset and a single *k* sub-dataset is used for model validation. The cross-validation process is then repeated *k* times, with each of the *k* sub-datasets used as a validation dataset. Thus, all data are used for both calibration and validation. Here, we used a 10-fold ($k = 10$) cross-validation procedure (Pérez-Planells et al., 2015; Verrelst et al., 2015b).

2.3. CWC spectral sensitivity analysis for real and simulated data

As mentioned above, water produces maximum absorptions features mainly at 970, 1200, 1450, 1940 and 2500 nm (Carter, 1991; Knipling, 1970; Tucker, 1980). These maximum absorptions can be observed for several crop types of the SPARC03 campaign with contrasting CWC (Fig. 1).

In Fig. 1 the maximum CWC-related absorptions in the NIR region, i.e. around 970 and 1200 nm, can be inspected. In these points, the depth of the spectrum (difference between the absorption minimums, 850 nm and 1080 nm, and the NIR shoulder) is maximized as the CWC increases. For this reason, the sugar beet spectrum (CWC = 2200 g/m^2) has the largest depth while the lucerne spectrum (CWC = 359 g/m^2) the smallest.

These water absorption maxima can also be observed when simulating vegetation reflectance with PROSAIL. In Fig. 2, two PROSAIL simulations are plotted where CWC is expressed as the water sheet thickness of the leaf (Cw, in cm). One spectrum (solid line) corresponds with a high CWC (Cw = 0.05 cm) and the other (dashed line) with a low CWC (Cw = 0.025 cm), both with LAI = 3. In addition, the atmospheric WV transmittance simulated with the atmospheric RTM MODTRAN (Berk et al., 2006) is shown (blue lines in Fig. 2).

Next, a spectral sensitivity analysis for varying CWC was conducted to inspect the spectral behaviour when water content is approaching zero, while varying LAI. In Fig. 3, TOC reflectance spectra were modelled for multiple LAI values ranging between 0.5 and 6 (in m^2 leaf/m^2 surface or without units) and three representative values of Cw: the minimum (0 cm), intermediate (0.025 cm) and maximum (0.05 cm) of the variable setting. The other model variables, maintained default values (Chl = 30 μg/cm^2; Dry matter = 0.012 g/cm^2).

Fig. 3 shows that for the simulations when Cw is zero, the TOC reflectance is characterized by a straight line without absorptions

Table 2
Generic vegetation indices introduced in ARTMO, where indices based on commonly CWC indices are shown shaded. Rλ represents reflectance at the wavelength λ (nm). The generic name of each index has been established in this study. Dash and Curran (2004), Gao (1996), Gitelson et al. (2002), Gower (1980), Hunt et al. (2013), Vincini et al. (2008), Zarco-Tejada and Ustin (2001).

Based reference	Formula	Generic name	Abbreviation	Generic formula
Hunt & Rock, 1989	$\frac{R_{1600}}{R_{820}}$	Ratio Generic Index	RGI	$\frac{R_1}{R_2}$
Peñuelas et al., 1997	$\frac{R_{900}}{R_{970}}$			
Zarco-Tejada & Ustin, 2001	$\frac{R_{860}}{R_{1240}}$			
Hardisky et al., 1983	$\frac{R_{820}-R_{1650}}{R_{820}+R_{1650}}$	Normalized Difference Water Generic Index	NDWGI	$\frac{R_1-R_2}{R_1+R_2}$
Gao, 1996	$\frac{R_{860}-R_{1240}}{R_{860}+R_{1240}}$			
Rollin & Milton, 1998	$\frac{R_{1116}-min(R_{1120},R_{1150})}{R_{1116}} \times 100$	Relative Depth Generic Index	RDGI	$\frac{R_1-R_2}{R_1} \times 100$
Wang & Qu, 2007	$\frac{R_{860}-(R_{1640}-R_{2130})}{R_{860}+(R_{1640}-R_{2130})}$	Normalized Multi-band Drought Generic Index	NMDGI	$\frac{R_1-(R_2-R_3)}{R_1+(R_2-R_3)}$
Vincini et al., 2008	$\frac{R_{500-590}+R_{610-680}}{R_{780-890}}$	Three Ratio Band Generic Index	TRBGI	$\frac{R_1+R_2}{R_3}$
Dash and Curran, 2004	$\frac{R_{753}-R_{708}}{R_{708}-R_{681}}$	Multi-band Simple Generic Ratio	MSGR	$\frac{R_1-R_3}{R_2-R_3}$
Gitelson et al., 2002 - le Maire et al., 2008	$\frac{R_{520-600}-R_{630-690}}{R_{520-600}+R_{630-690}-2R_{450-520}}$	Multi-band Normalized Generic Index	MNGI	$\frac{R_1-R_2}{R_1+R_2-2R_3}$
Hunt et al., 2013	$0.02(R_{670}-R_{550})+0.01(R_{670}-R_{480})$	Triangular Difference Generic Index	TDGI	$0.02(R_1-R_2)+0.01(R_2-R_3)$
Gower, 1980	$R_{676}-0.5(R_{746}+R_{665})$	Water Line Height Generic Index	WLHGI	$R_1-0.5(R_2+R_3)$

features between 800 nm and 1200 nm approximately. The slope and the magnitude of this reflectance line varies only as a function of LAI. This water absorption-free reference line between 800 and 1200 nm was subsequently used as a starting point to define a new index.

2.4. Development of the Water Absorption Area Index

Here, the so-called Water Absorption Area Index (WAAI), is proposed with the purpose of being generally applicable to a diversity of

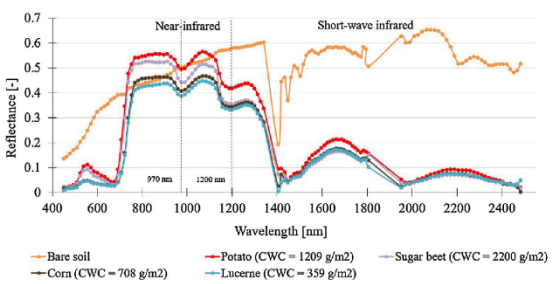

Fig. 1. Lucerne, corn, sugar beet and potato TOC spectra, with a bare soil spectrum of the field campaign SPARC03. CWC is expressed in g water/m^2 surface.

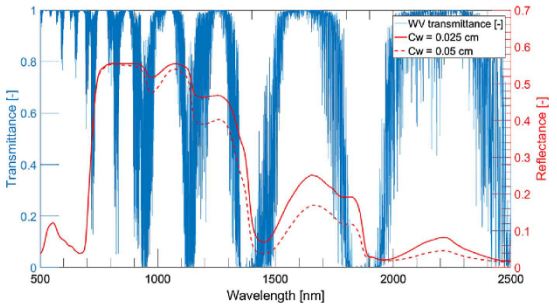

Fig. 2. Vegetation reflectance spectrum with more (solid line) and less (dashed line) CWC expressed as leaf water sheet thickness (Cw), LAI = 3, simulated with PROSAIL, together with atmospheric water vapour transmittance, simulated with MODTRAN (blue). (For interpretation of the references to colour in this figure legend, the reader is referred to the web version of this article.)

crop types. WAAI is based not only on the reflectance of a few bands, but instead on a wide spectral range with the purpose of minimizing estimation errors. The WAAI is defined as the difference between the area under the reference line (Cw = 0 cm) and the area under the curve, between the integration limits 800 nm and 1200 nm. The specific area covered by this index is shown in Fig. 4, with Cw the leaf water thickness in cm.

The first step to calculate WAAI, therefore, was to obtain the reference line. Fig. 5 shows R_{1200} as a function of R_{800} with Cw = 0 cm of PROSAIL simulations of varying LAI, in which a clearly linear relation ($R^2 = 1$) is observed.

The linear relationship contained in Fig. 5 together with the area under the line formed between 800 nm and 1200 nm (Eq. (1)) and the integral between these same limits (Eq. (2)) were required for defining the area index:

$$\text{Area under the reference line (Trapezium area)} = \frac{R_{800} + R_{1200}}{2}(1200 - 800) \quad (1)$$

$$\text{Area under curve} = \int_{800}^{1200} R(\lambda)d\lambda \quad (2)$$

where R_λ represents reflectance at the wavelength λ.

Thus, substituting the linear relationship ($R_{1200} = 0.857 * R_{800} + 0.097$) into Eq. (1) and subtracting (2) from Eq. (1), the Water Absorption Area Index is defined as:

$$WAAI = 200(1.857R_{800} + 0.097) - \int_{800}^{1200} R(\lambda)d\lambda \quad (3)$$

After the WAAI calculation, the optimal integration limits were determined. To do so, multiple spectral analyses were conducted on the SPARC03 dataset, i.e. by varying both integration limits within the NIR region (750–1300 nm) to observe the index response and to determine the spectral range that leads to the best correlation for estimating water content.

2.5. Development of the Depth Water Index

The WAAI is an area index essentially developed for high spectral resolution data, i.e. coming from hyperspectral imaging spectrometers. However, since hardly any of the currently operational satellite sensors are equipped with such a high spectral resolution the so-called Depth Water Index (DWI) is proposed as a possible guide for the configuration of future optical superspectral sensors. The DWI makes use of only four specific bands, providing the sum of the depth at 970 nm (d_1) and at 1200 nm (d_2), i.e., the difference between the corresponding reflectance at the baseline (y_i) and the TOC reflectance at 970 nm for d_1 and 1200 nm for d_2 (Fig. 6). The baseline y_i is formed from the TOC reflectance points at 850 nm and 1080 nm.

Therefore, the Depth Water Index presents the following general form:

$$DWI = (y_1 - R_{970}) + (y_2 - R_{1200}) \quad (4)$$

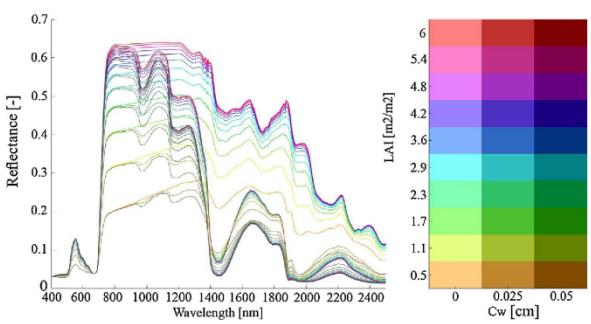

Fig. 3. TOC reflectance modelled by PROSAIL varying LAI and water content (Cw) variables.

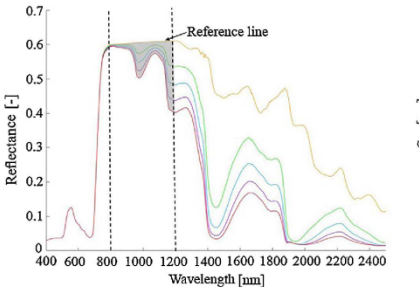

Fig. 4. TOC reflectance obtained with PROSAIL with different water content (Cw: leaf water thickness in cm), at a fixed LAI = 4.5, the shaded area corresponds with the area calculated by the WAAI.

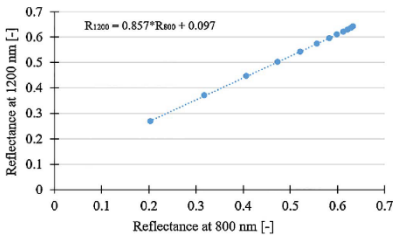

Fig. 5. Relationship between R_{800} and R_{1200} in vegetation spectra modelled, with Cw = 0 cm for LAI ranging from 0 to 6.

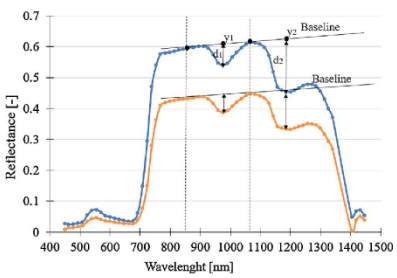

Fig. 6. Graphic representation of the DWI, which is the sum of the depths at 970 and at 1200 nm of the TOC reflectance, with respect to the baseline formed between the peaks at 850 and 1080 nm. The two spectra correspond to different CWC value (blue spectrum 459 g/m^2, orange spectrum 359 g/m^2). (For interpretation of the references to colour in this figure legend, the reader is referred to the web version of this article.)

Specifically, the baseline has the following form, from which y_i can be calculated for $x_i = 970$ and 1200 nm:

$$y_i = \frac{R_{1080} - R_{850}}{230} x_i + \frac{R_{1080} * 850 - R_{850} * 1080}{-230} \quad (5)$$

Consequently, substituting Eq. (5) into (4), the Depth Water Index equation is obtained:

$$DWI = 2.044R_{1080} - 0.044R_{850} - R_{970} - R_{1200} \quad (6)$$

Lastly, to analyse the statistical response of the WAAI and DWI, the coefficient of determination, R^2 (ranging from 0 to 1), is used.

3. Results

3.1. Performance of established CWC indices for a multi-crop dataset

The above-described established indices as given in Table 2 were evaluated with the multi-crop SPARC03 dataset. To start with, the established CWC indices have been tested with their default bands. The R^2 obtained with different types of fitting functions ranged between 0.114–0.598 when applying the respective indices on the multi-crop dataset (Table 3). Hence, the accuracies of each index obtained with linear, exponential and polynomial fitting were rather low. All three fitting functions performed similar, with the linear fitting performing slightly better than the exponential and polynomial fitting. Therefore, only linear fitting is used in further analysis.

In order to be more generic, the following step involved systematically calculating all bands combinations. Table 4 lists the best statistical results obtained for each of the generic indices and the corresponding bands with a linear fit.

Comparing to the afore-tested established indices, these results already show a more promising correlation with a R^2 ranging between 0.811 and 0.908. However, questions arose when evaluating the obtained wavelengths of the resulting best-performing bands from a physical point of view. In most cases, the selected bands were physically not only influenced by CWC, but also by other leaf constituents such as Chl pigments (e.g., 738 nm, 753 nm, etc.), while other bands were located in the NIR (e.g., 1272 nm, 927 nm, 943 nm) but not closely

Table 3
R^2 obtained with a linear, exponential and polynomial fitting for each index with their default bands.

Index	Formula	R^2 (linear fitting)	R^2 (exponential fitting)	R^2 (polynomial fitting)
RGI	$\frac{R_{1500}}{R_{820}}$	0.485	0.478	0.473
	$\frac{R_{900}}{R_{970}}$	0.576	0.565	0.542
	$\frac{R_{860}}{R_{1240}}$	0.598	0.592	0.584
NDWGI	$\frac{R_{820} - R_{1650}}{R_{820} + R_{1650}}$	0.556	0.551	0.564
	$\frac{R_{860} - R_{1240}}{R_{860} + R_{1240}}$	0.597	0.585	0.579
RDGI	$\frac{R_{1216} - \min(R_{1120}, R_{1150})}{R_{1114}} \times 100$	0.525	0.521	0.491
NMDGI	$\frac{R_{860} - (R_{1640} - R_{2130})}{R_{860} + (R_{1640} - R_{2130})}$	0.124	0.119	0.114

Table 4
Best combination of bands for each generic vegetation indices introduced in ARTMO, ordered from highest to lowest R^2, with a linear fitting.

Index	Bands	RMSE (g/m²)	NRMSE (%)	R^2
MNGI	1006;753;1113	210	10	0.908
TDGI	1022;829;738	220	11	0.895
WLHGI	1022;829;738	220	11	0.895
MSGR	1022;927;753	240	12	0.876
TRBGI	943;539;1272	230	11	0.876
NMDGI	1157;1006;753	250	12	0.867
RDGI	1272;738	270	13	0.825
RGI	738;1272	270	13	0.825
NDWGI	1006;943	290	14	0.811

located at the depth features 970 and 1200 nm. Consequently, the development of alternative multi-band indices with a stronger physically meaningful basis is needed.

3.2. Fitting and validation of the Water Absorption Area Index

As outlined in Eq. (3), the WAAI was defined as an integration index between the limits of 800 and 1200 nm. After multiple spectral analyses, the best regression result was achieved with the integration limits set at 911 nm and 1271 nm (R^2 of 0.808, RMSE = 290 g/m²), using Eq. (7), with an exponential fitting (Eq. (8)). This may be due to the fact that at 911 nm the first absorption peak begins and at 1271 nm the water content maximum influence ends. Fig. 7 shows the area index response between these values.

$$WAAI_{optimized} = 180(1.812R_{911} + 0.271) - \int_{911}^{1271} R(\lambda)d\lambda \quad (7)$$

$$CWC\,(g/m^2) = 42.98exp^{0.061\,WAAI_{optimized}} \quad (8)$$

This optimized WAAI led to a good correlation and at the same time is physically sound since the crop types with low CWC (garlic and lucerne) have minimum index values, and crop types with high CWC (sugar beet and potato) show maximum WAAI values. It should be mentioned that garlic usually has a high LWC, but because it also has low LAI (lower than 1), the derived CWC is consequently also low. Moreover, garlic has a scarce and dispersed coverage which translates into a low FVC. In the case of corn, the crop was planted late on the season and the plants were not fully grown at the time of measurements, it was in the swelling ear stage. Also, lucerne has a low CWC because it was in a bud stage and sparse with ray grass. On the other hand, potato and sugar beet crops typically have high CWC because these plants are usually leafy.

3.3. Fitting and validation of the Depth Water Index

The DWI, a four-bands index (Eq. (6)), was defined based on the hyperspectral WAAI with the purpose of being applicable to lower spectral resolution sensors. After fitting the DWI with the SPARC03 dataset, a good statistical behaviour, ($R^2 = 0.719$, RMSE = 400 g/m²) with an exponential fit was obtained:

$$CWC\,(g/m^2) = 113.9exp^{10.72DWI} \quad (9)$$

The DWI varies from −0.01, corresponding to bare soils, to a maximum of 0.26, in the case of sugar beet, in which CWC is high, around 2000 g/m² (Fig. 8). This index functions in a similar way than the WAAI, with sugar beet showing highest CWC values and, therefore, likewise expressing DWI values. By contrast, garlic leads to lowest CWC (344 g/m²) estimations given by its low FVC (12%) and low LAI (0.58 m² leaf/m² surface), despite having a high LWC (595 g/m²).

In order to demonstrate the validity of the four-bands DWI index for CWC estimation, DWI-estimated CWC values were plotted against the WAAI-estimated CWC values (Fig. 9). When comparing both CWC estimations, a R^2 of 0.85 is obtained. Although the WAAI index presents more accurate results because it uses information from a greater number of bands influenced by CWC, this result suggests that the four-bands DWI index closely approaches the original WAAI integration index, despite some over- and under-estimations.

Finally, we applied both indices to the 14th of July HyMap flight line as acquired over the Barrax region. The resulting maps are shown in Fig. 10. A visual inspection reveals that both indices estimate the CWC consistently with higher CWC values in the irrigated circular parcels. When observing the maps with more detail, the WAAI estimates CWC sometimes higher and sometimes lower than the DWI, depending on the crop type. Given that DWI is a simplification of WAAI and somewhat poorer validated, it can be reasonably assumed that the WAAI map displays CWC with a better accuracy.

4. Discussion

Established vegetation indices commonly used for CWC estimation are usually simple arithmetic formulations based on two spectral bands, i.e. a water content sensitive band and another control band that is not influenced by any variable. At the same time, these indices have been typically developed for a specific plant species. The challenge arose when we tried using these established indices in a general way for a multi-crop dataset, i.e. the SPARC03 dataset, because very low correlations (R^2 between 0.114 and 0.598) were obtained. In an attempt to improve estimations over this multi-crop dataset, all band combinations were systematically calculated for each index in order to achieve the highest possible correlation for the estimation of CWC. For the simple ratio index, the best combination of bands ($R^2 = 0.825$) was achieved with R_{738}/R_{1272}, and for the normalized index was $(R_{1006} - R_{943})/$

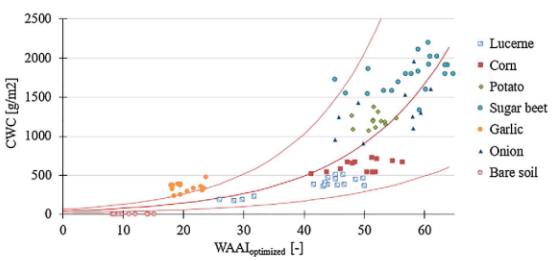

Fig. 7. CWC as a function of WAAI between the limits 911 and 1271 nm, with exponential fit and 95% of confidence interval.

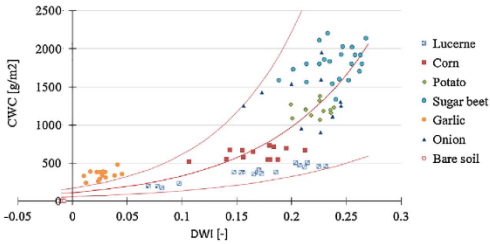

Fig. 8. CWC as a function of DWI, with exponential fit and 95% of confidence interval.

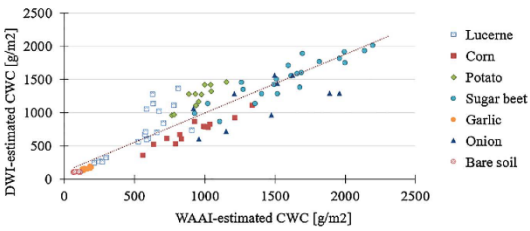

Fig. 9. CWC estimations, calculated with DWI and WAAI.

($R_{1006} + R_{943}$) with $R^2 = 0.811$. However, when inspecting these sensitive bands whether they are physically meaningful, i.e. if the selected bands are actually influenced only or mostly by water absorption features, then these indices turned out to be questionable. For instance, the band at 738 nm in the ratio index is mainly influenced by Chl content (Peng et al., 2017; Zarco-Tejada et al., 2004) and, thus, it cannot be used as a reference band. Also in the case of the normalized index, both bands (1006 nm and 943 nm) are influenced by water content, which potentially increases the level of error because there is no reference band to compare with.

At the field or landscape scale, canopy reflectance patterns represent the integrated effects of all biophysical parameters. Because at this scale most aircraft and satellite remote sensing instrument observations are made, interpreting the data can be challenging. Co-variation mechanisms of leaf constituents is typically causing the selection of bands related to other covarying biochemicals such as pigments, starch or lignin due to their high effect on spectral variability (Ollinger, 2011). Similarly, it was earlier observed that due to the covariation between water content and Chl content, typically bands in the Chl absorption region are selected as most sensitive (Van Wittenberghe et al., 2014).

It was shown that given a dataset of five common crop types (lucerne, corn, potato, sugar beet and onion) the two newly proposed indices, i.e. WAAI and DWI, estimate CWC with R^2 of 0.8 and 0.7, respectively, outperforming established indices in predicting CWC (Table 3) and being applicable to zones with different crop types (Fig. 10). When inspecting these indices more closely, there are some aspects that indicated that WAAI and DWI may be promising indices for CWC estimation. One aspect is that both have been designed in such a way that they are applicable to hyperspectral (WAAI) and multispectral

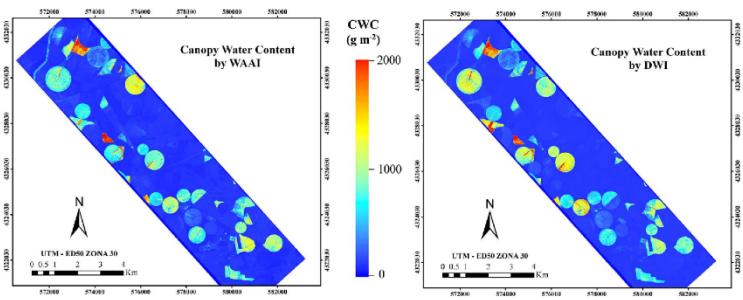

Fig. 10. CWC maps estimated with WAAI (left) and DWI (right) for the Barrax crop fields, using the 14th of July atmospherically corrected HyMap data.

(DWI) sensors. They are able to generate estimations closer to reality than established two-bands indices due to the greater number of bands located in the water absorption spectral regions. Results also suggested that the more bands influenced by CWC are used, the better correlation is obtained; the WAAI, an integration index that uses spectral information contained from 911 nm to 1271 nm, led to better results (R^2 of 0.808) than the four-bands DWI (R^2 = 0.719). However, another aspect to be remarked is that the performances of both WAAI and DWI are only optimal when there is presence of a minimal FVC; in our experience, typically higher than 30%. The role of bare soil is a common problem for the majority of VIs and is mostly apparent over the garlic fields, for which both indices do not provide adequate values. Garlic fields are characterized by an extremely low FVC, about 12% (Table 1). Earlier CWC studies already noted poor estimations for crop types where FVC values were very low due to the predominant role of soil reflectance (Zarco-Tejada et al., 2003). It is therefore not recommended to apply these indices for crop types with low FVC values, e.g. below 30%. Another limitation is that the CWC data is based on the LAI variable, which is actually an effective LAI with accumulation of errors, i.e. mainly the internal error of the LiCor LAI-2000 digital analyser and the human error in taking the measures. It is important to realize this when extrapolating these results to CWC estimation obtained with direct and destructive measures. Moreover, atmospheric correction is essential in VIs studies and especially for water indices because the observed TOC reflectance will be strongly influenced by atmospheric WV in the water absorbing regions (Goetz and Boardman, 1995). A precise removal of atmospheric effects to obtain good physical parameter retrievals by vegetation indices is therefore critical. Also, a widely applicable CWC index should not only work for multiple species with various structures and FVC, but also for temporal intra-species variability due to changing crop development stages. Since different crop development stages of multiple species were represented in the dataset, we have good assumptions that intra-species structural variability (and resulting biophysical changes) will also be better dealt by WAAI/DWI as opposed to simple VIs.

Finally, in order to avoid underestimating CWC in crops with scarce coverage, further work should focus on introducing a FVC-based adjustment in the newly proposed indices, as well to include data from other crop types in the analysis to confirm their generic validity. In addition, given that the DWI already leads to satisfactory estimations, when moving towards delivering CWC maps in a more operational framework, it would be interesting to configure operational optical superspectral sensors with the specific bands used in DWI. For instance, both indices can be applied to data of forthcoming imaging spectroscopy missions such as the German EnMAP–Environmental Mapping and Analysis Program (Guanter et al., 2015) and the Italian PRISMA–PRecursore IperSpettrale della Missione Applicativa (Candela et al., 2016).

5. Conclusions

Although numerous VIs have been proposed for the estimation of water content over various crop types, the problem found with these indices is that they show low estimation accuracies when applied to heterogeneous crop zones. Also, when systematically deducing the VIs best band combinations, the optimal bands produced a good correlation (R^2) but lacked physical meaning with water absorption. Hence, new indices are required that not only lead to accurate estimations but also are physically sound, and thus applicable to a great variety of crop types. Two new spectral indices were formulated capable of estimating canopy water content (CWC) over common crop types and therefore applicable to large spatial scales. The validity of these indices was based on a large multi-crop dataset (SPARC03), composed of field CWC and LAI values, as well as their corresponding hyperspectral TOC reflectance coming from a HyMap image. On the one hand, the WAAI was defined as the area between the line formed when the CWC is zero and the spectrum between the limits 911 and 1271 nm. On the other hand, DWI was formulated as a simpler and thus more applicable index to conventional sensors, which is based on the estimation of the spectral depths produced by the absorption of water at 970 and 1200 nm. Both WAAI and DWI improved the CWC estimations (R^2 = 0.8 and 0.7, respectively) compared to established indices, and are applicable to heterogeneous agricultural areas, given crop areas with sufficiently high FVC (> 30%). The validation of both indices proved good, with a RMSE of 290 and 400 g/m^2 for WAAI and DWI respectively, resulting in HyMap-generated maps over the Barrax agricultural area.

Acknowledgments

This work was supported by the pre-doctoral scholarship of the Generalitat Valenciana Vali+d (file number ACIF/2016/378). S.V.W. was funded by the European Union's H2020 Marie Skłodowska-Curie fellowship under the FLUOPHOT project (grant agreement 701815). J. V. was supported by the European Research Council (ERC) under the ERC-2017-STG SENTIFLEX project (grant agreement 755617). We thank the two reviewers for their valuable suggestions.

References

Alderfasi, A.A., Nielsen, D.C., 2001. Use of crop water stress index for monitoring water status and scheduling irrigation in wheat. Agric. Water Manag. 47, 69–75. http://dx.doi.org/10.1016/S0378-3774(00)00096-2.

Alonso, L., Moreno, J., 2005. Advances and limitations in a parametric geometric correction of CHRIS/PROBA data. Eur. Sp. Agency (Special Publ. ESA SP 7.13).

Berk, A., Anderson, G., Acharya, P., Bernstein, L., Muratov, L., Lee, J., Fox, M., Adler-Golden, S.; Chetwynd, J., Hoke, M., Lockwood, R., Gardner, J., Cooley, T., Borel, C., Lewis, P., Shettle, E., 2006. MODTRAN TM5: 2006 update.

Broge, N.H., Leblanc, E., 2000. Comparing prediction power and stability of broadband and hyperspectral vegetation indices for estimation of green leaf area index and canopy chlorophyll density. Remote Sens. Environ. 76, 156–172. http://dx.doi.org/10.1016/S0034-4257(00)00197-8.

Candela, L., Formaro, R., Guarini, R., Loizzo, R., Longo, F., Varacalli, G., 2016. The PRISMA mission. In: Int. Geosci. Remote Sens. Symp. 2016–November. pp. 253–256. http://dx.doi.org/10.1109/IGARSS.2016.7729057.

Carlson, J.D., Burgan, R.E., 2003. Review of users' needs in operational fire danger estimation: the Oklahoma example. Int. J. Remote Sens. 24, 1601–1620.

Carter, G.A., 1991. Primary and secondary effects of water content on the spectral reflectance of leaves. Am. J. Bot. 916–924.

Chuvieco, E., Cocero, D., Aguado, I., Palacios, A., Prado, E., 2004. Improving burning efficiency estimates through satellite assessment of fuel moisture content. J. Geophys. Res. Atmos. 109. http://dx.doi.org/10.1029/2003JD003467.

Clevers, J.G.P.W., Kooistra, L., Schaepman, M.E., 2010. Estimating canopy water content using hyperspectral remote sensing data. Int. J. Appl. Earth Obs. Geoinf. 12, 119–125. http://dx.doi.org/10.1016/j.jag.2010.01.007.

Colombo, R., Bellingeri, D., Fasolini, D., Marino, C.M., 2003. Retrieval of leaf area index in different vegetation types using high resolution satellite data. Remote Sens. Environ. 86, 120–131. http://dx.doi.org/10.1016/S0034-4257(03)00094-4.

Dash, J., Curran, P.J., 2004. The MERIS terrestrial chlorophyll index. Int. J. Remote Sens. 2523, 5403–5413. http://dx.doi.org/10.1080/01431160400274015.

Datt, B., 1999. Remote sensing of water content in eucalyptus leaves. Aust. J. Bot. 47, 909–923. http://dx.doi.org/10.1071/BT98042.

Delegido, J., Alonso, L., González, G., Moreno, J., 2010. Estimating chlorophyll content of crops from hyperspectral data using a normalized area over reflectance curve (NAOC). Int. J. Appl. Earth Obs. Geoinf. 12, 165–174. http://dx.doi.org/10.1016/j.jag.2010.02.003.

Delegido, J., Verrelst, J., Meza, C.M., Rivera, J.P., Alonso, L., Moreno, J., 2013. A red-edge spectral index for remote sensing estimation of green LAI over agroecosystems. Eur. J. Agron. 46, 42–52. http://dx.doi.org/10.1016/j.eja.2012.12.001.

Delegido, J., Verrelst, J., Rivera, J.P., Ruiz-Verdú, A., Moreno, J., 2015. Brown and green LAI mapping through spectral indices. Int. J. Appl. Earth Obs. Geoinf. 35, 350–358. http://dx.doi.org/10.1016/j.jag.2014.10.001.

Gandía, S., Fernández, G., García, J.C., Moreno, J., 2004. Retrieval of vegetation biophysical variables from CHRIS/PROBA data in the SPARC campaing. Eur. Sp. Agency (Special Publ. ESA SP 40–48).

Gao, B.-C., Goetz, A.F.H., 1990. Column atmospheric water vapor and vegetation liquid water retrievals from Airborne Imaging Spectrometer data. J. Geophys. Res. 95, 3549. http://dx.doi.org/10.1029/JD095iD04p03549.

Gao, B.C., 1996. NDWI – A normalized difference water index for remote sensing of vegetation liquid water from space. Remote Sens. Environ. 58, 257–266. http://dx.doi.org/10.1016/S0034-4257(96)00067-3.

Gitelson, A.A., Kaufman, Y.J., Stark, R., Rundquist, D., 2002. Novel algorithms for remote estimation of vegetation fraction. Remote Sens. Environ. 80, 76–87. http://dx.doi.org/10.1016/S0034-4257(01)00289-9.

Gitelson, A.A., Viña, A., Arkebauer, T.J., Rundquist, D.C., Keydan, G., Leavitt, B., 2003. Remote estimation of leaf area index and green leaf biomass in maize canopies. Geophys. Res. Lett. 30. http://dx.doi.org/10.1029/2002GL016450.

Gitelson, A.A., Viña, A., Ciganda, V., Rundquist, D.C., Arkebauer, T.J., 2005. Remote estimation of canopy chlorophyll content in crops. Geophys. Res. Lett. 32, 1–4.

http://dx.doi.org/10.1029/2005GL022688.
Glenn, E.P., Huete, A.R., Nagler, P.L., Nelson, S.G., 2008. Relationship between remotely-sensed vegetation indices, canopy attributes and plant physiological processes: what vegetation indices can and cannot tell us about the landscape. Sensors 8, 2136–2160. http://dx.doi.org/10.3390/s8042136.
Goetz, A.F., Boardman, J.W., 1995. Spectroscopic measurement of leaf water status. In: Geoscience and RemoteSensing Symposium. (IGARSS). pp. 978–980.
Gower, J.F.R., 1980. Observations of in situ fluorescence of chlorophyll-a in Saanich Inlet. Boundary-Layer Meteorol. 18, 235–245.
Guanter, L., Alonso, L., Moreno, J., Member, A., 2005. A method for the surface reflectance retrieval from PROBA/CHRIS data over land: application to ESA SPARC campaigns. IEEE Trans. Geosci. 43, 2908–2917.
Guanter, L., Kaufmann, H., Segl, K., Foerster, S., Rogass, C., Chabrillat, S., Kuester, T., Hollstein, A., Rossner, G., Chlebek, C., Straif, C., Fischer, S., Schrader, S., Storch, T., Heiden, U., Mueller, A., Bachmann, M., Mühle, H., Müller, R., Habermeyer, M., Ohndorf, A., Hill, J., Buddenbaum, H., Hostert, P., Van Der Linden, S., Leitão, P.J., Rabe, A., Doerffer, R., Krasemann, H., Xi, H., Mauser, W., Hank, T., Locherer, M., Rast, M., Staenz, K., Sang, B., 2015. The EnMAP spaceborne imaging spectroscopy mission for earth observation. Remote Sens. 7, 8830–8857. http://dx.doi.org/10.3390/rs70708830.
Haboudane, D., Miller, J.R., Tremblay, N., Zarco-Tejada, P.J., Dextraze, L., 2002. Integrated narrow-band vegetation indices for prediction of crop chlorophyll content for application to precision agriculture. Remote Sens. Environ. 81, 416–426. http://dx.doi.org/10.1016/S0034-4257(02)00018-4.
Hardisky, M., Klemas, V., Smart, R., 1983. The influence of soil salinity, growth form, and leaf moisture on the spectral radiance of Spartina alterniflora canopies. Photogramm. Eng. Remote Sens. 49, 77–83.
Hunt, E.R., Rock, B.N., 1989. Detection of changes in leaf water content using near- and middle-rnfrared reflectances. Remote Sens. Environ. 30, 43–54. http://dx.doi.org/10.1016/0034-4257(89)90046-1.
Hunt, E.R., Rock, B.N., Nobel, P.S., 1987. Measurement of leaf relative water content by infrared reflectance. Remote Sens. Environ. 22, 429–435. http://dx.doi.org/10.1016/0034-4257(87)90094-0.
Hunt, E.R., Doraiswamy, P.C., McMurtrey, J.E., Daughtry, C.S.T., Perry, E.M., Akhmedov, B., 2013. A visible band index for remote sensing leaf chlorophyll content at the Canopy scale. Int. J. Appl. Earth Obs. Geoinf. 21, 103–112. http://dx.doi.org/10.1016/j.jag.2012.07.020.
Inoue, Y., Morinaga, S., Shibayama, M., 1993. Non-destructive estimation of water status of intact crop leaves based on spectral reflectance measurements. Jpn. J. Crop Sci. 62, 462–469.
Jackson, T.J., Chen, D., Cosh, M., Li, F., Anderson, M., Walthall, C., Doriaswamy, P., Hunt, E.R., 2004. Vegetation water content mapping using Landsat data derived normalized difference water index for corn and soybeans. Remote Sens. Environ. 92, 475–482. http://dx.doi.org/10.1016/j.rse.2003.10.021.
Jackson, R.D., 1986. Remote sensing of biotic and abiotic plant stress. Annu. Rev. Phytopathol. 24, 265–287.
Jacquemoud, S., Baret, F., 1990. PROSPECT: a model of leaf optical properties spectra. Remote Sens. Environ. 34, 75–91. http://dx.doi.org/10.1016/0034-4257(90)90100-Z.
Jacquemoud, S., Ustin, S.L., Verdebout, J., Schmuck, G., Andreoli, G., Hosgood, B., 1996. Estimating leaf biochemistry using the PROSPECT leaf optical properties model. Remote Sens. Environ. 56, 194–202. http://dx.doi.org/10.1016/0034-4257(95)00238-3.
Jacquemoud, S., Verhoef, W., Baret, F., Bacour, C., Zarco-Tejada, P.J., Asner, G.P., François, C., Ustin, S.L., 2009. PROSPECT + SAIL models: a review of use for vegetation characterization. Remote Sens. Environ. 113, S56–S66. http://dx.doi.org/10.1016/j.rse.2008.01.026.
Kira, O., Nguy-Robertson, A.L., Arkebauer, T.J., Linker, R., Gitelson, A.A., 2016. Informative spectral bands for remote green LAI estimation in C3 and C4 crops. Agric. For. Meteorol. 218–219, 243–249. http://dx.doi.org/10.1016/j.agrformet.2015.12.064.
Knipling, E.B., 1970. Physical and physiological basis for the reflectance of visible and near-infrared radiation from vegetation. Remote Sens. Environ. 1, 155–159. http://dx.doi.org/10.1016/S0034-4257(70)80021-9.
Kumar, L., 2007. High-spectral resolution data for determining leaf water content in Eucalyptus species: leaf level experiments. Geocarto Int. 22, 3–16. http://dx.doi.org/10.1080/10106040701204396.
le Maire, G., François, C., Soudani, K., Berveiller, D., Pontailler, J.Y., Bréda, N., Genet, H., Davi, H., Dufrêne, E., 2008. Calibration and validation of hyperspectral indices for the estimation of broadleaved forest leaf chlorophyll content, leaf mass per area, leaf area index and leaf canopy biomass. Remote Sens. Environ. 112, 3846–3864. http://dx.doi.org/10.1016/j.rse.2008.06.005.
Malenovský, Z., Ufer, C., Lhotáková, Z., Clevers, J.G.P., Schaepman, M., Albrechtová, J., Cudlín, P., 2006. A new hyperspectral index for chlorophyll estimation of a forest canopy: area under curve normalised to maximal band depth between 650 and 725 nm. EARSeL eProc. 5, 161–172. http://dx.doi.org/10.5167/uzh-62112.
Mutanga, O.M.C., Skidmore, A.K., Kumar, L., Ferwerda, J., 2005. Estimating tropical pasture quality at canopy level using band depth analysis with continuum removal in the visible domain. Int. J. Remote Sens. 26, 1093–1108. http://dx.doi.org/10.1080/01431160512331326738.
Ollinger, S.V., 2011. Sources of variability in canopy reflectance and the convergent properties of plants. New Phytol. 189, 375–394. http://dx.doi.org/10.1111/j.1469-8137.2010.03536.x.
Oppelt, N., Mauser, W., 2004. Hyperspectral monitoring of physiological parameters of wheat during a vegetation period using AVIS data. Int. J. Remote Sens. 25, 145–159.
Pérez-Planells, L., Delegido, J., Rivera-Caicedo, J.P., Verrelst, J., 2015. Análisis de métodos de validación cruzada para la obtención robusta de parámetros biofísicos. Rev. Teledetec. 44, 55–65. http://dx.doi.org/10.4995/raet.2015.4153.
Peñuelas, J., Filella, I., Biel, C., Serrano, L., Savé, R., 1993. The reflectance at the 950–970 nm region as an indicator of plant water status. Int. J. Remote Sens. 14, 1887–1905. http://dx.doi.org/10.1080/01431169308954010.
Peñuelas, J., Pinol, J., Ogaya, R., Filella, I., 1997. Estimation of plant water concentration by the reflectance water index WI (R900/R970). Int. J. Remote Sens. 18, 2869–2875. http://dx.doi.org/10.1080/014311697217396.
Peng, Y., Nguy-Robertson, A., Arkebauer, T., Gitelson, A., 2017. Assessment of canopy chlorophyll content retrieval in maize and soybean: implications of hysteresis on the development of generic algorithms. Remote Sens. 9, 226. http://dx.doi.org/10.3390/rs9030226.
Pu, R., Ge, S., Kelly, N.M., Gong, P., 2003. Spectral absorption features as indicators of water status in coast live oak (Quercus agrifolia) leaves. Int. J. Remote Sens. 24, 1799–1810. http://dx.doi.org/10.1080/0143116021015596.
Riaño, D., Vaughan, P., Chuvieco, E., Zarco-Tejada, P.J., Ustin, S.L., 2005. Estimation of fuel moisture content by inversion of radiative transfer models to simulate equivalent water thickness and dry matter content: analysis at leaf and canopy level. IEEE Trans. Geosci. Remote Sens. 43, 819–826. http://dx.doi.org/10.1109/TGRS.2005.843316.
Rivera, J., Verrelst, J., Delegido, J., Veroustraete, F., Moreno, J., 2014. On the semi-automatic retrieval of biophysical parameters based on spectral index optimization. Remote Sens. 6, 4927–4951. http://dx.doi.org/10.3390/rs6064927.
Rollin, E.M., Milton, E.J., 1998. Processing of high spectral resolution reflectance data for the retrieval of canopy water content information. Remote Sens. Environ. 65, 86–92. http://dx.doi.org/10.1016/S0034-4257(98)00013-3.
Sabater, N., Vicent, J., Alonso, L., Verrest, J., Moreno, J., 2014. An atmospheric correction algorithm for the Flex/S3 tandem mission. 5th Int. Work. Remote Sens. Veg. Fluoresc. 3–8.
Snee, R., 1977. Validation and regression models: methods and examples. Technometrics 19, 415–428.
Stimson, H.C., Breshears, D.D., Ustin, S.L., Kefauver, S.C., 2005. Spectral sensing of foliar water conditions in two co-occurring conifer species: Pinus edulis and Juniperus monosperma. Remote Sens. Environ. 96, 108–118. http://dx.doi.org/10.1016/j.rse.2004.12.007.
Tucker, C.J., 1980. Remote sensing of leaf water content in the near infrared. Remote Sens. Environ. 10, 23–32. http://dx.doi.org/10.1016/0034-4257(80)90096-6.
Van Wittenberghe, S., Verrelst, J., Rivera, J.P., Alonso, L., Moreno, J., Samson, R., 2014. Gaussian processes retrieval of leaf parameters from a multi-species reflectance, absorbance and fluorescence dataset. J. Photochem. Photobiol. B Biol. 134, 37–48. http://dx.doi.org/10.1016/j.jphotobiol.2014.03.010.
Verhoef, W., 1984. Light scattering by leaf layers with application to canopy reflectance modeling: the SAIL model. Remote Sens. Environ. 16, 125–141. http://dx.doi.org/10.1016/0034-4257(84)90057-9.
Verrelst, J., Romijn, E., Kooistra, L., 2012. Mapping vegetation density in a heterogeneous river floodplain ecosystem using pointable CHRIS/PROBA data. Remote Sens. 4, 2866–2889. http://dx.doi.org/10.3390/rs4092866.
Verrelst, J., Camps-Valls, G., Muñoz-Marí, J., Rivera, J.P., Veroustraete, F., Clevers, J.G.P.W., Moreno, J., 2015a. Optical remote sensing and the retrieval of terrestrial vegetation bio-geophysical properties – A review. ISPRS J. Photogramm. Remote Sens. 108, 273–290. http://dx.doi.org/10.1016/j.isprsjprs.2015.05.005.
Verrelst, J., Rivera, J.P., Veroustraete, F., Muñoz-Marí, J., Clevers, J.G.P.W., Camps-Valls, G., Moreno, J., 2015b. Experimental Sentinel-2 LAI estimation using parametric, non-parametric and physical retrieval methods – A comparison. ISPRS J. Photogramm. Remote Sens. 108, 260–272. http://dx.doi.org/10.1016/j.isprsjprs.2015.04.013.
Verrelst, J., Rivera, J.P., Gitelson, A., Delegido, J., Moreno, J., Camps-Valls, G., 2016. Spectral band selection for vegetation properties retrieval using Gaussian processes regression. Int. J. Appl. Earth Obs. Geoinf. 52, 554–567. http://dx.doi.org/10.1016/j.jag.2016.07.016.
Vicent, J., Sabater, N., Tenjo, C., Delegido, J., Pe, R., 2015. Hico L1 and L2 data processing: radiometric recalibration, atmospheric correction and retrieval of water quality parameters. Geosci. Remote Sens. 102–105.
Vicent, J., Sabater, N., Verrelst, J., Alonso, L., Moreno, J., 2017. Assessment of approximations in aerosol optical properties and vertical distribution into FLEX atmospherically-corrected surface reflectance and retrieved sun-Induced fluorescence. Remote Sens. 9, 675. http://dx.doi.org/10.3390/rs9070675.
Vincini, M., Frazzi, E., D'Alessio, P., 2008. A broad-band leaf chlorophyll vegetation index at the canopy scale. Precis. Agric. 9, 303–319. http://dx.doi.org/10.1007/s11119-008-9075-z.
Wang, L., Qu, J., 2007. NMDI: a normalized multi-band drought index for monitoring soil and vegetation moisture with satellite remote sensing. Geophys. Res. Lett. 34. http://dx.doi.org/10.1029/2007GL031021.
Welles, J.M., Norman, J.M., 1991. Instrument for indirect measurement of canopy architecture. Agron. J. 83, 818–825.
Yang, Y., Huang, S., 2014. Suitability of five cross validation methods for performance evaluation of nonlinear mixed-effects forest models–a case study. Forestry 87, 654–662. http://dx.doi.org/10.1093/forestry/cpu025.
Zarco-Tejada, P.J., Ustin, S.L., 2001. Modeling canopy water content for carbon estimates from MODIS data at land EOS validation sites. IGARSS 2001. Scanning Present Resolv. Futur. Proceedings. IEEE 2001 Int. Geosci. Remote Sens. Symp. (Cat. No.01CH37217) 1, 342–344. http://dx.doi.org/10.1109/IGARSS.2001.976152.
Zarco-Tejada, P.J., Rueda, C.A., Ustin, S.L., 2003. Water content estimation in vegetation with MODIS reflectance data and model inversion methods. Remote Sens. Environ. 85, 109–124. http://dx.doi.org/10.1016/S0034-4257(02)00197-9.
Zarco-Tejada, P.J., Miller, J.R., Morales, A., Berjón, A., Agüera, J., 2004. Hyperspectral indices and model simulation for chlorophyll estimation in open-canopy tree crops. Remote Sens. Environ. 90, 463–476. http://dx.doi.org/10.1016/j.rse.2004.01.017.
Zhang, J., Xu, Y., Yao, F., Wang, P., Guo, W., Li, L., Yang, L., 2010. Advances in estimation methods of vegetation water content based on optical remote sensing techniques. Sci. China Technol. Sci. 53, 1159–1167. http://dx.doi.org/10.1007/s11431-010-0131-3.

ARTÍCULO 2

"Multi-crop green LAI estimation with a new simple Sentinel-2 LAI Index (SeLI)"

This article was published in "Sensors" in 2019. This journal had in 2018 an impact factor of 3.031 and the position of 15/61 (Q1) in Instruments & Instrumentation category.

sensors

MDPI

Article

Multi-Crop Green LAI Estimation with a New Simple Sentinel-2 LAI Index (SeLI)

Nieves Pasqualotto [1,*], Jesús Delegido [1], Shari Van Wittenberghe [1], Michele Rinaldi [2] and José Moreno [1]

[1] Image Processing Laboratory (IPL), University of Valencia, 46980 Valencia, Spain; jesus.delegido@uv.es (J.D.); shari.wittenberghe@uv.es (S.V.W.); jose.moreno@uv.es (J.M.)

[2] Council for Agricultural Research and Economics—Research Centre for Cereal and Industrial Crops, S.S. 673 km 25, 200, 71122 Foggia, Italy; michele.rinaldi@crea.gov.it

* Correspondence: m.nieve.pasqualotto@uv.es; Tel.: +34-963-544-068

Received: 14 January 2019; Accepted: 18 February 2019; Published: 21 February 2019

check for updates

Abstract: The spatial quantification of green leaf area index (LAI_{green}), the total green photosynthetically active leaf area per ground area, is a crucial biophysical variable for agroecosystem monitoring. The Sentinel-2 mission is with (1) a temporal resolution lower than a week, (2) a spatial resolution of up to 10 m, and (3) narrow bands in the red and red-edge region, a highly promising mission for agricultural monitoring. The aim of this work is to define an easy implementable LAI_{green} index for the Sentinel-2 mission. Two large and independent multi-crop datasets of in situ collected LAI_{green} measurements were used. Commonly used LAI_{green} indices applied on the Sentinel-2 10 m × 10 m pixel resulted in a validation R^2 lower than 0.6. By calculating all Sentinel-2 band combinations to identify high correlation and physical basis with LAI_{green}, the new Sentinel-2 LAI_{green} Index (SeLI) was defined. SeLI is a normalized index that uses the 705 nm and 865 nm centered bands, exploiting the red-edge region for low-saturating absorption sensitivity to photosynthetic vegetation. A R^2 of 0.708 (root mean squared error (RMSE) = 0.67) and a R^2 of 0.732 (RMSE = 0.69) were obtained with a linear fitting for the calibration and validation datasets, respectively, outperforming established indices. Sentinel-2 LAI_{green} maps are presented.

Keywords: crops; leaf area index; vegetation indices; remote sensing; Sentinel-2; red-edge

1. Introduction

Leaf area index (LAI), or the total one-sided leaf area per unit of ground area (m^2 leaf per m^2 surface or dimensionless), can be distinguished in two types. On the one hand, there is the green leaf area index (LAI_{green}), representing the leaves which are photosynthetically active, being the most common type of LAI [1], and, on the other hand, there is the brown leaf area index (LAI_{brown}), representing the leaf area normalized which is senescent and losing photosynthetic function [2]. The Sentinel-2 mission from the European Space Agency (ESA) has, with the improved optical sensor bands in the red-edge, an increased sensitivity towards LAI_{green} [2], while the shortwave infrared bands are sensitive to cellulose and lignin (dry matter) absorption [2]. Such improved capabilities to obtain more accurate quantifications of LAI_{green} over large areas provides an important aspect in climatic [3], ecological [4] and biogeochemical [5] cycles models, as well as for estimating crop vegetation status [6], developing soil maps [7] and estimating light-use efficiency [8]. Its determination is crucial for the understanding of biophysical processes of crop canopies, being the main morphological parameter used for determining crop growth through the correlation with crop productivity [1,9,10]. In the context of agricultural monitoring, there is a strong interest in estimate LAI_{green} parameter. Near real-time LAI_{green} estimates provides the tool for farmers to obtain the crop health and growth

status, further improving the effective technical support in farming practices such as fertilizer application and water management. In this way, increased crop yields and reduced costs and input resources for the agricultural sector are envisaged [11,12]. Remote sensing from satellite, aerial and unmanned aerial vehicle platforms has become a popular technique in monitoring crop LAI_{green} because of its ability to acquire synoptic information at different times and spatial scales [13–15]. For agricultural monitoring by remote sensing, the spatial resolution should be at least 20 m and, preferably, 10 m in order to make site-specific management possible [16]. A temporal resolution of less than a week would be required to follow-up acute changes in crop condition and provide timely response in management practices. These requirements are fulfilled by the ESA's Sentinel-2 mission, providing 10 m pixel size products with a 10-day temporal resolution. Sentinel-2 is a polar-orbiting, superspectral high-resolution imaging mission with twin polar-orbiting satellites, Sentinel-2A and 2B. The mission's main objective is providing quality information for agricultural and forestry practices and, hence, helping manage food security [17]. With Sentinel-2A in orbit (launched 23 June 2015), the temporal resolution was not yet sufficient for real applications at the individual farmer's level. But with the additional availability of data from Sentinel-2B (launched 7 March 2017) the revisit period goes down to five days under cloud-free conditions.

LAI_{green} is functionally linked to the canopy spectral reflectance, so its retrieval from optical remote-sensing data has prompted many studies using various techniques [18,19]. Essentially, these retrieval techniques can be classified into two groups, i.e., (1) empirical retrieval methods, which typically consist of relating the biophysical parameter of interest against spectral data through linear (e.g., vegetation indices) or nonlinear (e.g., machine learning approaches) regression techniques [20–23] and (2) physically-based retrieval methods, which refers to inversion of radiative transfer models (RTMs) against remote sensing observations [24–26]. Concerning physical models, experimental studies using RTMs have shown great flexibility in retrieving plant cover variables, because of being able to parameterize these models to a wide range of land cover situations and sensor configurations [27,28]. However, two main drawbacks limit the use of the inversion of RTMs for operational applications. First, RTM approaches typically require some ancillary information to enable the parameterization of the physical model, which may not always be available [13,29]. An additional problem hereby is that if uncertainties are introduced the likelihood increases that the model inversion will not lead to a unique solution and extra steps are required to overcome the ill-posed problem [30]. Second, regardless of the availability of auxiliary data, there is the intrinsic risk of oversimplifying the architecture of canopy for those RTMs fast enough for operational applications. The difficulty in describing canopy structure increases in heterogeneous scenes, such as mosaics of crops at different phenological stages or complex mixtures of woodlands and/or grasslands [2,31,32]. Non-linear regression techniques are standardly used for operational LAI products. For Sentinel-2 an operational LAI product, associated with a quality indicator, is provided through the SNAP (Sentinel Application Platform) toolbox and produced through a neural network which has been trained by simulated spectra generated from well-known RTMs [33]. The algorithm is trained with simulated LAI_{green} values generated from the SAIL radiative transfer model [34], which describes the canopy as a homogenous and horizontal turbid-medium, and the PROSPECT radiative transfer model [35], which considers the leaf as a succession of absorption layers. However, the accuracy of this product is shown improvable [36]. Other machine learning algorithms than neural networks have been proposed to study the retrieval opportunities of LAI from Sentinel-2 and -3 [37], solving the black box problem. However, although machine learning approaches can be fast and can capture the non-linear relationship between different parameters, they are time variant and location dependent [38].

Alternatively, linear empirical models, i.e., vegetation indices (VIs), are one of the most straightforward implementable method in an operational data processing chain. These indices relate a few spectral bands with the biophysical parameter of interest [39] in a way that enhances the spectral characteristics of a given vegetation property while minimizing the soil, atmospheric, and sun-target-sensor geometry effects [22]. Despite the positive aspects of VIs developed for LAI

retrieval, their major weakness is the lack of a generally applicable index for multiple vegetation types. The best way to find efficient and robust indices is to use large and diverse field datasets, with a large variety of canopy structures [22,40]. Early studies identified the red and near-infrared (NIR) regions as sensitive to LAI_{green}, resulting in the common use of the reflectance broad-bands in these regions through simple ratios [41] or normalized difference ratios [42,43]. It should be mentioned that while these indices were found to be sensitive to low LAI_{green} values, they usually lose sensitivity as LAI_{green} increases (typically above 2–3 according to Haboudane et al. [19]). This saturation of the reflectance at moderate to high LAI_{green} values in the red range (600–700 nm) is due to the high chlorophyll absorption in this spectral range [9]. The wavelength region located in the visible–near infrared (VIS-NIR) transition, i.e., between 690 and 750 nm, generally referred as the "red-edge", is the region between maximum chlorophyll absorption in the red, and maximum reflection (high scattering) in the NIR caused by leaf cellular structure abundance, i.e., LAI [44–46]. Reflectance in the red-edge transition region is much higher than in the visible range especially for these moderate to high LAI_{green} values, where the upwelling radiance in the red-edge range provides a higher and less noisy signal compared to the low values in the red region. It has been specifically demonstrated, through real [47,48] and simulated spectral data [42,46], that the shape of the red-edge region and mainly the slope is strongly influenced by chlorophyll density and, hence, by LAI_{green}. Despite this well-known sensitivity, practically no established indices use the red-edge region for the LAI_{green} retrieval as until now no free operational satellites had narrow-bands in this region. With the Sentinel-2 satellites (13 spectral bands) not only optimal and temporal resolution for crop monitoring is guaranteed, but, moreover, also spectral configuration in the red-edge is improved, with narrow-bands centred at 705 nm (B5) and 740 nm (B6). Recent studies have explored the potential of Sentinel-2 for the LAI_{green} retrieval based on simulated datasets [49,50]. But at this moment, few studies have used real Sentinel-2 images in combination with in situ datasets for agricultural applications. Moreover, these studies using the red-edge Sentinel-2 bands for LAI_{green} retrieval, calibrated and validated their products for only a few crop types [51,52], leaving the robustness of a generic retrieval application still an open issue.

In this respect, we aim to develop a simple, accurate empirical algorithm for deriving LAI_{green} from Sentinel-2 real data of multi-crop agricultural fields, using two large in situ field datasets. The first objective is to determine if the commonly used VIs for estimating LAI_{green} may be applicable for a variety of crop types. Secondly, we want to identify the Sentinel-2 spectral bands that present the highest correlation for the estimation of a wide variation in crop LAI_{green}. Based on this analysis and on a parallel study of the importance of the new Sentinel-2 red-edge bands, a new robust LAI_{green} index is defined. The performance of the new index and established VIs indices are validated and applied over two distinct agricultural test sites.

2. Materials and Methods

2.1. Study Sites

Field data was collected at two study sites in the Mediterranean region (Figure 1). The first site located in Valencia (Spain), named Huerta of Valencia, is an area in an alluvial plain between the Turia river, the Mediterranean Sea and Albufera lake, with an approximate area of 12,000 hectares. The climate is typically Mediterranean with mild, wet winters and hot dry summers, and a yearly average temperature around 18 °C. Seasonal rainfall is minimal in summer and maximal in autumn and spring, with an average annual value of 454 mm [53]. A complex historical irrigation system based on irrigation ditches brings water to this fertile soil in which cereals, vineyards and olive trees were originally the main crops and nowadays accompanied by rice, tigernut and new species of vegetables and citric orchards. All these crop types are currently cultivated in small plots of size 40–100 m. For this study, crop fields were measured in the Burjassot, Moncada and Alboraya municipalities (study site central coordinates 39°31'11.73" N, 0°23'20.48" W, 18 m above sea level, Datum WGS84).

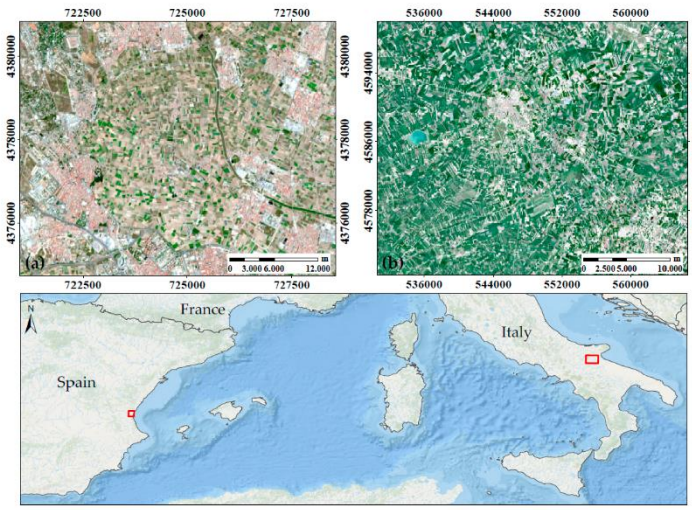

Figure 1. Test site locations. **(a)** Valencia (Spain) from the Sentinel-2 image of 6 April 2017, UTM-WGS84 Zone 30S **(b)** Foggia (Italy) from the Sentinel-2 image of 8 April 2017, UTM-WGS84 Zone 33T.

The second test site is an Italian agricultural area located near Foggia (study site central coordinates 41°27′36.76″ N, 15°32′45.33″ E, 70 m a.s.l., Datum WGS84). The climate is Mediterranean, but with a marked continental influence being 30 km distant from the coast. This promotes abrupt seasonal and daily temperature changes, sometimes as high as 20 °C. The average annual temperature is 15.8 °C but summers can be very hot and dry, with temperatures easily exceeding 35 °C, and winters with temperatures close to 0 °C. Rainfall is usually between 350 mm and 700 mm (average 469 mm), occurring mainly during autumn and winter [54]. The agricultural sector is the mainstay of Foggia's economy, where grapefruit, olives, durum wheat and tomato are the majority crops for centuries. The industries present are mostly devoted to food processing, with tomato processing the major industry branch.

2.2. Green Leaf Area Index (LAI_{green}) Datasets

At each study site, a large LAI_{green} dataset was collected with the LAI-2200 Plant Canopy Analyzer [55], which uses a fish-eyes lens with a hemispheric field of view (±45°). The detector is composed of five concentric rings (sensitive to radiation below 490 nm). Each ring responds over a different range of zenith angles and radiation is, thus, azimuthally integrated. The measurements were collected in one sensor mode using a 180° view cap, in clear sky condition, to avoid interferences from a user's shadow, following the Land European Remote-Sensing Instruments (VALERI) field protocol (http://w3.avignon.inra.fr/valeri/). The VALERI protocol is a sampling strategy corresponding to high spatial-resolution satellite imagery, choosing elementary sampling units (ESUs) of 20 m × 20 m for each measuring plot. Each ESU was chosen in the middle of the crop field which had minimum dimensions of 40 m × 40 m in Valencia and 100 m × 100 m in Foggia. A minimum distance of 20 m from the edges of the field was kept. To account for the spatial LAI_{green} variability within each ESU, measuring points were sampled following a square spatial sampling with 5 measurements at each

point (A, B, C, D and E), providing a statistically mean LAI_{green} estimate per ESU (Figure 2). The centre of the ESU (sampling point A) was geo-located using a GPS providing an accuracy of less than 5 m for later matching the mean LAI_{green} estimate with the corresponding Sentinel-2 reflectance data. The field protocol was identic for both study sites.

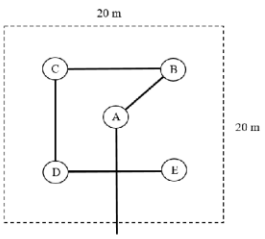

Figure 2. Sampling approach for each elementary sampling unit (ESU).

The field dataset collected in Valencia (Figure 1a), hereafter called "VLC17_ES", consists of 79 average LAI_{green} values for the respective ESUs sampled on 22 and 23 May; 18 and 19 July; and 8 and 9 November 2017. Several dates throughout the season were selected to cover a wider variety of growth stages. In total, LAI_{green} data from 79 ESUs were taken containing orange tree (*Citrus x sinensis*), collard (*Brassica oleracea*), tigernut (*Cyperus esculentus*), potato (*Solanum tuberosum*), artichoke (*Cynara scolymus*), squash (*Cucurbita pepo*), alfalfa (*Medicago sativa*), broad bean (*Vicia faba*), watermelon (*Citrullus lanatus*), pumpkin (*Cucurbita maxima*), onion (*Allium cepa*), celery (*Apium graveolens*) and lettuce (*Lactuca sativa*). The number of ESUs, classified by LAI_{green} value range, is given in the corresponding histogram of the VLC17_ES dataset (Figure 3a). Furthermore, 13 bare soil ESUs were included ($LAI_{green} = 0$), with the aim to create a more robust and general method.

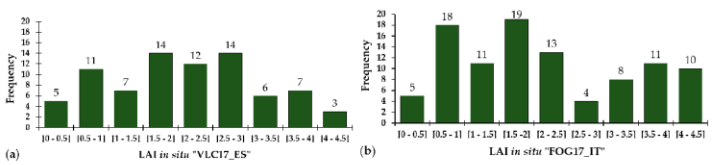

Figure 3. ESUs frequency histogram classified for LAI_{green} value range, for (**a**) the VLC17_ES testing dataset and (**b**) the FOG17_IT validation dataset. Bare soil ESUs are not included.

The field dataset collected in Foggia (Figure 1b), hereafter called "FOG17_IT", was taken in the framework of the H2020 SENSAGRI (Sentinels Synergy for Agriculture, http://sensagri.eu/) project. This dataset consists of 99 average LAI_{green} values collected on the 16, 21, 22 and 29 March; 5 and 13 April; 11, 17 and 30 May; 12, 15 and 21 June 2017. Mean LAI_{green} data of durum wheat (*Triticum durum*), tomato (*Solanum lycopersicum*) and horse bean (*Vicia faba*) ESUs were measured, with the number of ESU's specified in the histogram of Foggia test site (Figure 3b). In addition, 10 bare soil ESUs were included.

The two standard and independently collected field datasets VLC17_ES (n = 79) and FOG17_IT (n = 99) were, respectively, used as testing and validation dataset for the LAI_{green} index testing and development. Both datasets are covering a wide range of crop LAI values, i.e., from 0 to 4.5, providing an optimal experimental dataset for the definition of a new general methodology.

2.3. Sentinel-2 Imagery and Sentinel Application Platform (SNAP) LAI Product

All field campaigns were carried out on days close, with a maximum of five days' difference, to overpass dates of Sentinel-2 over the study area. Each Sentinel-2 satellite carries a Multi-Spectral Imager (MSI) instrument/sensor with a swath of 290 km on board. The MSI provides a versatile set of 13 spectral bands spanning from the visible and NIR to the shortwave infrared (SWIR) (443–2190 nm), featuring four bands at 10 m (VIS and NIR bands), six bands at 20 m (red-edge and SWIR) and three bands at 60 m spatial resolution for atmospheric correction (Table 1).

Table 1. Sentinel-2 bands setting.

Band Number	Function	Central Wavelength (nm)	Bandwidth (nm)	Spatial Resolution (m)
1	Coastal aerosol	443	27	60
2	Blue	490	98	10
3	Green	560	45	10
4	Red	665	38	10
5	Vegetation red-edge	705	19	20
6	Vegetation red-edge	740	18	20
7	Vegetation red-edge	783	28	20
8	Near infrared (NIR)	842	145	10
8a	Vegetation red-edge	865	33	20
9	Water vapour	945	26	60
10	Shortwave infrared (SWIR)-cirrus	1380	75	60
11	SWIR	1610	143	20
12	SWIR	2190	242	20

The images were downloaded directly and free of charge from the ESA server (https://scihub.copernicus.eu/). ESA provides Level-1C images, being geometrically corrected [56], with top-of-atmosphere (TOA) reflectance; and Level-2A images, being geometrically and atmospherically corrected, with top-of-canopy (TOC) reflectance. We downloaded 11 available cloud-free Level-1C acquisitions of Sentinel-2 over Valencia and Foggia study areas (Table 2). In addition, we used the SNAP toolbox to process these Level-1C images into Level-2A data, with the retrieval of the LAI_{green} product accompanied by a product quality indicator [33].

Table 2. Sentinel-2 images used in each field campaign.

Location	Field Work Date (2017 year)	Sentinel-2 Image Code
Valencia	22 and 23 May	S2A_MSIL1C_20170526T105031_N0205_R051_T30SYJ_20170526T105518
	18 and 19 July	S2A_MSIL1C_20170720T105029_N0205_R051_T30SYJ_20170720T105641
	8 and 9 November	S2A_MSIL1C_20171107T105229_N0206_R051_T30SYJ_20171107T131035
Foggia	16 March	S2A_MSIL1C_20170319T095021_N0204_R079_T33TWF_20170319T095021
	21 and 22 March	S2A_MSIL1C_20170319T095021_N0204_R079_T33TWG_20170319T095021
	29 March	S2A_MSIL1C_20170329T095021_N0204_R079_T33TWF_20170329T095024
	5 and 13 April	S2A_MSIL1C_20170408T095031_N0204_R079_T33TWF_20170408T095711
	11 and 17 May	S2A_MSIL1C_20170518T095031_N0205_R079_T33TWF_20170518T095716
	3 May	S2A_MSIL1C_20170528T095031_N0205_R079_T33TWF_20170528T095531
	12 June	S2A_MSIL1C_20170607T095031_N0205_R079_T33TWF_20170607T095031
	15 and 21 June	S2A_MSIL1C_20170617T095031_N0205_R079_T33TWF_20170617T095546

For each ESU the TOA reflectance spectrum was obtained from the central pixel of the corresponding plot of the Sentinel-2 image. These images were atmospherically corrected using the Sen2Cor procedure available in the Sentinel-2 SNAP toolbox, converting TOA reflectance into TOC reflectance [57]. The Sentinel images were resampled to 10 m pixel size with all selected pixels falling entirely inside the corresponding ESU. Subsetting was done to reduce the image size and the processing time, and to cover only the study areas.

2.4. Established Vegetation Indices Analysis

The performance of commonly used LAI_{green} indices was tested (Table 3, indices shaded), with the specific bands as defined by the original authors. The accuracies of each index was specifically analyzed with linear ($f(x) = ax + b$), polynomial of second order ($f(x) = ax^2 + bx + c$), exponential ($f(x) = a \times \exp(bx)$) and exponential of second order fitting ($f(x) = a \times \exp(bx) + c \times \exp(dx)$). Additionally, we introduced several generic index formulations, i.e., with undefined specific bands, into a Matlab-based graphical user interface toolbox called ARTMO (Automated Radiative Transfer Models Operator) [58]. ARTMO consists of multiple RTMs and several retrieval toolboxes that enable the development and optimization of retrieval algorithms to convert optical images into maps of vegetation properties. The indices formulation introduced in ARTMO was based on commonly used LAI_{green} indices, among other VIs typically used to estimate various biophysical variables such as chlorophyll (Table 3, non-shaded indices). The spectral indices assessment toolbox [59] was used to calibrate and validate generic indices, i.e., looking for those wavelengths that provide the best correlation with LAI_{green}, using the VLC17_ES testing dataset. A cross-validation method with the k-fold technique was used to ensure more robust results [60]. This method divides the available data into k subsets. From these k sub-datasets, k-1 sub-datasets are selected as a calibration dataset and a single k sub-dataset is used for model validation. The cross-validation process is then repeated k times, with each of the k sub-datasets used as validation dataset. Thus, all VLC17_ES field data are used for both calibration and validation. Here, we used a 4-fold (k = 4) cross-validation procedure.

Table 3. Generic vegetation indices introduced in Automated Radiative Transfer Models Operator (ARTMO), where indices based on commonly LAI_{green} indices are shown shaded and typically indices used to estimate other biophysical parameters are shown non-shaded. R_λ represents reflectance at the wavelength λ. The generic name of each index has been established in this study.

Based Reference	Formula	Generic Name	Abbreviation	Generic Formula
[41]	$\frac{R_{800}}{R_{635}}$	Ratio Index	RI	$\frac{R_1}{R_2}$
[43]	$\frac{R_{800}-R_{670}}{R_{800}+R_{670}}$	Normalized Difference Generic Index	NDGI	$\frac{R_1-R_2}{R_1+R_2}$
[42]	$\frac{R_{704}-R_{668}}{R_{704}+R_{668}}$			
[61]	$\frac{R_{520-600}+R_{670-690}}{R_{760-800}}$	Three Ratio Band Index	TRBI	$\frac{R_1+R_2}{R_3}$
[62]	$\frac{R_{680}-R_{500}}{R_{790}}$	Three Difference Band Index	TDBI	$\frac{R_1-R_2}{R_3}$
[63]	$\frac{R_{753}-R_{733}}{R_{733}-R_{673}}$	MERIS Terrestrial Generic Index Normalized Difference 3 band	MTGI ND3b	$\frac{R_1-R_2}{R_2-R_3}$ $\frac{R_1-R_2}{R_2+R_3}$
[64]	$\frac{R_{753}-R_{705}}{R_{705}+R_{705}-2R_{445}}$	Multi-band Normalized Index	MNI	$\frac{R_1-R_2}{R_1+R_2-R_3}$
[65]	$\frac{R_{800}-R_{670}}{R_{800}+R_{670}-R_{490}}$			
[66]	$R_{676}-0.5(R_{746}+R_{665})$	Generic Line Height	GLH	$R_1-0.5(R_2+R_3)$
[67]	$0.5[120(R_{750}-R_{550})-200(R_{670}-R_{550})]$	Triangular Generic Index	TGI	$0.5[120(R_1-R_2)-200(R_3-R_2)]$
[68]	$\lvert(R_{700}-R_{670})-0.2(R_{700}-R_{550})\rvert(R_{700}/R_{670})$	Modified Chlorophyll Generic Index	MCGI	$\lvert(R_1-R_2)-0.2(R_1-R_3)\rvert(R_1/R_2)$

The selection of the index and, accordingly, the best performing bands based on the testing dataset will rely on a series of criteria. First, it should be a simple index, preferably using only two bands to minimize processing time and improve its operational use. Secondly, the index must have physical sense, that is, it should be based on areas of the spectrum with high influence of the LAI_{green} parameter. As mentioned earlier, the red, red-edge and NIR regions are the areas with the greatest influence of this parameter, so the Sentinel-2 bands used by the proposed index will be from these spectral regions. Third, it must present good statistics when applied to the completely independent validation dataset (FOG17_IT). The coefficient of determination (R^2) and root mean squared error (RMSE) will be selected as indicators of the accuracy of the statistical estimation models.

3. Results

In this section we first present the quality results of Sentinel-2 LAI product, comparing them with both the Valencia and Foggia LAI_{green} in situ datasets. In the same way, we show the performance of the common indices used by the bibliography, presenting graphs with the best settings for each index. Next, the best band combination for each commonly used index, obtained with ARTMO toolbox, are shown, defining finally the new SeLI index and showing its validation assessment with the Foggia dataset.

3.1. Performance of the Sentinel-2 Level-2A LAI_{green} Product

The LAI_{green} products of both Valencia and Foggia Sentinel-2 images were obtained and compared with the in situ LAI_{green} of the corresponding pixel. The analysis was carried out with only 31 LAI_{green} VLC17_ES values and 99 FOG17_ES values, because only those corresponding pixels indicated with a good product quality flag were selected. Figure 4 shows the Sentinel-2 LAI_{green} product values and the in situ LAI_{green} values, with the 1:1 line (black), its statistics and the linear fitting (red). A clear underestimation of the product values is shown in Figure 4.

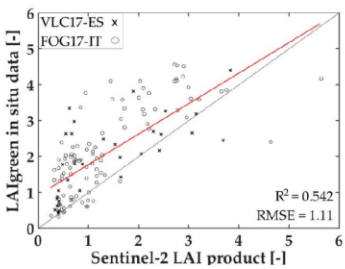

Figure 4. Green leaf area index (LAI_{green}) in situ values in comparison to the Sentinel-2 LAI_{green} product, with 1:1 line (black), its statistics and linear fitting (red).

3.2. Performance of Common LAI_{green} Indices for a Multi-Crop Dataset

Commonly used LAI_{green} indices (Table 3, indices shaded) were evaluated with their default bands using the multi-crop VLC17_ES dataset. The R^2 obtained with different types of fitting functions ranged between 0.234–0.663 when applying the respective indices on the multi-crop dataset (Table 4). Hence, the accuracies of each index obtained with linear, polynomial of second order, exponential and exponential of second order fitting, were rather low. The p-value is <0.001 in all cases except for the ratio index (RI).

Table 4. Statistics obtained with a linear, polynomial of second order, exponential and exponential of second order fitting for each index. The best fitting is boldfaced.

Index	References	Linear Fitting		Polynomial Fitting, Second Order		Exponential Fitting		Exponential Fitting, Second Order	
		R^2	RMSE	R^2	RMSE	R^2	RMSE	R^2	RMSE
RI	[41]	0.355	0.91	0.314	0.93	0.234	1.13	**0.663**	0.75
		$y = 0.15x + 1.11$		$y = -0.01x^2 + 0.33x + 0.55$		$y = 1.51\exp(0.04x)$		$y = 2.59\exp(0.01x) - 6.19\exp(-0.71x)$	
NDGI	[43]	**0.659**	0.72	0.612	0.74	0.571	0.85	0.629	0.79
		$y = 3.93x - 0.18$		$y = -1.98x^2 + 5.93x - 0.55$		$y = 0.68\exp(1.78x)$		$y = -1547\exp(3.96x) + 1548\exp(3.96x)$	
	[42]	0.402	0.86	0.389	0.89	0.310	1.07	**0.549**	0.88
		$y = 3.58x + 0.91$		$y = -6.51x^2 + 9.33x + 0.16$		$y = 1.33\exp(1.18x)$		$y = -3.61\exp(-0.08x) - 3.84\exp(-4.21x)$	
TRBI	[61]	**0.663**	0.75	0.639	0.75	0.625	0.79	0.659	0.76
		$y = -2.55x + 3.62$		$y = 0.44x^2 - 3.27x + 3.84$		$y = 4.39\exp(-1.42x)$		$y = -7.13\exp(-3.34x) - \exp(-3.34x)$	

Each established index was represented as a function of the VLC17_ES LAI_{green} values, to show its predicting performance (Figure 5). As can be seen, they generally present a scattered performance and all indices present a saturation problem with high and/or low LAI_{green} values. Concretely, the RI index (Figure 5a) overestimates to an extreme extent at low and high LAI_{green} values. The TRBI (Figure 5d) shows a saturation process with LAI_{green} values close to 3. And both normalized indices (Figure 5b,c) already present their greater value (the unit), with also LAI_{green} values close to 3. The normalized index defined by Delegido et al. (2011) uses a red-edge band (705 nm), but as it is used in combination with the red band (665 nm) [42], the saturation problem at high LAI_{green} values appears. So, the effectiveness of LAI_{green} indices depends entirely on the combination of bands used.

Another demonstration of the saturation produced by the band located at the red region (B4: 665 nm) is Figure 6. In this Figure, real Sentinel-2 spectra of artichoke (LAI = 2.8 in blue, 3.4 in orange) and orange tree crops (LAI = 2.3 in blue, 3.9 in orange) with moderate-high LAI_{green} values of the VLC17_ES dataset are represented. Values higher than 2 have been chosen because it is usually the limit at which saturation process starts with common LAI_{green} indices (Figure 5). As can be seen, they have the same reflectance value in the 665 nm band, that is, at moderate-high LAI_{green} values, chlorophyll maximally absorbs in this region, producing saturation. At the same time, the red-edge band close to the red (B5: 705 nm) does not show such entire absorption saturation, which brings the advantage of using red-edge Sentinel-2 bands for LAI_{green} estimation.

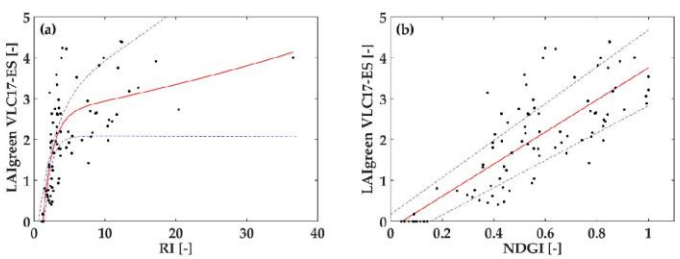

Figure 5. *Cont.*

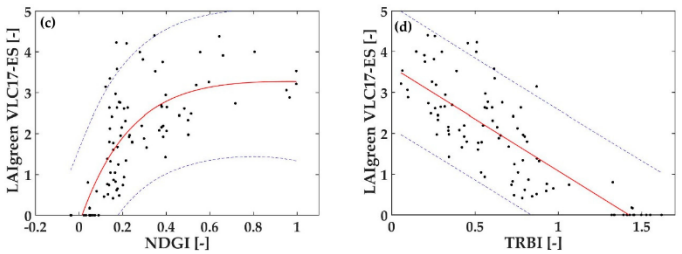

Figure 5. Graphic representation of the LAI_{green} of VLC17_ES dataset as a function of the established LAI_{green} indices, with the best fitting function and 95% of confidence interval. (**a**) RI [41]; (**b**) NDGI [43]; (**c**) NDGI [42]; (**d**) TRBI [61].

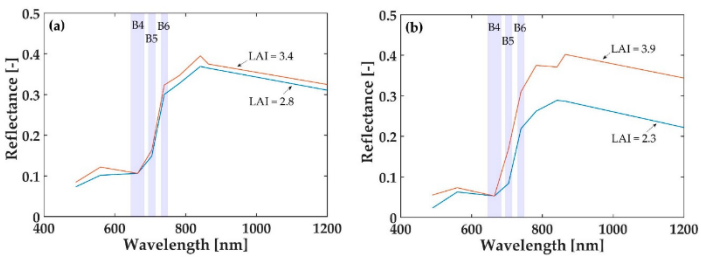

Figure 6. Representation of real Sentinel-2 top-of-canopy (TOC) reflectance spectra of (**a**) artichoke crops (20/07/2017 Sentinel-2 image used) and (**b**) orange tree crops (07/11/2017 Sentinel-2 image used). The red and red-edge Sentinel-2 bands (B4, B5 and B6) are represented with their corresponding bandwidth.

3.3. Sensitivity of Spectral Bands against LAI_{green} Parameter

In order to investigate more generic index options, the following step involved systematically calculating all band combinations with the ARTMO toolbox. Table 5 lists the 10 best statistical results obtained for each generic index and the corresponding bands with a linear fit, using the VLC17_ES dataset and a cross-validation process. The analysis was performed with linear fitting, because the aim of this study is to define a simple relationship between the LAI_{green} parameter and Sentinel-2 bands, analysing whether there is a linear relationship between the LAI_{green} in situ values and the estimated values. Furthermore, as seen in Table 4, linear fitting produces one of the best statistical results.

Comparing to the tested established indices, these results already show a more promising correlation with a R^2 ranging between 0.701 and 0.737. However, questions arose when evaluating the obtained wavelengths of the resulting best-performing bands from a physical point of view. In the majority of cases, the selected bands were physically not only influenced by chlorophyll absorption, but mainly by other leaf constituents such as lignin, cellulose and water (e.g., 1610 nm, 2190 nm) affecting the scattering properties in the NIR and SWIR [69,70]. The only case where physical chlorophyll-related bands were chosen, was the NDGI, using one of the new red-edge bands (705 nm, in the tail of the chlorophyll absorption peak) and the other in the NIR region (865 nm). The red band (B4) appeared not to be chosen at all.

Table 5. Best band combination for each generic vegetation index introduced in ARTMO from cross-validation of the testing dataset (VLC17_ES), ordered from highest to lowest R^2, with a linear fit.

Index	Bands	R^2	RMSE	NRMSE (%)	p-Value
TRBI	2190;740;865	0.737	0.63	14	<0.001
TDBI	2190;865;740	0.732	0.64	15	<0.001
ND3b	2190;865;740	0.731	0.64	15	<0.001
MNI	2190;865;1610	0.731	0.64	15	<0.001
RI	2190;865	0.728	0.64	15	<0.001
MCGI	1610;865;740	0.717	0.65	15	<0.001
TGI	1610;842;2190	0.713	0.66	15	<0.001
GLH	2190;1610;842	0.708	0.67	15	<0.001
NDGI	865;705	0.708	0.67	15	<0.001
MTGI	2190;865;490	0.701	0.68	15	<0.001

3.4. Optimized Simple Index for LAI_{green} Retrieval from Sentinel-2 Data: SeLI

According to the previous outcome of the NDGI, we used this index structure and analysed all band combinations in red, red-edge and NIR regions, i.e., the bands 4, 5, 6, 7, 8 and 8a (Table 1). Table 6 summarizes the normalized difference ratio index band combinations with their corresponding statistics for the independent testing and validation datasets. The statistical results are ranked according their performance for the testing dataset. All indices perform better compared to the common used indices, apart from those listed at the bottom. The top four performing combinations do not use the red band, but instead, all use the red-edge band at 705 nm in combination with a far-red or NIR band.

Table 6. Linear cross-validation fitting results of the normalized difference ratio index with different band combinations and LAI_{green} values from the testing and validation datasets, ordered from highest to lowest R^2 according to the testing dataset.

Bands	Testing (VLC17_ES)		Validation (FOG17_IT)	
	R^2	RMSE	R^2	RMSE
865;705	0.708	0.67	0.732	0.69
783;705	0.702	0.68	0.711	0.71
842;705	0.688	0.69	0.717	0.71
740;705	0.685	0.71	0.686	0.74
783;665	0.675	0.71	0.678	0.75
842;665	0.665	0.72	0.684	0.74
783;740	0.531	0.85	0.674	0.76

As expected, the best result for the testing dataset is again the 705 (B5)–865 (B8a) nm combination (R^2 = 0.708), and, moreover, confirmed by the validation dataset (R^2 = 0.732). These both independent datasets on real in situ data give us the strong experimental proof that the LAI_{green} parameter presents a linear behavior up to values of five, proposing therefore a physiologically-based LAI_{green} index, hereafter called the Sentinel-2 LAI_{green} Index (SeLI) (Equation (1)). For the in situ VLC17_ES LAI_{green} dataset (Figure 7a), it is observed that SeLI values vary from 0.03, corresponding to bare soils, to a maximum of 0.76, corresponding to LAI_{green} values up to 4.5, with potato and alfalfa crops showing the highest LAI_{green} values. We do not observe any saturation at these high LAI_{green} values, while previously shown indices did. Hence, SeLI showed the potential to be used in a unified algorithm for LAI_{green} estimation in different crop types.

$$\mathrm{SeLI} = \frac{R_{865} - R_{705}}{R_{865} + R_{705}} \quad (1)$$

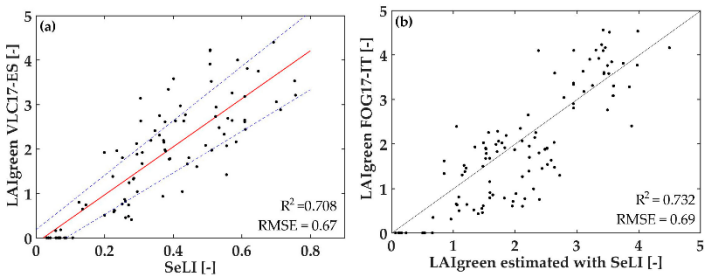

Figure 7. (**a**) Graphic representation of the LAI_{green} of the testing VLC17_ES dataset (n = 92) as a function of SeLI, the index proposed, with linear fit and 95% of confidence interval, (**b**) LAI_{green} in situ validation data from FOG17_IT (n = 109) as a function of LAI_{green} estimated with SeLI, with 1:1 line and its statistics.

From Figure 7a, the LAI_{green} estimation equation through SeLI index is extracted, with a linear fit (Equation (2)). We have tested, besides the linear fitting (R^2 = 0.708, RMSE = 0.67), also an exponential fitting (R^2 = 0.603, RMSE = 0.78) and a polynomial of second order (R^2 = 0.727, RMSE = 0.65) to fit the index with in situ LAI values. The polynomial fitting presents slightly higher statistics, but the adjustment is negative, not presenting much physical sense.

$$LAI_{green} = 5.405 \times SeLI - 0.114 \quad (2)$$

Figure 7b shows the LAI_{green} values estimated with Equation (2) together to the validation dataset taken in Foggia, obtaining a correlation R^2 of 0.732 and RMSE of 0.69 (1:1 line), showing strong validation statistics.

Finally, we applied the SeLI to both field sites, using the 26 May 2017 and 8 April 2017 Sentinel-2 images for the Huerta of Valencia and Foggia site, respectively. The resulting maps are shown in Figure 8, demonstrating the applicability of SeLI at high spatial resolution for two distinct agricultural areas. In brown, the pixels with the lowest value of LAI_{green} are shown, mainly corresponding to bare soils, and in green colour, the pixels with the highest LAI_{green} value, corresponding to potato and alfalfa crops in the case of Valencia, and wheat in the case of Foggia. A zoom of each map is shown to demonstrate the high spatial resolution of Sentinel-2, being able to observe individual agricultural plots of 40 m × 40 m (Valencia) and 100 m × 100 m (Foggia) based on LAI, while also observing slight LAI variability within these plots.

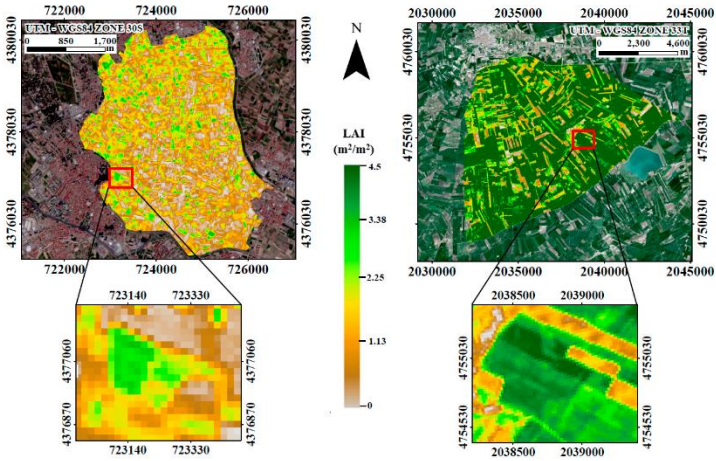

Figure 8. LAI_{green} maps estimated with SeLI proposed index in Valencia test site using the Sentinel-2 image of 26 May 2017 (left) and Foggia test site using the Sentinel-2 image of 8 April 2017 (right). Note the different scale of both study sites and their respective agricultural areas.

4. Discussion

With the availability of a narrow band in the red-edge region by Sentinel-2, an improved and simple estimation of LAI_{green} based on a simple index becomes possible at high spatial resolution. The proposed SeLI index shows a significant improvement towards indices using the saturating bands in the red (B4 in Sentinel-2). Moreover, no saturation appeared in the obtained LAI_{green} product based on the red-edge bands (B5: 705 nm and B6: 740 nm). The B4 (665 nm) saturation at high LAI_{green} values is clearly shown with real Sentinel-2 TOC reflectance spectra for different LAI_{green} values, higher than 2 (Figures 5 and 6). The red-edge bands (B5: 705 nm and B6: 740 nm) in contrast are both affected by higher scattering, whereby the B5 band is still driven by chlorophyll absorption. This agrees with numerous authors who emphasize the importance of the red-edge bands for the estimation of biophysical parameters, mainly the LAI_{green} and chlorophyll estimation [42,46,71]. The proposed Sentinel-2 LAI Index (SeLI) exploits the B5 red-edge band, which has been widely demonstrated that is highly influenced by the LAI_{green} parameter [46–48], and the B8a NIR band, which is driven by the scattering changes in moderate-to-high LAI values in crops [72]. Very few previous indices have used bands in the red-edge region because no free operational previous sensors had narrow bands in this spectral area [42]. Both linear and non-linear empirical regression techniques have been tested for the LAI retrieval on simulated spectrally resampled airborne data [50,73] and recently on real Sentinel-2 data [10,52]. The band selection obtained from these methodologies appeared to favor (1) green and SWIR bands in the case of linear regression by VIs, and (2) red, NIR and SWIR bands in the case of non-linear regression by machine learning approaches [74]. These bands were also chosen by several of our tested VIs (Table 5), with the difference that the NDGI formulation indicated the use of red-edge (705 nm) and a NIR band (865 nm) as best band selection.

The robustness and generality of the SeLI index is demonstrated by applying it to an independent in situ field dataset from a distinct geographical location with crop types different from those included in the testing dataset, obtaining equally good statistics (R^2 of 0.732, RMSE of 0.69). Specifically, SeLI

does not present problems of saturation when it is applied to a multi-crop Valencia in situ dataset composed of 13 different crop types and LAI_{green} values that go up to 4.5, obtaining R^2 of 0.708 and RMSE of 0.67. Furthermore, when SeLI is applied to the Foggia region, characterized by high LAI_{green} values, the limits of the different crop fields and LAI_{green} variability within the crop field appears even for the high value ranges, indicating variable growing conditions. Such a clear distinction in LAI_{green} variability allows evaluation of management practices at the field level. Hence, it is shown that the SeLI index generally can be applied for LAI_{green} retrieval of different crop types and distinct areas. A limitation of the index is that it has been calibrated and validated with LAI data up to 5, so it is only applicable to agricultural areas with this range of values, although it is the common range of in situ LAI measured values in a lot of studies with a great variety of crop types; such as wheat [75,76], corn [19], potato [10] and sugar beet [2,47]. Currently, ongoing scientific debate is taking place on the discussion if there is a linear relationship or not between in situ LAI values and estimated values [77]. Our study shows that in situ data are linearly related to SeLI, in the value range of 0 to 5. This result is in accordance with other results in which also LAI of agricultural areas is estimated through indices and linear models in similar ranges [10,75,78–80]. Generally, no values higher than 5 are used in these studies constraining the model applicability to this range. As SeLI has a physiological foundation, the index will be applicable to a higher value range, but the SeLI-LAI fitting relationship might change depending on the dataset range. To verify this, a LAI in situ data range >5 would be required. However, one must also consider the instrumental limitations for in situ measurements. The LAI-2200 Plant Canopy Analyzer [55] calculates LAI by comparing differential light measurements above and below canopy. The maximum measurable LAI is generally lower for these devices measuring gap fraction with LAI reaching an asymptotic saturation level at a value of about 5, compared to that assessed via destructive methods. The cause for this is gap fraction saturation as LAI approaches five or six [81–83].

In this work, the Sentinel-2 LAI_{green} product obtained from the SNAP toolbox was also tested with the multi-crop dataset from Valencia. The results show underestimated LAI estimations ($R^2 = 0.475$, RMSE = 0.91). There are some studies, which have also compared this Sentinel-2 LAI_{green} product with in situ LAI_{green} crop data, that obtain better R^2 [84,85], but they only tested the product with few crop types. When the product is analysed in different areas and plant species, the results can be improved [36]. This finding could be explained by the fact that the Sentinel-2 algorithm used for land surface parameters, including LAI_{green} product, ingests almost all spectral bands and applies a nonlinear regression to estimate each parameter [33], in addition to the fact that it has been proven that there is a substantial sensitivity of Sentinel-2 biophysical products to the implemented rugged terrain corrections [36].

The other main challenge in the retrieval of biophysical parameters with vegetation indices is the difficulty of finding a simple index with such a general character that it can estimate the parameter of a wide variety of crop types. In this work it has also been shown that the established indices do not present this general character. This may be because they were developed and calibrated based on limited experimental data in terms of species, presenting improvable statistics (R^2 between 0.234–0.663) when applied to multi-crop datasets. In an attempt to improve estimations over this multi-crop dataset, all band combinations were systematically calculated for each index in order to achieve the highest possible correlation for the estimation of LAI_{green}. More promising results were obtained, with a R^2 between 0.701 and 0.737. However, when inspecting these sensitive bands whether they are physically meaningful, i.e., if the selected bands are actually influenced only or mostly by LAI_{green}, then these indices turned out to be questionable. In the majority of cases, the selected bands were influenced by leaf constituents such as lignin, cellulose and water (e.g., 1610 nm, 2190 nm) affecting the scattering properties in the NIR and SWIR [69,70], and being less related to photosynthetically based LAI_{green}. At the field or landscape scale, canopy reflectance patterns represent the integrated effects of all biophysical parameters. Co-variation mechanisms of leaf constituents is typically causing the selection of bands related to other covarying biochemicals such as pigments or lignin due to their

high effect on spectral variability [86]. Similarly, it was earlier observed that due to the covariation between water content and chlorophyll content (related with LAI parameter), typically bands in the water content absorption region are selected as most sensitive [87]. To improve the estimation of LAI_{green} (aside from LAI_{brown}), bands only affected by structural leaf components should be omitted. Structurally-related NIR and SWIR bands may improve the LAI_{green} retrieval when the model is trained on healthy vegetation [74] but may be less generally applicable for scenarios with different structural types or stress conditions. With the band selection B5 and B8a, SeLI is functionally related to green LAI, avoiding absorption saturation in the red region.

It should be mentioned that this is the first time that this kind of LAI_{green} retrieval can be carried out for agricultural areas with plots sizes of only 40–100 m, such as Huerta of Valencia, due to the lack of an operational satellite with the required spatial and temporal resolution. ESA's satellite Sentinel-2 aims to replace and improve the older generation of satellite sensors such as Landsat and SPOT, with improved spectral and spatial capabilities. Therefore, the Sentinel-2 satellites provide a great opportunity for global vegetation monitoring, and specifically crop field monitoring, due to its enhanced spatial, spectral and temporal characteristics [42].

Finally, further validation is required with other field campaigns and synthetic Sentinel-2 data to reinforce findings. Considering appropriate instrumental tools, the index behavior for LAI_{green} values higher than 5 should be tested, as well as the fitting behavior of these further ranges.

5. Conclusions

Numerous VIs have been proposed for the estimation of green leaf area index (LAI_{green}) over various crop types, but the general problem appears when they are applied to multi-crop datasets, obtaining low estimation accuracies and additionally at LAI_{green} values higher than 2, saturation problems appear. Based on the availability of Sentinel-2 narrow red-edge bands, we explored new index possibilities for accurate LAI_{green} estimations for heterogeneous agricultural areas, based on spectral areas influenced mainly by photosynthesis-related absorption regions. The proposed Sentinel-2 LAI Index (SeLI) is a normalized index that uses the new Sentinel-2 narrow B5-band located at the beginning of the red-edge region (705 nm), a spectral area which balances the influence of strong chlorophyll absorption and minimal scattering at moderate-high LAI_{green} values, and a NIR band (865 nm) influenced by leaf scattering, as a reference band. SeLI was calibrated with a multi-crop Valencia dataset composed of LAI_{green} values of 13 different crop types, obtaining a R^2 of 0.708 and RMSE of 0.67. The validation of SeLI proved good, with a R^2 of 0.732 and RMSE of 0.69. This work demonstrated the existence of a linear relationship between in situ LAI_{green} and the spectral information of Sentinel-2, in the range of 0 to 5. Sentinel-2 generated maps over the Valencia and Foggia test sites convincingly illustrate the great potential of high spatial resolution LAI_{green} monitoring at the single agricultural plot level, even for small- and medium-scale agricultural activities.

Author Contributions: N.P., J.D. and M.R. designed the field campaigns and collected in situ LAI multi-crop data; N.P. and J.D. analyzed the data and obtained the results; N.P. and S.V.W. wrote the paper and J.M. designed the experiments and guided and supervised the work.

Funding: This research was funded by SENSAGRI (Sentinels Synergy for Agriculture) project (H2020-EO-2016-730074).

Acknowledgments: This work was supported by the pre-doctoral scholarship of the Generalitat Valenciana Vali+d (ACIF/2016/378) of the first author. S.V.W. acknowledges the European Union's Marie Sklodowska-Curie fellowship (MSCA-IF-2015-701815) and the Generalitat Valenciana Vali+d (APOSTD/2018/162). We would also like to thank the SENSAGRI project (H2020-EO-2016-730074) and especially to the EOLAB spin-off from the University of Valencia.

Conflicts of Interest: The authors declare no conflict of interest.

References

1. Daughtry, C.S.T.; Gallo, K.P.; Goward, S.N.; Prince, S.D.; Kustas, W.P. Spectral estimates of absorbed radiation and phytomass production in corn and soybean canopies. *Remote Sens. Environ.* **1992**, *39*, 141–152. [CrossRef]

2. Delegido, J.; Verrelst, J.; Rivera, J.P.; Ruiz-Verdú, A.; Moreno, J. Brown and green LAI mapping through spectral indices. *Int. J. Appl. Earth Obs. Geoinf.* **2015**, *35*, 350–358. [CrossRef]
3. Zaroug, M.A.H.; Sylla, M.B.; Giorgi, F.; Eltahir, E.A.B.; Aggarwal, P.K. A sensitivity study on the role of the swamps of southern Sudan in the summer climate of North Africa using a regional climate model. *Theor. Appl. Climatol.* **2013**, *113*, 63–81. [CrossRef]
4. Richardson, A.D.; Dail, D.B.; Hollinger, D.Y. Leaf area index uncertainty estimates for model-data fusion applications. *Agric. For. Meteorol.* **2011**, *151*, 1287–1292. [CrossRef]
5. Bréda, N.J.J. Ground-based measurements of leaf area index: A review of methods, instruments and current controversies. *J. Exp. Bot.* **2003**, *54*, 2403–2417. [CrossRef] [PubMed]
6. Sakamoto, T.; Gitelson, A.; Nguy-Robertson, A.; Arkebauer, T.; Wardlow, B.; Suyker, A.; Verma, S.; Shibayama, M. An alternative method using digital cameras for continuous monitoring of crop status. *Agric. For. Meteorol.* **2012**, *154*, 113–126. [CrossRef]
7. Coops, N.C.; Waring, R.H.; Hilker, T. Prediction of soil properties using a process-based forest growth model to match satellite-derived estimates of leaf area index. *Remote Sens. Environ.* **2012**, *126*, 160–173. [CrossRef]
8. Boegh, E.; Soegaard, H.; Broge, N.; Hasager, C.B.; Jensen, N.O.; Schelde, K.; Thomsen, A. Airborne multispectral data for quantifying leaf area index, nitrogen concentration, and photosynthetic efficiency in agriculture. *Remote Sens. Environ.* **2002**, *81*, 179–193. [CrossRef]
9. Kira, O.; Nguy-Robertson, A.L.; Arkebauer, T.J.; Linker, R.; Gitelson, A.A. Informative spectral bands for remote green LAI estimation in C3 and C4 crops. *Agric. For. Meteorol.* **2016**, *218–219*, 243–249. [CrossRef]
10. Clevers, J.G.P.W.; Kooistra, L.; van den Brande, M.M.M. Using Sentinel-2 data for retrieving LAI and leaf and canopy chlorophyll content of a potato crop. *Remote Sens.* **2017**, *9*, 405. [CrossRef]
11. Brisco, B.; Brown, R.J.; Hirose, T.; McNairn, H.; Staenz, K. Precision agriculture and the role of remote sensing: A review. *Can. J. Remote Sens.* **1998**, *24*, 315–327. [CrossRef]
12. Houlès, V.; Guérif, M.; Mary, B. Elaboration of a nitrogen nutrition indicator for winter wheat based on leaf area index and chlorophyll content for making nitrogen recommendations. *Eur. J. Agron.* **2007**, *27*, 1–11. [CrossRef]
13. Bsaibes, A.; Courault, D.; Baret, F.; Weiss, M.; Olioso, A.; Jacob, F.; Hagolle, O.; Marloie, O.; Bertrand, N.; Desfond, V.; et al. Albedo and LAI estimates from FORMOSAT-2 data for crop monitoring. *Remote Sens. Environ.* **2009**, *113*, 716–729. [CrossRef]
14. Yao, X.; Wang, N.; Liu, Y.; Cheng, T.; Tian, Y.; Chen, Q.; Zhu, Y. Estimation of wheat LAI at middle to high levels using unmanned aerial vehicle narrowband multispectral imagery. *Remote Sens.* **2017**, *9*, 1304. [CrossRef]
15. Campos-Taberner, M.; García-Haro, F.J.; Camps-Valls, G.; Grau-Muedra, G.; Nutini, F.; Crema, A.; Boschetti, M. Multitemporal and multiresolution leaf area index retrieval for operational local rice crop monitoring. *Remote Sens. Environ.* **2016**, *187*, 102–118. [CrossRef]
16. Mulla, D.J. Twenty five years of remote sensing in precision agriculture: Key advances and remaining knowledge gaps. *Biosyst. Eng.* **2013**, *114*, 358–371. [CrossRef]
17. Drusch, M.; Del Bello, U.; Carlier, S.; Colin, O.; Fernandez, V.; Gascon, F.; Hoersch, B.; Isola, C.; Laberinti, P.; Martimort, P.; et al. Sentinel-2: ESA's optical high-resolution mission for GMES operational services. *Remote Sens. Environ.* **2012**, *120*, 25–36. [CrossRef]
18. Baret, F.; Guyot, G. Potential and limitations of vegetation indices for LAI and APAR assessment. *Remote Sens. Environ.* **1991**, *35*, 161–173. [CrossRef]
19. Haboudane, D.; Miller, J.R.; Pattey, E.; Zarco-Tejada, P.J.; Strachan, I.B. Hyperspectral vegetation indices and novel algorithms for predicting green LAI of crop canopies: Modeling and validation in the context of precision agriculture. *Remote Sens. Environ.* **2004**, *90*, 337–352. [CrossRef]
20. Verrelst, J.; Romijn, E.; Kooistra, L. Mapping vegetation density in a heterogeneous river floodplain ecosystem using pointable CHRIS/PROBA data. *Remote Sens.* **2012**, *4*, 2866–2889. [CrossRef]
21. Broge, N.H.; Mortensen, J.V. Deriving green crop area index and canopy chlorophyll density of winter wheat from spectral reflectance data. *Remote Sens. Environ.* **2002**, *81*, 45–57. [CrossRef]
22. Glenn, E.P.; Huete, A.R.; Nagler, P.L.; Nelson, S.G. Relationship between remotely-sensed vegetation indices, canopy attributes and plant physiological processes: What vegetation indices can and cannot tell us about the landscape. *Sensors* **2008**, *8*, 2136–2160. [CrossRef] [PubMed]
23. Myneni, R.B.; Maggion, S.; Iaquinta, J.; Privette, J.L.; Gobron, N.; Pinty, B.; Kimes, D.S.; Verstraete, M.M.; William, D.L. Optical remote sensing of vegetation: Modeling, caveates, and algorithms. *Remote Sens. Environ.* **1995**, *51*, 169–188. [CrossRef]

24. Gobron, N.; Pinty, B.; Verstraete, M.M.; Widlowski, J.L. Advanced vegetation indices optimized for up-coming sensors: Design, performance, and applications. *IEEE Trans. Geosci. Remote Sens.* **2000**, *38*, 2489–2505. [CrossRef]
25. Houborg, R.; Boegh, E. Mapping leaf chlorophyll and leaf area index using inverse and forward canopy reflectance modeling and SPOT reflectance data. *Remote Sens. Environ.* **2008**, *112*, 186–202. [CrossRef]
26. Jacquemoud, S.; Baret, F.; Andrieu, B.; Danson, M.; Jaggard, K. Extraction of vegetation biophysical parameters by inversion of the PROSPECT+SAIL model on sugar beet canopy reflectance data: Application to TM and AVIRIS sensors. *Remote Sens. Environ.* **1995**, *52*, 163–172. [CrossRef]
27. Zheng, G.; Moskal, L.M. Retrieving leaf area index (LAI) using remote sensing: Theories, methods and sensors. *Sensors* **2009**, *9*, 2719–2745. [CrossRef]
28. González-Sanpedro, M.C.; Le Toan, T.; Moreno, J.; Kergoat, L.; Rubio, E. Seasonal variations of leaf area index of agricultural fields retrieved from Landsat data. *Remote Sens. Environ.* **2008**, *112*, 810–824. [CrossRef]
29. Combal, B.; Baret, F.; Weiss, M.; Trubuil, A.; Macé, D.; Pragnère, A.; Myneni, R.; Knyazikhin, Y.; Wang, L. Retrieval of canopy biophysical variables from bidirectional reflectance: Using prior information to solve the ill-posed inverse problem. *Remote Sens. Environ.* **2002**, *84*, 1–15. [CrossRef]
30. Atzberger, C. Object-based retrieval of biophysical canopy variables using artificial neural nets and radiative transfer models. *Remote Sens. Environ.* **2004**, *93*, 53–67. [CrossRef]
31. España, M.L.; Baret, F.; Aries, F.; Chelle, M.; Andrieu, B.; Prévot, L. Modeling maize canopy 3D architecture: Application to reflectance simulation. *Ecol. Model.* **1999**, *122*, 25–43. [CrossRef]
32. Casa, R.; Baret, F.; Buis, S.; Lopez-Lozano, R.; Pascucci, S.; Palombo, A.; Jones, H.G. Estimation of maize canopy properties from remote sensing by inversion of 1-D and 4-D models. *Precis. Agric.* **2010**, *11*, 319–334. [CrossRef]
33. Weiss, M.; Baret, F. S2ToolBox Level 2 products: LAI, FAPAR, FCOVER. Available online: http://step.esa.int/docs/extra/ATBD_S2ToolBox_L2B_V1.1.pdf (accessed on 9 November 2018).
34. Verhoef, W. Light scattering by leaf layers with application to canopy reflectance modeling: The SAIL model. *Remote Sens. Environ.* **1984**, *16*, 125–141. [CrossRef]
35. Jacquemoud, S.; Baret, F. PROSPECT: A model of leaf optical properties spectra. *Remote Sens. Environ.* **1990**, *34*, 75–91. [CrossRef]
36. Djamai, N.; Fernandes, R. Comparison of SNAP-derived Sentinel-2A L2A product to ESA product over Europe. *Remote Sens.* **2018**, *10*, 926. [CrossRef]
37. Verrelst, J.; Muñoz, J.; Alonso, L.; Delegido, J.; Rivera, J.P.; Camps-Valls, G.; Moreno, J. Machine learning regression algorithms for biophysical parameter retrieval: Opportunities for Sentinel-2 and -3. *Remote Sens. Environ.* **2012**, *118*, 127–139. [CrossRef]
38. Cui, Z.; Kerekes, J.P. Potential of red edge spectral bands in future landsat satellites on agroecosystem canopy green leaf area index retrieval. *Remote Sens.* **2018**, *10*, 1458. [CrossRef]
39. Verrelst, J.; Camps-Valls, G.; Muñoz-Marí, J.; Rivera, J.P.; Veroustraete, F.; Clevers, J.G.P.W.; Moreno, J. Optical remote sensing and the retrieval of terrestrial vegetation bio-geophysical properties—A review. *ISPRS J. Photogramm. Remote Sens.* **2015**, *108*, 273–290. [CrossRef]
40. le Maire, G.; François, C.; Soudani, K.; Berveiller, D.; Pontailler, J.Y.; Bréda, N.; Genet, H.; Davi, H.; Dufrêne, E. Calibration and validation of hyperspectral indices for the estimation of broadleaved forest leaf chlorophyll content, leaf mass per area, leaf area index and leaf canopy biomass. *Remote Sens. Environ.* **2008**, *112*, 3846–3864. [CrossRef]
41. Jordan, C.F. Derivation of leaf area index from quality of light on the forest floor. *Ecology* **1969**, *50*, 663–666. [CrossRef]
42. Delegido, J.; Verrelst, J.; Alonso, L.; Moreno, J. Evaluation of sentinel-2 red-edge bands for empirical estimation of green LAI and chlorophyll content. *Sensors* **2011**, *11*, 7063–7081. [CrossRef] [PubMed]
43. Rouse, J.W.; Hass, R.H.; Schell, J.A.; Deering, D.W. Monitoring vegetation systems in the great plains with ERTS. In *Third Earth Resources Technology Satellite-1 Symposium*; NASA: Washington, DC, USA, 1973; Volume 1, pp. 309–317.
44. Guyot, G.; Baret, F.; Jacquemond, S. Imaging spectroscopy for vegetation studies. *Imaging Spectrosc. Fundam. Prospect. Appl.* **1992**, *2*, 145–165.
45. Baret, F.; Jacquemoud, S.; Guyot, G.; Leprieur, C. Modeled analysis of the biophysical nature of spectral shifts and comparison with information content of broad bands. *Remote Sens. Environ.* **1992**, *41*, 133–142. [CrossRef]

46. Liu, J.; Miller, J.R.; Haboudane, D.; Pattey, E. Exploring the relationship between red edge parameters and crop variables for precision agriculture. In Proceedings of the IGARSS 2004. 2004 IEEE International Geoscience and Remote Sensing Symposium, Anchorage, AK, USA, 20–24 September 2004; Volume 2, pp. 1276–1279. [CrossRef]
47. Delegido, J.; Fernandez, G.; Gandia, S.; Moreno, J. Retrieval of chlorophyll content and LAI of crops using hyperspectral techniques: Application to PROBA/CHRIS data. *Int. J. Remote Sens.* **2008**, *29*, 7107–7127. [CrossRef]
48. Herrmann, I.; Pimstein, A.; Karnieli, A.; Cohen, Y.; Alchanatis, V.; Bonfil, D.J. LAI assessment of wheat and potato crops by VENμS and Sentinel-2 bands. *Remote Sens. Environ.* **2011**, *115*, 2141–2151. [CrossRef]
49. Campos-Taberner, M.; García-Haro, F.J.; Camps-Valls, G.; Grau-Muedra, G.; Nutini, F.; Busetto, L.; Katsantonis, D.; Stavrakoudis, D.; Minakou, C.; Gatti, L.; et al. Exploitation of SAR and optical sentinel data to detect rice crop and estimate seasonal dynamics of leaf area index. *Remote Sens.* **2017**, *9*, 248. [CrossRef]
50. Kira, O.; Nguy-Robertson, A.L.; Arkebauer, T.J.; Linker, R.; Gitelson, A.A. Toward generic models for green LAI estimation in maize and soybean: Satellite observations. *Remote Sens.* **2017**, *9*, 318. [CrossRef]
51. Nguy-Robertson, A.L.; Peng, Y.; Gitelson, A.A.; Arkebauer, T.J.; Pimstein, A.; Herrmann, I.; Karnieli, A.; Rundquist, D.C.; Bonfil, D.J. Estimating green LAI in four crops: Potential of determining optimal spectral bands for a universal algorithm. *Agric. For. Meteorol.* **2014**, *192–193*, 140–148. [CrossRef]
52. Xie, Q.; Dash, J.; Huang, W.; Peng, D.; Qin, Q.; Mortimer, H.; Casa, R.; Pignatti, S.; Laneve, G.; Pascucci, S.; et al. Vegetation indices combining the red and red-edge spectral information for Leaf Area Index retrieval. *IEEE J. Sel. Top. Appl. Earth Obs. Remote Sens.* **2018**, *11*, 1482–1493. [CrossRef]
53. AEMET. Agencia Estatal de Meteorología. Available online: http://www.aemet.es/es/portada (accessed on 20 November 2018).
54. METEOBLUE Weather. Climate Foggia. Available online: https://www.meteoblue.com/en/weather/forecast/modelclimate/foggia_italy_3176885 (accessed on 20 November 2018).
55. LI-COR. *Licor 2200 Instruction Manual*; LI-COR: Lincoln, NE, USA, 2012; ISBN 4024672819.
56. Pandžić, M.; Mihajlović, D.; Pandžić, J.; Pfeifer, N. Assessment of the geometric quality of sentinel-2 data. *Int. Arch. Photogramm. Remote Sens. Spat. Inf. Sci. ISPRS Arch.* **2016**, *41*, 489–494. [CrossRef]
57. Louis, J.; Debaecker, V.; Pflug, B.; Main-Knorn, M.; Bieniarz, J.; Mueller-Wilm, U.; Cadau, E.; Gascon, F. Sentinel-2 SEN2COR: L2A processor for users. In Proceedings of the Living Planet Symposium, Prague, Czech Republic, 9–13 May 2016; pp. 1–8.
58. Verrelst, J.; Rivera, J.P.; Alonso, L.; Moreno, J. ARTMO: An Automated Radiative Transfer Models Operator toolbox for automated retrieval of biophysical parameters through model inversion. In Proceedings of the EARSeL 7th SIG-Imaging Spectroscopy Workshop, Edinburgh, UK, 11–13 April 2011; pp. 11–13.
59. Rivera, J.; Verrelst, J.; Delegido, J.; Veroustraete, F.; Moreno, J. On the semi-automatic retrieval of biophysical parameters based on spectral index optimization. *Remote Sens.* **2014**, *6*, 4927–4951. [CrossRef]
60. Snee, R. Validation and regression models: Methods and examples. *Technometrics* **1977**, *19*, 415–428. [CrossRef]
61. Vincini, M.; Frazzi, E.; D'Alessio, P. Comparison of narrow-band and broad-band vegetation indices for canopy chlorophyll density estimation in sugar beet. In Proceedings of the 6th European Conference on Precision Agriculture, Skiathos, Greece, 3–6 June 2007; pp. 189–196.
62. Merzlyak, M.N.; Gitelson, A.A.; Chivkunova, O.B.; Rakitin, V.Y. Non-destructive optical detection of leaf senescence and fruit ripening. *Physiol. Plant.* **1999**, *106*, 135–141. [CrossRef]
63. Dash, J.; Curran, P.J. The MERIS terrestrial chlorophyll index. *Int. J. Remote Sens.* **2004**, *2523*, 5403–5413. [CrossRef]
64. Sims, D.A.; Gamon, J.A. Relationships between leaf pigment content and spectral reflectance across a wide range of species, leaf structures and developmental stages. *Remote Sens. Environ.* **2002**, *81*, 337–354. [CrossRef]
65. Gitelson, A.A.; Kaufman, Y.J.; Stark, R.; Rundquist, D. Novel algorithms for remote estimation of vegetation fraction. *Remote Sens. Environ.* **2002**, *80*, 76–87. [CrossRef]
66. Gower, J.F.R. Observations of in situ fluorescence of chlorophyll-a in Saanich Inlet. *Bound. Layer Meteorol.* **1980**, *18*, 235–245. [CrossRef]
67. Broge, N.H.; Leblanc, E. Comparing prediction power and stability of broadband and hyperspectral vegetation indices for estimation of green leaf area index and canopy chlorophyll density. *Remote Sens. Environ.* **2000**, *76*, 156–172. [CrossRef]
68. Daughtry, C.S.T.; Walthall, C.L.; Kim, M.S.; De Colstoun, E.B.; McMurtrey, J.E. Estimating corn leaf chlorophyll concentration from leaf and canopy reflectance. *Remote Sens. Environ.* **2000**, *74*, 229–239. [CrossRef]

69. Pasqualotto, N.; Delegido, J.; Van Wittenberghe, S.; Verrelst, J.; Rivera, J.P.; Moreno, J. Retrieval of canopy water content of different crop types with two new hyperspectral indices: Water Absorption Area Index and Depth Water Index. *Int. J. Appl. Earth Obs. Geoinf.* **2018**, *67*, 69–78. [CrossRef]
70. Dawson, T.P.; Curran, P.J.; North, P.R.J.; Plummer, S.E. The propagation of foliar biochemical absorption features in forest canopy reflectance: A theoretical analysis. *Remote Sens. Environ.* **1999**, *67*, 147–159. [CrossRef]
71. Clevers, J.G.P.W.; Gitelson, A.A. Remote estimation of crop and grass chlorophyll and nitrogen content using red-edge bands on Sentinel-2 and -3. *Int. J. Appl. Earth Obs. Geoinf.* **2013**, *23*, 344–351. [CrossRef]
72. Gitelson, A.A. Wide dynamic range vegetation index for remote quantification of biophysical characteristics of vegetation. *J. Plant Physiol.* **2004**, *161*, 165–173. [CrossRef] [PubMed]
73. Liang, L.; Di, L.; Zhang, L.; Deng, M.; Qin, Z.; Zhao, S.; Lin, H. Estimation of crop LAI using hyperspectral vegetation indices and a hybrid inversion method. *Remote Sens. Environ.* **2015**, *165*, 123–134. [CrossRef]
74. Verrelst, J.; Rivera, J.P.; Veroustraete, F.; Muñoz-Marí, J.; Clevers, J.G.P.W.; Camps-Valls, G.; Moreno, J. Experimental Sentinel-2 LAI estimation using parametric, non-parametric and physical retrieval methods—A comparison. *ISPRS J. Photogramm. Remote Sens.* **2015**, *108*, 260–272. [CrossRef]
75. Tanaka, S.; Kawamura, K.; Maki, M.; Muramoto, Y.; Yoshida, K.; Akiyama, T. Spectral index for quantifying leaf area index of winter wheat by field hyperspectral measurements: A case study in Gifu Prefecture, Central Japan. *Remote Sens.* **2015**, *7*, 5329–5346. [CrossRef]
76. Duveiller, G.; Baret, F.; Defourny, P. Remotely sensed green area index for winter wheat crop monitoring: 10-Year assessment at regional scale over a fragmented landscape. *Agric. For. Meteorol.* **2012**, *166–167*, 156–168. [CrossRef]
77. Fernandes, R.; Omari, K.; Canisius, F.; Maloley, M.; Rochdi, N. A theoretical basis for the observed linear relationship between LAI and normalized differences of red edge reflectance with implications for LAI retrieval from Sentinel-2. In Proceedings of the Recent Advances in Quantitative Remote Sensing RAQRS, Torrent, Spain, 18–22 September 2017.
78. Darvishzadeh, R.; Skidmore, A.; Atzberger, C.; van Wieren, S. Estimation of vegetation LAI from hyperspectral reflectance data: Effects of soil type and plant architecture. *Int. J. Appl. Earth Obs. Geoinf.* **2008**, *10*, 358–373. [CrossRef]
79. Wu, C.; Han, X.; Niu, Z.; Dong, J. An evaluation of EO-1 hyperspectral Hyperion data for chlorophyll content and leaf area index estimation. *Int. J. Remote Sens.* **2010**, *31*, 1079–1086. [CrossRef]
80. Fernandes, R.; Omari, K.; Canisius, F.; Rochdi, N.; Baret, F. Robust leaf area index retrieval using Sentinel-2 red edge bands. In Proceedings of the First Sentinel-2 Preparatory Symposium, Frascati, Italy, 23–27 April 2012.
81. Gower, S.T.; Kucharik, C.J.; Norman, J.M. Direct and indirect estimation of leaf area index, f(APAR), and net primary production of terrestrial ecosystems. *Remote Sens. Environ.* **1999**, *70*, 29–51. [CrossRef]
82. Küßner, R.; Mosandl, R. Comparison of direct and indirect estimation of leaf area index in mature Norway spruce stands of eastern Germany. *Can. J. For. Res.* **2000**, *30*, 440–447. [CrossRef]
83. Leblanc, S.G.; Chen, J.M. A practical scheme for correcting multiple scattering effects on optical LAI measurements. *Agric. For. Meteorol.* **2001**, *110*, 125–139. [CrossRef]
84. Vuolo, F.; Zóltak, M.; Pipitone, C.; Zappa, L.; Wenng, H.; Immitzer, M.; Weiss, M.; Baret, F.; Atzberger, C. Data service platform for Sentinel-2 surface reflectance and value-added products: System use and examples. *Remote Sens.* **2016**, *8*, 938. [CrossRef]
85. Vanino, S.; Nino, P.; De Michele, C.; Falanga, S.; Urso, G.D.; Di, C.; Pennelli, B.; Vuolo, F.; Farina, R.; Pulighe, G. Capability of Sentinel-2 data for estimating maximum evapotranspiration and irrigation requirements for tomato crop in Central Italy. *Remote Sens. Environ.* **2018**, *215*, 452–470. [CrossRef]
86. Ollinger, S.V. Sources of variability in canopy reflectance and the convergent properties of plants. *New Phytol.* **2011**, *189*, 375–394. [CrossRef] [PubMed]
87. Van Wittenberghe, S.; Verrelst, J.; Rivera, J.P.; Alonso, L.; Moreno, J.; Samson, R. Gaussian processes retrieval of leaf parameters from a multi-species reflectance, absorbance and fluorescence dataset. *J. Photochem. Photobiol. B Biol.* **2014**, *134*, 37–48. [CrossRef] [PubMed]

ARTÍCULO 3

"Retrieval of evapotranspiration from Sentinel-2: Comparison of vegetation indices, semi-empirical models and SNAP Biophysical Processor approach"

This article was published in "Agronomy-Basel" in 2019. This journal had in 2018 an impact factor of 2.259 and the position of 19/89 (Q1) in Agronomy category.

agronomy

MDPI

Article

Retrieval of Evapotranspiration from Sentinel-2: Comparison of Vegetation Indices, Semi-Empirical Models and SNAP Biophysical Processor Approach

Nieves Pasqualotto [1,*], Guido D'Urso [2], Salvatore Falanga Bolognesi [3], Oscar Rosario Belfiore [3], Shari Van Wittenberghe [1], Jesús Delegido [1], Alejandro Pezzola [4], Cristina Winschel [4] and José Moreno [1]

1 Image Processing Laboratory (IPL), University of Valencia, 46980 Valencia, Spain; shari.wittenberghe@uv.es (S.V.W.); jesus.delegido@uv.es (J.D.); jose.moreno@uv.es (J.M.)
2 Department of Agricultural Sciences, University of Naples Federico II, I-80055 Portici, Italy; durso@unina.it
3 ARIESPACE s.r.l., Spin-off Company University of Napoli "Federico II", Centro Direzionale IS. A3, 80143 Naples, Italy; salvatore.falanga@ariespace.com (S.F.B.); oscar.belfiore@ariespace.com (O.R.B.)
4 Remote Sensing and SIG Laboratory, Hilario Ascasubi Agricultural Experimental Station, National Institute of Agricultural Technology, 8142 Hilario Ascasubi, Argentina; pezzola.alejandro@inta.gob.ar (A.P.); winschel.cristina@inta.gob.ar (C.W.)
* Correspondence: m.nieve.pasqualotto@uv.es; Tel.: +34-963-544-068

Received: 16 August 2019; Accepted: 18 October 2019; Published: 22 October 2019

Abstract: Remote sensing evapotranspiration estimation over agricultural areas is increasingly used for irrigation management during the crop growing cycle. Different methodologies based on remote sensing have emerged for the leaf area index (LAI) and the canopy chlorophyll content (CCC) estimation, essential biophysical parameters for crop evapotranspiration monitoring. Using Sentinel-2 (S2) spectral information, this study performed a comparative analysis of empirical (vegetation indices), semi-empirical (CLAIR model with fixed and calibrated extinction coefficient) and artificial neural network S2 products derived from the Sentinel Application Platform Software (SNAP) biophysical processor (ANN S2 products) approaches for the estimation of LAI and CCC. Four independent in situ collected datasets of LAI and CCC, obtained with standard instruments (LAI-2000, SPAD) and a smartphone application (PocketLAI), were used. The ANN S2 products present good statistics for LAI ($R^2 > 0.70$, root mean square error (RMSE) < 0.86) and CCC ($R^2 > 0.75$, RMSE < 0.68 g/m^2) retrievals. The normalized Sentinel-2 LAI index (SeLI) is the index that presents good statistics in each dataset ($R^2 > 0.71$, RMSE < 0.78) and for the CCC, the ratio red-edge chlorophyll index ($CI_{red-edge}$) ($R^2 > 0.67$, RMSE < 0.62 g/m^2). Both indices use bands located in the red-edge zone, highlighting the importance of this region. The LAI CLAIR model with a fixed extinction coefficient value produces a $R^2 > 0.63$ and a RMSE < 1.47 and calibrating this coefficient for each study area only improves the statistics in two areas (RMSE ≈ 0.70). Finally, this study analyzed the influence of the LAI parameter estimated with the different methodologies in the calculation of crop potential evapotranspiration (ET_c) with the adapted Penman–Monteith (FAO-56 PM), using a multi-temporal dataset. The results were compared with ET_c estimated as the product of the reference evapotranspiration (ET_o) and on the crop coefficient (K_c) derived from FAO table values. In the absence of independent reference ET data, the estimated ET_c with the LAI in situ values were considered as the proxy of the ground-truth. ET_c estimated with the ANN S2 LAI product is the closest to the ET_c values calculated with the LAI in situ ($R^2 > 0.90$, RMSE < 0.41 mm/d). Our findings indicate the good validation of ANN S2 LAI and CCC products and their further suitability for the implementation in evapotranspiration retrieval of agricultural areas.

Keywords: evapotranspiration in standard condition; leaf area index; canopy chlorophyll content; Sentinel-2; vegetation indices; artificial neural network

1. Introduction

Monitoring the growth of agricultural crops during the whole growing season is important for increasing crop yields and reducing costs and input resources for the agricultural sector [1]. Spatially-explicit knowledge of biophysical variables, such as the leaf area index (LAI) and the chlorophyll content (Chl), is fundamental for the understanding of agricultural ecosystems [2]. Moreover, the variables as LAI are used as inputs of important agricultural models, such as the adapted FAO-56 Penman-Monteith (FAO-56 PM) model [3] which derives the reference (ET_o) and potential (ET_c) crop evapotranspiration. Different empirical methods to estimate evapotranspiration (ET) have been developed over the last 50 years by numerous specialists worldwide. Testing the accuracy of these methods in situ is however time-consuming and costly, and yet ET data are frequently needed at short notice for irrigation scheduling design. The Penman-Monteith model (FAO-56 PM) [3], also referred as the one-step or direct approach, is considered to offer the best results with a minimum possible error. During recent years, there has been a consistent effort to estimate vegetation parameters from remotely sensed data, allowing to adapt the Penman-Monteith equation for direct use with Earth observation (EO) based LAI and surface albedo retrieval [4], minimizing time and cost. Consequently, nowadays it is the most commonly used method for the estimation of ET [5–7].

LAI is defined as the one half of the total leaf area per unit horizontal ground surface area (m^2 leaf per m^2 surface or dimensionless) [8] and Chl is given by the weight of green pigment per leaf surface (g Chl per m^2 leaf) [9]. By quantifying and monitoring both parameters, the photosynthetic capacity [10,11], nutrient stress [12,13] and development stage [14,15] of crops can be detected. There are two approaches to remotely estimate Chl in crops. One of them is by the assessment of the leaf chlorophyll content (LCC) [16] and the other approach is based on canopy chlorophyll content (CCC), the total crop chlorophyll content, which is defined as the product of LCC and LAI [17]. Different studies have demonstrated that a direct estimation of CCC is more robust and accurate than an estimation based on the product of the individual estimation of LAI and LCC [18]. Therefore, the remote estimation of CCC has been preferred the one of the LCC.

The direct field measurements of biophysical parameters require continuous updates and can be extremely time-consuming and expensive [19]. Therefore, remote sensing from satellite, aerial and unmanned aerial vehicle platforms has become a popular technique for monitoring agricultural areas because of its ability to acquire synoptic information at different times and spatial scales [20,21]. There are different approaches for estimating biophysical parameters from remotely sensed data, i.e., (1) empirical retrieval methods, which consist of relating the biophysical parameter of interest against spectral data (e.g., vegetation indices—VIs), (2) statistical category, which defines regression functions according to information from remote sensing data (e.g., artificial neural network—ANN) and (3) physically-based retrieval methods, which refers typically to the inversion of radiative transfer models (RTMs) against remote sensing observations.

The empirical approaches provide an acceptable level of accuracy in the estimation of important biophysical parameters and can be calculated without high computational demands, but due to the sensitivity of VIs to vegetation type, the site and sensor characteristics, reliable ground measurements are required for model calibration. Furthermore, VIs are affected by the canopy structure, given different leaf angles, leaf spatial distribution and row orientation, which strongly influences canopy reflectance, which is further influenced by soil optical properties and sun-target-sensor geometry [15]. Additionally, VIs are generally based on only a few spectral bands and a single-angle observation, leading to an under-exploitation of the full spectral and directional range available from new generation sensors. Despite the above, there are VIs based models that have been improved because they also account for other factors such as the bare soil response affecting the canopy reflectance, as is the case of the Clevers leaf area index by reflectance (CLAIR) model [22].

The statistical methods can be either parametric or non-parametric [23]. Parametric models rely on physical knowledge of the problem and build explicit parameterized expressions, assuming a finite set of parameters. Therefore, the complexity of the model is bounded even if the amount of data is

unbounded. This makes them quite inflexible. Alternatively, non-parametric models are adjusted to predict a variable of interest using a training dataset of input-output data pairs, building a non-linear regression model using the observed parameters as inputs and without taking into account physical restrictions. This makes them more flexible.

On the other hand, the physically based models of canopy reflectance consider the crop architecture, illumination, soil backgrounds and viewing geometries, making them applicable across multiple operational applications for crop biophysical parameters retrieval [24]. Nevertheless, other restrictions, such as the intrinsic risk of oversimplifying the architecture of canopy for those RTMs fast enough for operational applications, have to be considered in this context [25]. They generally correspond to a simple description of canopy architecture which may not represent the actual one, particularly regarding the clumped nature of many vegetation types. Moreover, in these approaches, radiometric measurement uncertainties have to be added to the simulations when building up the training datasets [26]. The ill-posed problem has to be taken also into account when performing model inversion: The different parameter combinations may produce almost identical spectra, resulting in significant uncertainties in parameter estimation [27].

For agricultural monitoring by remote sensing, the spatial resolution should be at least 20 m and, preferably, 10 m in order to make site-specific management possible [28]. A temporal resolution of less than a week would be required to follow-up acute changes in the crop condition and provide a timely response in management practices. Specifically, extensive research has been carried out on ET crop estimation for management strategies using EO data, but to date, one of the major limitations for their applicability and technological transfer was the limited spatial and temporal resolution of the sensors [29]. In this context, the Sentinel-2 (S2) mission from the European Space Agency (ESA) [30] fulfills such operational requirements. S2 is a constellation of satellites, Sentinel-2A (S2A) and Sentinel-2B (S2B) at the moment, launched by the ESA on 23 June, 2015 and 7 March, 2017, respectively. They occupy the same sun-synchronous orbit at an altitude ~786 km, but are separated by 180°. Together, they provide better than 5-day revisit of the Earth's land surfaces under cloud-free conditions with a 10, 20 and 60 m of pixel size. S2A and S2B carry on board a virtually identical sensor, named the multi-spectral imager (MSI), covering the visible, the near-infrared (NIR) and the shortwave-infrared (SWIR) spectral regions. Hence, the S2 mission improves the temporal, spatial and spectral resolution of remote sensing data, compared to other multi-spectral missions, such as Landsat, and offers great opportunities for agricultural monitoring. For S2, the operational biophysical parameter products associated with a quality indicator are provided through the Sentinel Application Platform (SNAP) toolbox and produced through an ANN which has been trained by simulated spectra generated from well-known RTMs [31]. However, the accuracy of these products has been poorly tested, producing mostly improvable results [32,33]. It should be mentioned that both the S2 satellite images and the SNAP program are free of charge.

The present work aims at evaluating empirical (VIs), semi-empirical (CLAIR model) and ANN S2 products derived from SNAP biophysical processor methods for LAI and CCC estimation, the essential parameters to understand the evapotranspiration process. Section 2.1 describes the four test sites used in this study, a strong point of this research as they are totally independent zones with their specific characteristics. Section 2.2 details the field measurement protocol followed for the measurement of the LAI and LCC parameters in each of the zones, as well as the field instrument calibration equations. Section 2.3 specifies the four datasets obtained from the field campaigns, detailing the crop types sampled and the number of samples of each crop type, among other characteristics. From these in situ data and the corresponding S2 spectral information, the ANN S2 products are applied (Section 2.4), as well as the semi-empirical CLAIR model and the most commonly VIs used by the literature for the estimation of LAI and CCC (Section 2.5). Section 2.6 describes the FAO-56 PM equation adapted to remote sensing, specifying where the LAI parameter is within the equation. Section 3 details the results obtained for the estimation of the LAI and CCC parameters with each of the methodologies, as well as the impact obtained from the LAI parameter on the FAO-56 PM equation. Finally, Section 4 evaluates

the results, highlighting the positive and negative aspects of each method and comparing with other studies. Section 5 outlines the main conclusions, specifying the most optimal methodology for LAI and CCC retrieval and for the evapotranspiration estimation from the operational point of view.

2. Materials and Methods

2.1. Study Sites

Four different test areas have been used in this study. Two study sites are located in Italy, another in Argentina and, finally, one in Spain (Figure 1).

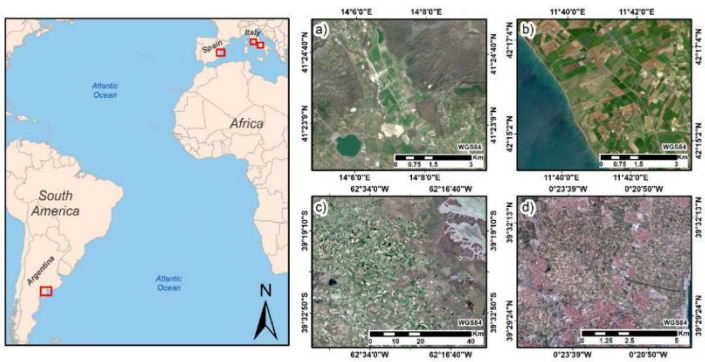

Figure 1. Test site locations. (**a**) Caserta test site located in the south of Italy from the S2 image of 7 March 2019, (**b**) Tarquina test area located in the center of Italy from the S2 image of 15 March, 2017, (**c**) Bahía Blanca test site located in the center south of Argentina from S2 image of 18 November, 2018 and (**d**) Valencia test site situated in the center south of Spain from S2 image of 3 October, 2018.

2.1.1. Caserta (Italy)

One test site is an Italian agricultural area near Caserta (study site central coordinates 41°24'8.86"N, 14°6'54.24"E, 134 m a.s.l., Datum WGS84), located 30 km from the coast. The climate is Mediterranean, but with a marked continental influence. Due to this influence, abrupt seasonal and daily temperature changes are produced, with an average annual temperature of 15.2 °C, but with hot and dry summers, with temperatures easily exceed 30 °C (July, August) and winters with temperatures close to 5 °C (December, January). The annual rainfall is approximately 580 mm, occurring mainly during autumn and winter [34]. This agricultural area is mainly composed of oat and alfalfa irrigated crop types, cultivated in plots in size of more than 100 m in length.

2.1.2. Tarquinia (Italy)

The second test site located in Italy is an agricultural area near Tarquinia municipality (study site central coordinates 42°17'12.30"N, 11°41'8.83"E, 25 m a.s.l., Datum WGS84), being 3 km from seashore. The climate is typical Mediterranean characterized by warm dry summers, mild winters, and with an average annual rainfall of approximately 600 mm, mainly concentrated in autumn and spring. The mean daily temperature is 15.3 °C (ranging from 7.7 °C in January and of 23.7 °C in July) [35]. The area is characterized by intensive agricultural management due to the production of irrigated crops, mainly tomato, cultivated in plots with a size smaller than 100 m in length.

2.1.3. Bahía Blanca (Argentina)

The third study area is located in the Buenos Aires province, south of Bahía Blanca (study site central coordinates 39°3′53.32″S, 62°40′21.50″W, 26 m a.s.l., Datum WGS84). It is situated in a plain with slopes that descend towards the coast. The climate is temperate, sub-humid with moderate temperatures but with high variability (ranging from 23 °C in January and of 7.6 °C in July) and there is no dry season. The average annual rainfall is 385 mm, being the rainiest months: February, March, October and November [36]. The study area is far from the coast in a range of 40 - 100 km. This test site is composed of irrigated and rain-fed multi-crop types, mainly wheat, onion and oat crop types, cultivated in plots of size larger than 300 m in length.

2.1.4. Valencia (Spain)

The last study site is located around Valencia city (Spain), in an area named Huerta of Valencia (study site central coordinates 39°31′11.73″ N, 0°23′20.48″ W, 18 m a.s.l., Datum WGS84). It is a zone in an alluvial plain with an approximate area of 12,000 hectares, located 6 km from the sea. The climate is typically Mediterranean with mild winters and hot dry summers and a yearly average temperature of approximately 18 °C (ranging from 11.8 °C in January and 25.6 °C in July). The seasonal rainfall is minimal in summer and maximal in autumn and spring, with an average annual value of 230 mm [37]. A complex historical irrigation system based on irrigation ditches brings water to this fertile soil in which cereals, vineyards and olive trees were originally the main crops. Nowadays, they have been replaced by rice, tigernut and new species of vegetables and citric orchards. All these crop types are currently cultivated in plots in size of 40–100 m in length (< 1 ha).

2.2. *Field Measurement Protocol*

The measurements were collected following the Land European Remote-Sensing Instruments (VALERI) field protocol [38]. The VALERI protocol is a sampling strategy corresponding to high spatial-resolution satellite imagery, choosing elementary sampling units (ESUs) of 20 m × 20 m for each measuring plot. Each ESU was chosen in the middle of the crop field, keeping a minimum distance of 20 m from the edges of the field. To account for the spatial LAI and LCC variability within each ESU, the measuring points were sampled following a square spatial sampling with 5 random measurements at each point (A, B, C, D and E), providing a statistically mean LAI and LCC estimate per ESU (Figure 2). The center of the ESU (sampling point A) was geo-located using a GPS providing an accuracy of less than 5 m for later matching the mean LAI and LCC estimate with the corresponding S2 reflectance data.

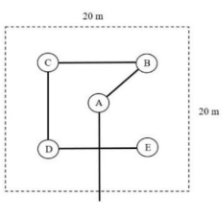

Figure 2. Land European Remote-Sensing Instruments (VALERI) sampling approach for each elementary sampling unit (ESU).

In the different field campaigns, the LAI and LCC biophysical parameter data were taken with different instruments. The LAI measurements were carried out by using the Plant Canopy Analyzer instruments LAI-2000 and LAI-2200 (Li-COR Inc., Lincoln, NE, USA) and PocketLAI smartphone application (University of Milan, DiSAA, Cassandra lab, version 1.6.5.2c) [39]. The LCC parameter, on the other hand, was taken with the MC-100 Chlorophyll Concentration Meter (MC) (Apogee

Instruments, Inc., Logan, UT, USA) and Chlorophyll Meter SPAD-502Plus (SPAD) (Konica Minolta Optics Inc., Japan). The field sampling protocol was identic for all study sites and instruments. Since the MC and SPAD instruments provide digital count values, a calibration equation is required to finally obtain the chlorophyll content. In the case of the MC instrument, it uses a calibration equation specific to each crop type. In this study, the equations for wheat (Equation (1)) and for tomato crop type (Equation (2)) were used concretely [40]. In the case of the SPAD instrument, an adjusted calibration equation for many plant species was used, so Equation (3) was applied as the standard equation for all crop types [9].

$$\text{(wheat) LCC}\left(\frac{\text{g}}{\text{m}^2}\right) = \left(-84 + 79\text{MC}^{0.6} \times 0.9\right)/1000 \quad (1)$$

$$\text{(tomato) LCC}\left(\frac{\text{g}}{\text{m}^2}\right) = \left(-328 + 304\text{MC}^{0.26} \times 0.9\right)/1000 \quad (2)$$

$$\text{(standard) LCC}\left(\frac{\text{g}}{\text{m}^2}\right) = \left(0.021752\text{SPAD}^{2.1129}\right)/100 \quad (3)$$

2.3. Datasets

Table 1 summarizes the characteristics of the four datasets used in this study. On the one hand, the field data of Caserta (Italy) were taken with LAI-2000 and SPAD, during the days 12 and 20 March, 2019, obtaining a dataset composed of 50 mean LAI and CCC (LAI × LCC) values of three different crop types. This dataset is hereafter called "CAS19_IT". Regarding Tarquinia dataset, hereafter called "TAR16_IT", is composed of 44 mean LAI and CCC values of two common crop types, taken with LAI-2000 and MC instruments during several dates to cover a wider variety of growth stages (17 March, 19 April, 6 May, 8 and 25 June, 8 and 28 July, 2016). The other two datasets are composed of multi-crop data. A dataset obtained in Argentina ("BAH18_AR"), composed of 50 LAI and CCC mean values taken with PocketLAI and SPAD during 16, 17, 21 and 23 November 2018. Further, another taken in Huerta of Valencia (Spain), hereafter called "VAL18_ES", composed of 48 LAI and CCC mean values obtained on 1, 3 and 4 October 2018. Furthermore, bare soil ESUs were included in all datasets (LAI = 0, LCC = 0 g/m^2), with the aim of creating a more robust and general method. All datasets are covering a wide range of crop LAI values, i.e., from 0 to 5, and CCC values, i.e., from 0 to 5.4 g/m^2, providing an optimal basis for the definition of a new general methodology.

2.4. Sentinel-2 Imagery and SNAP Biophysical Processor Products

All field campaigns were carried out on days close to the overpass dates of S2 over the study area with a maximum difference of three days. The technical characteristics of the MSI on-board the S2 satellites are outlined in Table 2 [41]. The images were downloaded directly and free of charge from the ESA server [42]. ESA provides Level-1C (L1C) images, which were geometrically corrected with top-of-atmosphere (TOA) reflectance and, in some places, Level-2A (L2A) images, which were geometrically and atmospherically corrected, with top-of-canopy (TOC) reflectance. Two available cloud-free L1C acquisitions of S2 over Caserta were downloaded, seven over Tarquinia, three over Argentina and one over Spain (Table 3). These images were atmospherically corrected using the Sen2Cor processor (version 2.5.5) available in the SNAP toolbox (version 6.0), converting TOA reflectance into TOC reflectance [43]. Further, they were resampled to 10 m pixel size with all selected pixels falling entirely inside the corresponding ESU, obtaining the TOC reflectance spectrum for each ESU.

Table 1. Mean values and standard deviation (SD) of the obtained variables for each crop species and test site.

Test Site	Crop Types	N° ESUs	LAI		LCC (g/m^2)		Total ESUs
			Mean	SD	Mean	SD	
CAS19_IT	Oat (*Avena sativa*)	44	2.65	0.93	0.96	0.15	50
	Ryegrass (*Secale cereale*)	3	2.22	0.14	0.45	0.27	
	Alfalfa (*Medicago sativa*)	3	1.58	0.25	0.96	0.09	
	Bare soil	10	0	0	0	0	10
TAR16_IT	Wheat (*Triticum durum*)	18	3.24	0.98	0.45	0.07	44
	Tomato (*Solanum lycopersicum*)	26	2.15	1.10	0.37	0.07	
	Bare soil	10	0	0	0	0	10
BAH18_AR	Wheat (*Triticum durum*)	8	1.51	1.28	0.50	0.07	50
	Alfalfa (*Medicago sativa*)	5	2.11	0.78	0.71	0.18	
	Onion (*Allium cepa*)	9	1.65	0.83	0.36	0.10	
	Oat (*Avena sativa*)	6	2.51	0.63	0.47	0.17	
	Agropiro (*Thinopyrum ponticum*)	9	3.24	0.95	0.57	0.10	
	Barley (*Hordeum vulgare*)	4	2.43	1.23	0.50	0.02	
	Potato (*Solanum tuberosum*)	9	2.09	0.52	0.64	0.06	
	Bare soil	12	0	0	0	0	12
VAL18_ES	Tigernut (*Cyperus esculentus*)	7	1.78	0.64	0.28	0.09	48
	Potato (*Solanum tuberosum*)	2	0.95	0.15	0.73	0.03	
	Orange tree (*Citrus x sinensis*)	7	2.68	0.41	1.40	0.29	
	Pumpkin (*Cucurbita maxima*)	4	1.54	0.36	0.52	0.23	
	Artichoke (*Cynara scolymus*)	6	1.94	0.35	0.98	1.12	
	Alfalfa (*Medicago sativa*)	3	2.33	0.22	0.82	0.09	
	Lettuce (*Lactuca sativa*)	5	3.15	0.90	0.34	0.08	
	Oleander (*Nerium oleander*)	5	1.64	0.78	1.08	0.30	
	Onion (*Allium cepa*)	2	0.44	0.01	0.39	0.04	
	Walnut tree (*Juglans regia*)	2	1.16	0.18	0.79	0.02	
	Olive tree (*Olea europaea*)	2	2.50	0.67	1.39	0.09	
	Fan palm (*Chamaerops humilis*)	3	2.26	0.44	1.07	0.04	
	Bare soil	10	0	0	0	0	10

Table 2. S2 band setting. The eight bands used for leaf area index (LAI) and canopy chlorophyll content (CCC) automatic estimation are highlighted.

Band Number	Function	Central Wavelength (nm)	Bandwidth (nm)	Spatial Resolution (m)
B1	Coastal aerosol	443	27	60
B2	Blue	490	98	10
B3	Green	560	45	10
B4	Red	665	38	10
B5	Vegetation red-edge	705	19	20
B6	Vegetation red-edge	740	18	20
B7	Vegetation red-edge	783	28	20
B8	Near-infrared (NIR)	842	145	10
B8a	Vegetation red-edge	865	33	20
B9	Water vapour	945	26	60
B10	SWIR	1380	75	60
B11	SWIR	1610	143	20
B12	SWIR	2190	242	20

Table 3. Satellite images used in this study with field measurement dates.

Test Site	Sentinel-2 Tile	N° of Images	Acquisition Dates	Field Measurement Dates
CAS19_IT	T33TVF	2	2019 (March 09, March 19)	2019 (March 12, March 20)
TAR16_IT	T32TQM	7	2016 (March 17, April 19, May 06, June 08, June 25, July 08, July 28)	2016 (March 17, April 19, May 06, June 08, June 25, July 08, July 28)
BAH18_AR	T20HNB T20HNC	3	2018 (November 18, November 23)	2018 (November 16, November 17, November 21, November 23)
VAL18_ES	T30SYJ	1	2018 (October 03)	2018 (October 01, October 03, October 04)

The SNAP toolbox additionally provides a scientific tool named the Biophysical Processor for the retrieval of LAI, CCC, canopy water content (CWC), fraction of photosynthetically active radiation absorbed (fAPAR) by the canopy green elements and the fraction of vegetation cover (FVC) variables. The retrieval algorithms for these parameters are based on an ANN approach, trained with a globally representative set of simulations from a canopy RTM (PROSAIL: PROSPECT [44] + SAIL [45]). The ANN algorithm hereby requires the input of eight S2 spectral bands (B3–B7, B8a, B11 and B12), which are all resampled to 10 m pixel size to derive LAI and CCC parameters. Additional, the quality indicators are attached to these SNAP biophysical products [31]. Through the Biophysical Processor, the LAI and CCC values together with the quality indicators from each ESU of all datasets were automatically obtained.

2.5. *Semi-Empirical and Empirical Methods*

To compare the ANN S2 products approach with semi-empirical and empirical ones, the LAI parameter was obtained with the CLAIR model and commonly used LAI VIs and CCC through the most commonly used VIs.

2.5.1. Semi-Empirical Method: The CLAIR Model

The simple and feasible approaches based on empirical relationships between LAI and nadir-viewing measurements in the red and near-infrared bands have been defined by several authors. One of these methods is the semi-empirical CLAIR model [22]. It is based on the logarithmic relationship between LAI and the Weighted Differences Vegetation Index (WDVI), using a soil line value to compensate for the errors related to soil background reflectance [46]:

$$\mathrm{LAI} = -\frac{1}{\alpha^*} \ln\left(1 - \frac{\mathrm{WDVI}}{\mathrm{WDVI}_{\infty}}\right) \quad (4)$$

$$\mathrm{WDVI} = \mathrm{R_i} - \mathrm{R_r}\frac{\mathrm{R_{soil,i}}}{\mathrm{R_{soil,r}}} \quad (5)$$

$$\mathrm{WDVI}_{\infty} = \mathrm{WDVI_{mean}} + 6\mathrm{WDVI_{SD}} \quad (6)$$

where α^* is an extinction coefficient expressing the increase of WDVI for a unitary increase of LAI, i.e., an empirical shape parameter, mainly depending on canopy architecture and computed from field measurements corresponding to the minimum error between the observed and estimated LAI. In this study, the commonly fixed values of 0.41 for herbaceous crop and 0.30 for tree were used [47,48]. The R_i and R_r variables indicate the reflectance of the observed canopy in near-infrared (B8—842 nm) and red (B4—665 nm) bands respectively, while $R_{soil,i}$ and $R_{soil,r}$ are the corresponding values for bare soil conditions. The ratio $R_{soil,i}/R_{soil,r}$ can be taken as the constant and is called the soil line slope [46]. In this work, the soil line slope was automatically estimated for each image, masking the vegetation, water and cloud pixels first with the Scene Classification (SCL) map derived by Sen2Cor and using the scatter plot between B4 and B8 S2 bands of all bare soil pixels [49]. Finally, $WDVI_{\infty}$ is the asymptotical value of WDVI for LAI→∞, and is calculated at each acquisition at the target "vegetation cover (not woody) very dense and uniform" or maximum vegetation (agricultural) cover. In order to estimate

this number automatically, the WDVI index was applied to the whole S2 image and with the SNAP statistics estimation option, the mean ($WDVI_{mean}$) and standard deviation ($WDVI_{SD}$) were calculated and used in Equation (6).

2.5.2. Empirical Method: Established Vegetation Indices

Table 4 shows the commonly used LAI and CCC indices evaluated in this study. The majority has a ratio form, with the structure of the NDVI and a quotient of addition and subtraction of three bands. The performance of these commonly used LAI and CCC indices were tested with the specific bands as defined by the original authors. The accuracies of each index were specifically analyzed with the coefficient of determination (R^2) and root mean square error (RMSE) obtained from applying them to the different datasets.

Table 4. Established LAI and CCC indices used in this study. R_λ represents reflectance at the wavelength λ (nm). The specific S2 band number to be used in each index is specified.

LAI			
Reference	**Abbreviation**	**Formula**	**Formula with S2 Bands**
[50]	RVI	$\frac{R_{842}}{R_{665}}$	$\frac{B8}{B4}$
[51]	NDVI	$\frac{R_{842}-R_{665}}{R_{842}+R_{665}}$	$\frac{B8-B4}{B8+B4}$
[52]	NDI	$\frac{R_{705}-R_{665}}{R_{705}+R_{665}}$	$\frac{B5-B4}{B5+B4}$
[53]	RENDVI	$\frac{R_{842}-R_{740}}{R_{842}+R_{740}}$	$\frac{B8-B6}{B8+B6}$
[33]	SeLI	$\frac{R_{865}-R_{705}}{R_{865}+R_{705}}$	$\frac{B8a-B5}{B8a+B5}$
[54]	TRBI	$\frac{R_{560}+R_{665}}{R_{842}}$	$\frac{B3+B4}{B8}$
[55]	IRECI	$(R_{783}-R_{665})/\frac{R_{705}}{R_{740}}$	$(B7-B4)/\frac{B5}{B6}$
[56]	EVI	$2.5(R_{842}-R_{665})/(R_{842}+6R_{665}-7.5R_{490}+1)$	$2.5(B8-B4)/(B8+6B4-7.5B2+1)$
CCC			
Reference	**Abbreviation**	**Formula**	**Formula with S2 bands**
[57]	$CI_{red\text{-}edge}$	$\frac{R_{783}}{R_{705}}-1$	$\frac{B7}{B5}-1$
[57]	CI_{green}	$\frac{R_{783}}{R_{560}}-1$	$\frac{B7}{B3}-1$
[58]	TCARI	$3\left[(R_{740}-R_{705})-0.2(R_{740}-R_{560})\left(\frac{R_{740}}{R_{705}}\right)\right]$	$3\left[(B6-B5)-0.2(B6-B3)\left(\frac{B6}{B5}\right)\right]$
[59]	OSAVI	$(1+0.16)(R_{740}-R_{705})/(R_{740}+R_{705}+0.16)$	$(1+0.16)(B6-B5)/(B6+B5+0.16)$
[60]	MTCI	$\frac{R_{740}-R_{705}}{R_{705}-R_{665}}$	$\frac{B6-B5}{B5-B4}$
[61]	NDRE1	$\frac{R_{740}-R_{705}}{R_{740}+R_{705}}$	$\frac{B6-B5}{B6+B5}$
[62]	NDRE2	$\frac{R_{783}-R_{705}}{R_{783}+R_{705}}$	$\frac{B7-B5}{B7+B5}$
[63]	NAOC	$1-\frac{\int_{665}^{783} R\ d\lambda}{R_{783}(783-665)}$	$1-\frac{\int_{B4}^{B7} R\ d\lambda}{B7(783-665)}$

2.6. Crop Potential Evapotranspiration (ETc) Based on LAI

The FAO-56 PM equation computes ET from standard climatological records of solar radiation, air temperature, relative humidity and wind speed, combined with active LAI (LAI_{active}, LAI of sun-exposed leaves), surface albedo (α, influences the net radiation of the surface, which is the primary source of the energy exchange for the evaporation process), crop height (h_c, influences the aerodynamic resistance term and the turbulent transfer of water vapour from the crop into the atmosphere) and resistance factors (Equation (7)). The resistance nomenclature distinguishes between aerodynamic resistance and surface resistance factors. The aerodynamic resistance (r_a) describes the resistance from the vegetation upward and involves friction from air flowing over vegetative surfaces. The bulk surface resistance parameter (r_s) describes the resistance of water vapour flow through the stomata openings and the active LAI (LAI_{active}, LAI of sun-exposed leaves).

$$ET\left(\frac{mm}{d}\right)=\frac{1}{\lambda}\times\frac{\Delta(R_{ns}-R_{nl}-G)+\rho_a c_p\frac{(e_s-e_a)}{r_a}}{\Delta+\gamma\left(1+\frac{r_s}{r_a}\right)} \quad (7)$$

Concretely, the α, the LAI and h_c are integrated in the Equation (7) as follows:

$$R_{ns} = (1 - \alpha) R_s \tag{8}$$

$$r_s = \frac{r_l}{LAI_{active}} \tag{9}$$

$$r_a = \frac{\ln\left(\frac{Z_U - \left(\frac{2}{3}\right)h_c}{0.123h_c}\right)\ln\left(\frac{Z_h - \left(\frac{2}{3}\right)h_c}{0.0123h_c}\right)}{0.168U_z} \tag{10}$$

where, R_s is the total incoming solar radiation (MJ/m^{2}d); r_l is the bulk stomatal resistance of the well-illuminated leaf (s/m), Z_U and Z_h are the measurement heights for wind and humidity, respectively (m); h_c is the crop height (m) and U is wind speed at height z (m/s).

A minimum and constant value of r_l is considered (100 s/m), so the surface resistance became only a function of LAI. To determine the aerodynamic resistance (r_a), this study set the zero plane displacement height (d = 2/3h_c), the roughness length for momentum Z_{0m} = 0.123h_c and the roughness length for heat Z_{0h} = 0.0123hc, following FAO-56 PM indications for full homogeneous vegetation canopies [3]. Regarding h_c, a mean of 0.4 m was applied for all crop types. It has been shown that a constant h_c value of 0.4 m determines an error percentage ranging from ±2% (as respect to the h_c of 0.1 m) and ±1% (as respect to the 0.6 m) on ET_c [64].

The surface albedo (α) is the spectrally integrated hemispherical solar reflectance and is the driving variable of the radiation budget of a surface. The estimation of α can be done using the measurements of the reflected solar radiance $K^{\uparrow}(\vartheta, \Phi, \lambda)$ (W/m^{2}sr) at a wavelength λ (nm) and can be expressed as a function of viewing zenith (ϑ) and azimuth (Φ) angles, respectively:

$$\alpha = \int_{300}^{2500} \frac{\left[\int_0^{2\pi}\int_0^{\frac{\pi}{2}} K^{\uparrow}(\vartheta, \Phi, \lambda)\cos\vartheta \sin\vartheta d\vartheta d\Phi\right]}{K^{\downarrow}(\lambda)} d\lambda \tag{11}$$

However, the current S2 sensor capabilities impose several simplifications. In the first instance, the observed surface is considered as Lambertian. Here, the dependence of $K^{\uparrow}$ on ϑ and Φ is neglected and α can be estimated from any direction of observation by means of Equation (12), using the S2 reflectance corrected values for atmospheric effects (R_λ) and the weighting coefficient (ω_λ) for a given S2 band λ [65,66]. The weighting coefficients for the calculation of α are summarized in [64] and compared to ground measurements in [67]. The weighting coefficient representing the solar radiation fraction derived from the solar irradiance spectrum within the spectral range for bands λ.

$$\alpha = \sum\nolimits_{\lambda} R_\lambda \times \omega_\lambda \tag{12}$$

Crop potential evapotranspiration (ET_c) is the maximum value of crop evapotranspiration under standard conditions, i.e., the evapotranspiration from disease-free, well-fertilized crops, under optimum soil water conditions and achieving full production under the given climatic conditions. ET_c is widely estimated by the bibliography as the product of the evapotranspiration from a reference surface (ET_o) and a dimensionless crop coefficient (K_c). The ET_o is a hypothetical grass reference crop with an assumed crop height of 0.12 m, a fixed surface resistance of 70 s/m, an albedo of 0.23 and a LAI value of 2.88. The reference surface closely resembles an extensive surface of green, well-watered grass of uniform height, actively growing and completely shading the ground. The K_c coefficient is specific to each crop and reflects the canopy development and water management practices over the course of the growing season. The standard K_c values were collected in FAO-56 [3], classified by the crop type and growing stage of the crop. Hence, ET_c was computed in the sense as the product of ET_o and the crop-defined K_c without any remote sensing data ($ET_o \times K_c$). Next, the influence of the S2 retrieved LAI value on the FAO-56 PM equation (Equation (7)) was verified. This influence was analyzed by estimating ET_c with LAI in situ data, and studying the variations produced by estimating ET_c using

ANN S2 LAI product, CLAIR model and the normalized Sentinel-2 LAI index (SeLI) index approaches. To evaluate ET_c throughout the season, the dataset from Tarquina test site was used due to availability of temporal data of two crop types, wheat and tomato.

3. Results

This section is composed of the different results obtained with each of the LAI retrieval methods, i.e., ANN S2 LAI product, the CLAIR model and VIs, applied to the four in situ datasets. Secondly, the results obtained with the different CCC methodologies are shown, both the ANN S2 CCC product and those obtained with the commonly used CCC VIs. Finally, an analysis of how the LAI input variable affects the estimation of evapotranspiration calculated with the FAO-56 PM equation is presented.

3.1. Performance of LAI Estimation Methods

For the application of the CLAIR model, two methods for α^* estimation were applied. In the first approach, simply named CLAIR, a fixed reference value for α^* was applied depending on the two general crop types (0.41 for herbaceous crops and 0.30 for tree crops). In a second approach, named $CLAIR_{opt}$, a calibrated α^* value was applied from S2 image for each study area. The calibration consists of a regression analysis technique applied to the observed and CLAIR estimated LAI values of the satellite image where there are more in situ values. The resulting calibrated α^* is considered the new constant α^* and it is used in the rest of the images of the corresponding study area. Table 5 specifies the values obtained for soil line slope, $WDVI_\infty$ and α^* calibrated for each of the study areas.

Table 5. Soil line slope, $WDVI_\infty$ and calibrated extinction coefficient (α^*) values used in the Clevers leaf area index by reflectance (CLAIR) model obtained for each satellite image in each test site. The satellite image used to calibrate α^* is boldfaced.

Test Site	Acquisition Dates	Soil Line Slope	$WDVI_\infty$	α^* (Calibrated)
CAS19_IT	March 09, 2019	0.990	0.728	0.27
	March 19, 2019	0.986	0.784	0.27
TAR16_IT	March 17, 2016	0.984	0.943	0.20
	April 19, 2016	0.983	0.971	0.20
	May 06, 2016	0.993	1.026	0.20
	June 08, 2016	0.978	0.927	0.20
	June 25, 2016	0.999	0.917	0.20
	July 08, 2016	0.995	0.788	0.20
	July 28, 2016	0.995	0.774	0.20
BAH18_AR	**November 18, 2018 (T20 HNB)**	0.984	0.590	0.69
	November 18, 2018 (T20 HNC)	0.989	0.534	0.69
	November 23, 2018 (T20 HNB)	0.985	0.571	0.69
VAL18_ES	**October 03, 2018**	0.998	0.519	0.58 (herb. crops) 0.27 (tree crops)

The ANN S2 product, CLAIR model, $CLAIR_{opt}$ model and the different VIs for LAI estimation were obtained for each test site and compared with the corresponding in situ LAI values of each dataset. Table 6 summarizes the different statistics (R^2 and RMSE) obtained for each test site, being the p-value < 0.001 in all cases. In general, almost all models produced results that came close to the ground-truth ($R^2 > 0.6$, RMSE < 0.9), except in the case of the Valencia dataset where all models obtained worse statistics, $R^2 < 0.6$ and a RMSE > 0.7. This may be due to the fact that this study area is mainly composed of crop types, e.g., lettuce, onion and orange tree which have a scarce and dispersed

coverage, translating into a strong soil influence. Additionally, it is shown how the $CLAIR_{opt}$ model results are similar to those obtained with the non-calibrated model, improving slightly in the CAS19_IT and TAR16_IT dataset, i.e., halving the RMSE. In the two other datasets, the results of the $CLAIR_{opt}$ model are worse than the CLAIR model with fixed values. This may be because α^* is optimized with only one satellite image per test site, which has the highest number of in situ values, making in some cases a possible error in α^* creating a large impact on the results.

Table 6. Statistics (R^2 and root mean square error, RMSE) obtained between each model and LAI in situ values, with linear fitting. The best result for each study site is boldfaced, prioritizing the RMSE.

Model		CAS19_IT		TAR16_IT		BAH18_AR		VAL18_ES		All Datasets	
		R^2	RMSE	R^2	RMSE	R^2	RMSE	R^2	RMSE	R^2	RMSE
ANN S2		0.863	0.79	0.742	0.86	0.702	0.78	0.473	1.19	0.639	0.92
CLAIR		0.798	0.90	0.715	1.47	0.631	0.86	0.460	0.84	0.529	1.04
$CLAIR_{opt}$		0.800	0.60	0.712	0.78	0.631	1.22	0.460	0.93	0.576	0.91
VI	RVI	0.802	0.56	0.433	1.09	0.493	0.90	0.346	0.86	0.540	0.87
	NDVI	0.736	0.65	0.696	0.80	0.714	0.68	**0.525**	**0.73**	0.689	0.71
	NDI	0.709	0.68	0.605	0.91	0.640	0.76	0.369	0.85	0.610	0.80
	RENDV	0.782	0.59	0.478	1.05	0.609	0.85	0.217	0.94	0.542	0.87
	SeLI	0.805	0.56	0.709	0.78	**0.721**	**0.67**	0.468	0.78	0.702	0.70
	TRBI	0.710	0.68	0.673	0.83	0.719	0.67	0.523	0.74	0.677	0.73
	IRECI	**0.852**	**0.49**	0.655	0.85	0.605	0.80	0.437	0.80	0.662	0.75
	EVI	0.802	0.56	**0.744**	**0.74**	0.673	0.72	0.520	0.74	0.708	0.69

The results of each model for all four study sites together are shown in Figure 3. Figure 3a represents the validation of ANN S2 LAI product, observing that all the data are close to 1:1 line, except for the LAI in situ data from Valencia, where the ANN LAI product underestimates the LAI values (Table 6, RMSE = 1.19). Figure 3b shows the LAI values obtained with the CLAIR model with fixed values. In this case, the LAI values are more dispersed, being the LAI estimated values corresponding to the Tarquinia study area the least close to the in situ values (Table 6, RMSE = 1.47). Finally, Figure 3c shows the LAI values estimated with the SeLI index together with the different in situ data (LAI = 4.885SeLI − 0.205). The SeLI index is an index that presents good statistics in the different datasets, hence, the reason for its selection. Observing the graph, the LAI values are less dispersed but a clear saturation of the estimated LAI values with LAI values greater than 4 can be distinguished. The ANN S2 LAI product is the retrieval methodology that presents the least saturation problems with high LAI values.

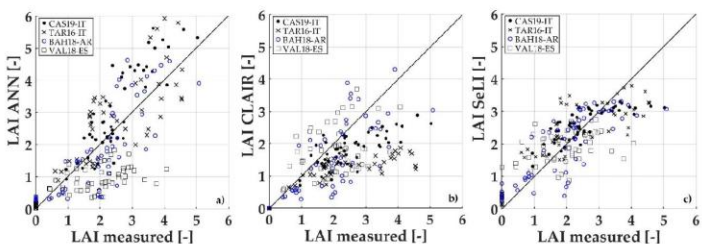

Figure 3. LAI validation for the different LAI retrieval methods. (**a**) ANN S2 LAI product, (**b**) LAI obtained with CLAIR model with a fixed α^* and (**c**) the normalized Sentinel-2 LAI index (SeLI) index method. All graphs present the 1:1 line.

3.2. Performance of CCC Estimation Methods

In the case of the CCC variable, the ANN S2 CCC product and the VIs most widely used by the bibliography for CCC retrieval were calculated. Table 7 shows the statistics obtained by applying both methodologies at each study site, being the *p*-value < 0.001 in all cases. The different CCC methods present similar results to those obtained for the LAI parameter. Almost all models present good statistics ($R^2 > 0.5$, RMSE < 0.8 g/m^2) in comparison with in situ CCC values, with only the Valencia test site presenting worse statistics ($R^2 < 0.5$, RMSE > 0.9 g/m^2). Eight VIs widely used in literature for the estimation of the CCC parameter were tested, being the $CI_{red\text{-}edge}$ one of the best indices in each of the datasets.

Table 7. Statistics (R^2 and RMSE) obtained between each model and CCC in situ values, with linear fitting. The best result for each study site is boldfaced, prioritizing the RMSE.

Model		CAS19_IT		TAR16_IT		BAH18_AR		VAL18_ES		All Datasets	
		R^2	RMSE (g/m^2)	R^2	RMSE (g/m^2)	R^2	RMSE (g/m^2)	R^2	RMSE (g/m^2)	R^2	RMSE (g/m^2)
ANN S2		0.847	0.68	0.775	0.67	0.745	0.45	0.473	1.45	0.502	0.89
VI	$CI_{red\text{-}edge}$	0.806	0.62	0.667	0.40	0.827	0.32	0.408	0.99	0.710	0.64
	CI_{green}	0.794	0.64	0.712	0.37	0.802	0.34	0.427	**0.98**	0.712	0.63
	TCARI	0.813	0.61	0.543	0.47	0.754	0.38	0.182	1.16	0.628	0.72
	OSAVI	0.684	0.79	0.582	0.45	0.819	0.32	0.315	1.07	0.630	0.72
	MTCI	0.705	0.76	0.569	0.46	0.777	0.36	0.371	1.06	0.637	0.71
	NDRE1	0.679	0.80	0.603	0.44	0.822	0.32	0.376	1.02	0.649	0.70
	NDRE2	0.690	0.78	0.639	0.42	**0.831**	**0.31**	0.422	0.98	0.670	0.68
	NACC	0.627	0.86	0.609	0.43	0.803	0.34	0.384	1.01	0.631	0.72

Figure 4 shows the in situ CCC values together with the values estimated using $CI_{red\text{-}edge}$ index and ANN S2 CCC product. Figure 4a shows the CCC values obtained with the ANN S2 CCC product, with a behaviour similar to that obtained with the ANN S2 LAI product, i.e., the values are close to 1:1 line, except for those corresponding to the Valencia dataset, in which there is a clear underestimation in comparison with the in situ values. Figure 4b, on the other hand, shows the CCC values estimated with the $CI_{red\text{-}edge}$ index, which is the index that presents good statistics in the different datasets (CCC (g/m^2) = 0.522$CI_{red\text{-}edge}$ + 0.198). In this case, the $CI_{red\text{-}edge}$ index does not produce as much saturation as the SeLI index (Figure 3c), with the CCC values approaching the 1:1 line, except in the case of the Valencia study area where the CCC values are still underestimated.

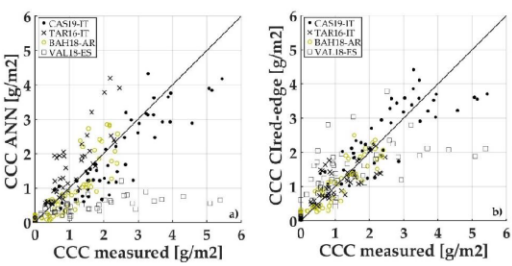

Figure 4. CCC validation for both CCC retrieval methods. (**a**) ANN S2 CCC product and (**b**) $CI_{red\text{-}edge}$ vegetation index method. Both graphs present the 1:1 line.

3.3. Impact of LAI Uncertainty on the Estimation of ETc in Irrigated Crops

Given the different LAI retrieval methodologies, this study applied the FAO-56 PM equation (Equation (7)) to estimate the ET_c of the wheat and tomato crop types in the seasonal dataset from Tarquinia (Italy) (Figure 5). Specifically, ET_c was calculated with both the albedo and LAI retrievals, estimated from the S2 images, together with the specific climatic conditions. In addition, the ET_c values obtained with the traditional reference evapotranspiration (ET_o) methodology by the corresponding crop-based K_c coefficient ($ET_o \times K_c$ in black) were added. Specifically, a constant K_c value of 1.15 was used for the wheat crop type and for tomato, first 1.15 and in the late season stage of the plant (end of July), a value of 0.8. In the absence of the reference and independent ET data, i.e., from an Eddy Covariance station, the estimated ET_c with the LAI in situ values were considered as the proxy of the ground-truth ET_c (in red). The error bars are also included in Figure 5, corresponding with the standard deviation obtained within each ESU that composes the TAR16_IT dataset. The $ET_o \times K_c$ method does not present error bars because for the whole wheat and tomato plot, it presents the same value without differences.

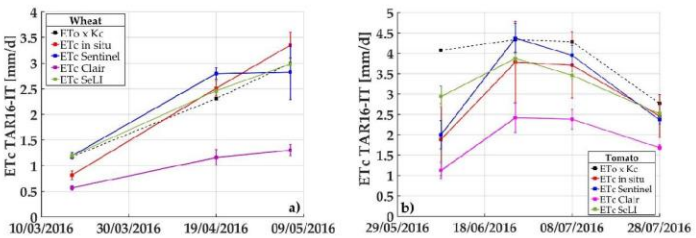

Figure 5. Short-seasonal evolution of ET_c (mm/d) estimated with the commonly used method (ET_o * Kc), with LAI in situ data, with ANN S2 LAI product, with LAI obtained with CLAIR model and with LAI from SeLI index, using TAR16-IT temporal dataset of **a**) wheat crop type and **b**) tomato crop type. Vertical bars correspond to the standard deviation on ET_c estimation for each ESU.

Figure 5a,b show the short-seasonal trend of ET_c for wheat (March to May) and tomato (May to July), respectively. Table 8 specifies the R^2 and RMSE between ET_c obtained by the different LAI retrievals and ET_c obtained by in situ LAI data, being the *p*-value < 0.001 in all cases. Observing Figure 5a, together with the values in Table 8, the ET_c estimated with the LAI values of the SeLI index are the closest to the ET_c values obtained with LAI in situ (R^2 = 0.998, RMSE = 0.31 mm/d), followed by the $ET_o \times K_c$ method (R^2 = 0.998, RMSE = 0.32 mm/d) and the ET_c estimated with ANN S2 LAI product (R^2 = 0.902, RMSE = 0.41 mm/d). On the other hand, in Figure 5b, this study identified that the ET_c values closest to those estimated with LAI in situ, are the ones obtained with the ANN S2 LAI product (R^2 = 0.971, RMSE = 0.33 mm/d), followed by ET_c estimated with the SeLI index (R^2 = 0.672, RMSE = 0.54 mm/d). In this case, the ET_c estimated with the $ET_o \times K_c$ method presents statistics that can be improved (R^2 = 0.240, RMSE = 1.17 mm/d). In both crop types, the ET_c estimated with LAI CLAIR presents a high RMSE, greater than 1 mm/d, according to the results obtained previously (Table 6).

Table 8. Statistics (R^2 and RMSE) obtained between ET_c estimated with LAI in situ and ET_c estimated with each of the models, with linear fitting. The best results are boldfaced.

Model	WHEAT		TOMATO	
	ET_c LAI In Situ			
	R^2	RMSE (mm/d)	R^2	RMSE (mm/d)
$ET_o \times K_c$	0.998	0.32	0.240	1.17
ET_c ANN LAI S2	0.902	0.41	**0.971**	**0.33**
ET_c LAI CLAIR	0.978	1.42	0.985	1.10
ET_c LAI SeLI	**0.998**	**0.31**	0.672	0.54

4. Discussion

The importance of estimating biophysical variables lies in their use as input parameters for various models dedicated to the monitoring of seasonal plant functioning and the optimization of agricultural zones. If the estimation of variables, such as LAI and CCC, is through satellites as S2, information of these key variables can be obtained with high frequency and spatial resolution, increasing the accuracy of the dynamical models fed by their input. This study analyzes different methodologies to estimate LAI and CCC, the essential parameters for the understanding of the evapotranspiration process. Specifically, empirical (VIs), semi-empirical (CLAIR model with fixed and calibrated extinction coefficient) and ANN S2 products are derived from SNAP biophysical processor approaches for the LAI and CCC estimation, using S2 spectral information. Previous S2 retrieval works are commonly based on simulated data [68] or on in situ data taken only in one test site [69]. The main strength of this study is the use of four datasets with in situ multi-crop information obtained with different instruments from totally diverse test sites.

The VIs most commonly used by the scientific community for the LAI and CCC remote retrieval were applied to the four study areas. These indices have produced good results in previous studies both in the analysis of a single crop type [54,58] and in the studies with a variety of crops [55,63,70]. In this study, one of the best indices, together with the EVI index, for the estimation of LAI in the four datasets i.e., successful in multi-crop data, was the SeLI index. This is a consistent result with a previous work that was done with LAI data taken in a multi-crop area [33]. SeLI uses the red-edge region as the area of greatest influence of the LAI (B5—705 nm) and the NIR region as the control band (B8a—865 nm). Furthermore, for the estimation of the CCC parameter, one of the VI with the best statistics in each dataset is the $CI_{red\text{-}edge}$, which uses a two bands ratio located in the red-edge region (B5—705 nm, B7—783 nm). The S2 bands located in the red-edge area have been identified as key bands for the biophysical parameters estimation, mainly the LAI [52] and CCC [71]. One of the main critics of VIs is that it does not take into account other parameters that affect reflectance [16]. Hence, the methodologies based on VIs have been developed and improved by incorporating the calibration factors, such as the influence of bare soil. This is the case of the semi-empirical CLAIR [22] model composed of the WDVI, soil line concept and a correction coefficient corresponding to the minimum error between the observed and estimated LAI (α^*). This model has been widely used for the estimation of the LAI parameter with different satellites such as DEIMOS-1 [72] or WorldView-2 [73], and even with the S2 satellite [74]. In this study, this model is first estimated with a fixed value of α^* parameter and after being checked with an optimized α^* for each test site. The results with the optimized CLAIR model ($CLAIR_{opt}$) are better in the CAS19_IT and TAR16_IT datasets, especially in the latter where RMSE is halved. However, the $CLAIR_{opt}$ model obtains worse results in the Bahía Blanca and Valencia test areas. This may be due to the fact that the fixed value of α^* is 0.41 and the optimized value is approximately 0.30 for the image with the highest number of in situ points. However, if the optimized α^* of another image is checked, it returns approximately 0.60, so 0.41 is an intermediate value, obtaining in the end better results with the non-optimized CLAIR model. Other studies have obtained also better results with a fixed α^* value than by performing a calibration process [72]. Therefore, from an operational point of view, the CLAIR model can be used with constant values. In case the area of study

is specific, a calibration can be made but it should include the maximum in situ points from several images for an optimal calibration. On the other hand, several authors who have used the CLAIR model in their studies obtained saturation problems with high LAI values when WDVI value tended to $WDVI_{\infty}$ [75]. This saturation process also occurs in our four datasets with the LAI values higher than 3. Generally, the studies based on the CLAIR model visually select approximately 50–100 bare soil pixels in the satellite image to estimate the soil line slope [72]. In this case, the soil line slope value has been estimated from all the bare soil pixels in the image, masking the rest of the pixels. In this case, the SCL map derived by Sen2Cor have been used for masking, producing good results.

Regarding the ANN S2 LAI and CCC products, the LAI product has been validated in several studies, obtaining results that can be improved ($R^2 = 0.5$), both when applied to a single crop type [76] and when validated with multi-crop data [33]. Even studies that have carried out an analysis of different retrieval methodologies concluded that VIs produce better results than the ANN S2 LAI product [77]. In this study, the ANN S2 LAI product obtains good results in the three datasets corresponding to Caserta, Tarquinia and Bahía Blanca test sites ($R^2 > 0.7$, RMSE < 0.9 g/m^2). The validation of the ANN S2 CCC product, on the other hand, has been done by very few studies and only for the wheat crop type. These studies obtained good results. A recent study [76] obtained a $R^2 = 0.72$ with the ANN S2 CCC product and in situ wheat data, and [78] has defined a relation between the ANN S2 CCC product and the canopy nitrogen, obtaining a $R^2 = 0.90$. The results of this study support and extend these results, obtaining a $R^2 > 0.7$ and RMSE < 0.7 g/m^2, for three totally different agricultural areas and with different crop types: Caserta, Tarquinia and Bahía Blanca test sites.

The special case of the Valencia study area should be mentioned. This study site is characterized by very small plots (40–100 m in length) and composed of some crop types (e.g., orange tree and lettuce) with a fraction vegetation cover (FVC) ≈ 50% [33], leaving the soil an important role. Therefore, the VIs and the ANN S2 products do not present good statistics in this area. The CLAIR model includes a soil correction factor, the soil line slope concept, which is expected to present better statistics. However, the model obtains improvable statistics ($R^2 = 0.46$, RMSE = 0.84). The FVC has always influenced remote sensing studies, not only in the biophysical retrieval models, also in studies related to evapotranspiration and irrigation management [79,80]. Therefore, it is necessary to incorporate the FVC parameter in the biophysical models, mainly when they are applied to areas such as Valencia. A possible solution is to use the ANN S2 FVC product, but this must be validated to a further extent as very few studies are available concerning the quality analysis of this product. For example, a recent study [77] has validated the ANN S2 FVC product in soybeans, canola, wheat, corn, oats, black beans and alfalfa crop types, obtaining good results.

In general, the Plant Canopy Analyzer (LAI-2000, LAI-2200) is the instrument most commonly used to measure in situ LAI parameter [81,82]. However, in many cases, this instrument is not available due to its high cost. In this study, the LAI data from Caserta, Tarquinia and Valencia were taken with the standard LAI instrument but the Bahía Blanca (Argentina) data were obtained with the PocketLAI smartphone application [83]. This application has been used in several previous works with satisfactory results, mainly on rice crop studies [84,85] but also on other crop types such as vineyards [86]. In this last study [86], both PocketLAI and the digital hemispherical photography (DHP) instrument were used and compared with destructive LAI values, observing that PocketLAI measurements were closer to the ground-truth (RRMSE = 43.00% for PocketLAI; RRMSE = 99.46% for DHP). Furthermore, in a recent comparative study of different LAI measurement instruments against destructive LAI values [39], the PocketLAI was found to a good alternative for the LAI operational measurement due to its cost-effective and similar results to destructive LAI values, obtaining a RMSE of < 0.65 for alfalfa, broad bean and maize crop types.

Finally, the influence of the biophysical parameter retrieval methodologies over the biophysical model outputs was analyzed. Crop potential evapotranspiration (ET_c) has been estimated using the FAO-56 PM equation adapted to remote sensing [3]. In general, the ET_c is estimated using the reference evapotranspiration (ET_o) by a crop specific coefficient (K_c), focusing the different studies on optimizing

this coefficient for the different crop types with satellite data. For example, [5] optimized the K_c coefficient for wheat using SPOT-4 satellite data and [7] optimized the K_c coefficient for vineyards with Landsat 8—RapidEye satellite data combination. In this study, on the other hand, the standard K_c values established by FAO [3] for each crop type and growth stage were selected and the impact of the LAI parameter on the model was analyzed. The LAI obtained with the different methodologies was used as an input. As a result, the ET_c estimated with the ANN S2 LAI product is the closest to the ET_c estimated with the in situ LAI. Previous satellite evapotranspiration estimation studies have also used the ANN S2 LAI product as an input, producing satisfactory results in comparison with the soil water balance module in the environmental policy integrated climate (EPIC) model [64]. In addition, this study found that the satellite retrieved LAI values provided a more pronounced seasonal trend compared to the K_c approach for both wheat and tomato crop types.

In short, the ANN S2 products are the closest match to the in situ data. From the operational point of view, this study provides evidence that ANN S2 LAI and CCC products have great potential to be used for the estimation and understanding of evapotranspiration, being one of the methodologies that provide similar results to ground-truth, without saturation problems. In future works, the authors want to validate the ANN S2 FVC product with the objective of incorporating this parameter in models applied to the study areas with low vegetation cover FVC $\leq$ 50%, as is the case of Valencia area.

5. Conclusions

This study performs a comparative analysis of commonly used methods, vegetation indices (VIs), CLAIR model and artificial neural network Sentinel-2 biophysical processor products (ANN S2 products), for the estimation of leaf area index (LAI) and canopy chlorophyll content (CCC) using the S2 satellite spectral information. Both parameters are essential for the estimation and understanding of the evapotranspiration process. The main strength of this study is that it is based on four in situ LAI and CCC datasets obtained in different parts of the world (Argentina, Italy and Spain), with diverse instruments, from standard instruments (LAI-2000, SPAD) to smartphone applications such as PocketLAI. By applying the methodologies to the different datasets, the ANN S2 products produced good retrieval results both for the LAI ($R^2 > 0.70$, RMSE < 0.86) and for the CCC ($R^2 > 0.75$, RMSE < 0.68 g/m^2) parameter. Regarding VIs, the normalized SeLI index is the one that obtains the best results in the different datasets for LAI retrieval and for the CCC, the $CI_{red\text{-}edge}$ ratio index. Both indices use bands located in the red-edge zone, highlighting the importance of this region. On the other hand, the CLAIR model estimated with fixed extinction values (α^*) of 0.41 for herbaceous crops and 0.30 for tree species obtained good statistics ($R^2 > 0.63$, RMSE < 1.47) and the CLAIR model optimizing the parameter α^* ($CLAIR_{opt}$) for each of the study areas only slightly improved the RMSE in the two Italian datasets (RMSE $\approx$ 0.70). It should be mentioned that with the Valencia area dataset, all the methodologies produce statistics that can be improved, due to the high soil influence in this area and the small size of the plots (< 1 ha). Finally, the influence of the LAI parameter on the FAO-56 PM evapotranspiration model adapted to remote sensing was analyzed. This analysis showed that the crop potential evapotranspiration (ET_c) values estimated with the ANN S2 LAI product are the closest to those estimated with the in situ LAI values ($R^2 > 0.90$, RMSE < 0.41 mm/d) using a dataset with seasonal information of wheat and tomato. Therefore, with all the above, it can be concluded that VIs produce the best statistics, but the ANN S2 products are the only ones that do not produce saturation, demonstrating the great potential of ANN S2 products for operational use in the monitoring of agricultural areas.

Author Contributions: N.P. and J.D. designed the field campaigns; N.P., J.D., S.F.B., O.R.B., A.P. and C.W. collected in situ multi-crop data; N.P., J.D., S.F.B. and O.R.B. analyzed the data and obtained the results; N.P. and S.V.W. wrote the paper; and J.M. and G.D. proposed the general objectives and goals of the research, designed the methodology and supervised all the procedure.

Funding: This research received no external funding.

Acknowledgments: This work was supported by the predoctoral scholarship of the Generalitat Valenciana Vali+d (file number ACIF/2016/378) of the first author. S.V.W. was supported by the postdoctoral scholarship APOSTD/2018/162 of the Generalitat Valenciana and co-funded by the 'Fondo Social Europeo'. We would also to thank SENSAGRI project (H2020-EO-2016-730074) and AVANFLEX project (ESP2016-79503-C2-1-P).

Conflicts of Interest: The authors declare no conflict of interest.

References

1. Brisco, B.; Brown, R.J.; Hirose, T.; McNairn, H.; Staenz, K. Precision agriculture and the role of remote sensing: A review. *Can. J. Remote Sens.* **1998**, *24*, 315–327. [CrossRef]
2. Wang, K.; Franklin, S.E.; Guo, X.; Cattet, M. Remote sensing of ecology, biodiversity and conservation: A review from the perspective of remote sensing specialists. *Sensors* **2010**, *10*, 9647–9667. [CrossRef] [PubMed]
3. Allen, R.G.; Pereira, L.S.; Raes, D.; Smith, M. *Crop Evapotranspiration—Guidelines for Computing Crop Water Requirements*; Food and Agriculture Organization of the United Nations: Rome, Italy, 1998; Volume 300.
4. D'Urso, G. Current status and perspectives for the estimation of crop water requirements from earth observation. *Ital. J. Agron.* **2010**, *5*, 107–120. [CrossRef]
5. Farg, E.; Arafat, S.M.; Abd El-Wahed, M.S.; El-Gindy, A.M. Estimation of evapotranspiration ETc and crop coefficient Kc of wheat, in south Nile Delta of Egypt using integrated FAO-56 approach and remote sensing data. *Egypt. J. Remote Sens. Sp. Sci.* **2012**, *15*, 83–89. [CrossRef]
6. Glenn, E.P.; Neale, C.M.U.; Hunsaker, D.J.; Nagler, P.L. Vegetation index-based crop coefficients to estimate evapotranspiration by remote sensing in agricultural and natural ecosystems. *Hydrol. Process.* **2011**, *25*, 4050–4062. [CrossRef]
7. Vanino, S.; Pulighe, G.; Nino, P.; de Michele, C.; Bolognesi, S.F.; D'Urso, G. Estimation of evapotranspiration and crop coefficients of tendone vineyards using multi-sensor remote sensing data in a mediterranean environment. *Remote Sens.* **2015**, *7*, 14708–14730. [CrossRef]
8. Chen, J.M.; Black, T.A. Defining leaf area index for non-flat leaves. *Plant. Cell Environ.* **1992**, *15*, 421–429. [CrossRef]
9. Delegido, J.; Van Wittenberghe, S.; Verrelst, J.; Ortiz, V.; Veroustraete, F.; Valcke, R.; Samson, R.; Rivera, J.P.; Tenjo, C.; Moreno, J. Chlorophyll content mapping of urban vegetation in the city of Valencia based on the hyperspectral NAOC index. *Ecol. Indic.* **2014**, *40*, 34–42. [CrossRef]
10. Gitelson, A.A.; Viña, A.; Verma, S.B.; Rundquist, D.C.; Arkebauer, T.J.; Keydan, G.; Leavitt, B.; Ciganda, V.; Burba, G.G.; Suyker, A.E. Relationship between gross primary production and chlorophyll content in crops: Implications for the synoptic monitoring of vegetation productivity. *J. Geophys. Res. Atmos.* **2006**, *111*, 1–13. [CrossRef]
11. Boegh, E.; Soegaard, H.; Broge, N.; Hasager, C.B.; Jensen, N.O.; Schelde, K.; Thomsen, A. Airborne multispectral data for quantifying leaf area index, nitrogen concentration, and photosynthetic efficiency in agriculture. *Remote Sens. Environ.* **2002**, *81*, 179–193. [CrossRef]
12. Gianquinto, G.; Orsini, F.; Fecondini, M.; Mezzetti, M.; Sambo, P.; Bona, S. A methodological approach for defining spectral indices for assessing tomato nitrogen status and yield. *Eur. J. Agron.* **2011**, *35*, 135–143. [CrossRef]
13. Houlès, V.; Guérif, M.; Mary, B. Elaboration of a nitrogen nutrition indicator for winter wheat based on leaf area index and chlorophyll content for making nitrogen recommendations. *Eur. J. Agron.* **2007**, *27*, 1–11. [CrossRef]
14. Solari, F.; Shanahan, J.; Ferguson, R.; Schepers, J.; Gitelson, A. Active sensor reflectance measurements of corn nitrogen status and yield potential. *Agron. J.* **2008**, *100*, 571–579. [CrossRef]
15. Sakamoto, T.; Gitelson, A.; Nguy-Robertson, A.; Arkebauer, T.; Wardlow, B.; Suyker, A.; Verma, S.; Shibayama, M. An alternative method using digital cameras for continuous monitoring of crop status. *Agric. For. Meteorol.* **2012**, *154*, 113–126. [CrossRef]
16. Daughtry, C.S.T.; Walthall, C.L.; Kim, M.S.; De Colstoun, E.B.; McMurtrey, J.E. Estimating corn leaf chlorophyll concentration from leaf and canopy reflectance. *Remote Sens. Environ.* **2000**, *74*, 229–239. [CrossRef]
17. Gitelson, A.A.; Viña, A.; Ciganda, V.; Rundquist, D.C.; Arkebauer, T.J. Remote estimation of canopy chlorophyll content in crops. *Geophys. Res. Lett.* **2005**, *32*, 1–4. [CrossRef]

18. Weiss, M.; Baret, F.; Myneni, R.; Pragnère, A.; Knyazikhin, Y. Investigation of a model inversion technique for the estimation of crop characteristics from spectral and directional reflectance data. *Agronomie* **2000**, *20*, 3–22. [CrossRef]
19. Bréda, N.J.J. Ground-based measurements of leaf area index: A review of methods, instruments and current controversies. *J. Exp. Bot.* **2003**, *54*, 2403–2417. [CrossRef]
20. Yao, X.; Wang, N.; Liu, Y.; Cheng, T.; Tian, Y.; Chen, Q.; Zhu, Y. Estimation of wheat LAI at middle to high levels using unmanned aerial vehicle narrowband multispectral imagery. *Remote Sens.* **2017**, *9*, 1304. [CrossRef]
21. Campos-Taberner, M.; García-Haro, F.J.; Camps-Valls, G.; Grau-Muedra, G.; Nutini, F.; Crema, A.; Boschetti, M. Multitemporal and multiresolution leaf area index retrieval for operational local rice crop monitoring. *Remote Sens. Environ.* **2016**, *187*, 102–118. [CrossRef]
22. Clevers, J.G.P.W. The application of a weighted infrared-red vegetation index for estimating leaf area index by correcting for soil moisture. *Remote Sens. Environ.* **1989**, *29*, 25–37. [CrossRef]
23. Lázaro-gredilla, M.; Titsias, M.K.; Verrelst, J.; Camps-valls, G.; Member, S. Retrieval of biophysical parameters with heteroscedastic gaussian processes. *IEEE Geosci. Remote Sens. Lett.* **2013**, *11*, 838–842. [CrossRef]
24. Bacour, C.; Baret, F.; Béal, D.; Weiss, M.; Pavageau, K. Neural network estimation of LAI, fAPAR, fCover and LAI×Cab, from top of canopy MERIS reflectance data: Principles and validation. *Remote Sens. Environ.* **2006**, *105*, 313–325. [CrossRef]
25. Casa, R.; Baret, F.; Buis, S.; Lopez-Lozano, R.; Pascucci, S.; Palombo, A.; Jones, H.G. Estimation of maize canopy properties from remote sensing by inversion of 1-D and 4-D models. *Precis. Agric.* **2010**, *11*, 319–334. [CrossRef]
26. Frederic, B.; Buis, S. Estimating canopy characteristics from remote sensing observations: Review of methods and associated problems. In *Advances in Land Remote Sensing*; Springer: Berlin, Germany, 2008; pp. 173–201. ISBN 978-1-4020-6449-4.
27. Atzberger, C. Object-based retrieval of biophysical canopy variables using artificial neural nets and radiative transfer models. *Remote Sens. Environ.* **2004**, *93*, 53–67. [CrossRef]
28. Mulla, D.J. Twenty five years of remote sensing in precision agriculture: Key advances and remaining knowledge gaps. *Biosyst. Eng.* **2013**, *114*, 358–371. [CrossRef]
29. Bisquert, M.; Sánchez, J.M.; López-Urrea, R.; Caselles, V. Estimating high resolution evapotranspiration from disaggregated thermal images. *Remote Sens. Environ.* **2016**, *187*, 423–433. [CrossRef]
30. Drusch, M.; Del Bello, U.; Carlier, S.; Colin, O.; Fernandez, V.; Gascon, F.; Hoersch, B.; Isola, C.; Laberinti, P.; Martimort, P.; et al. Sentinel-2: ESA's optical high-resolution mission for GMES operational services. *Remote Sens. Environ.* **2012**, *120*, 25–36. [CrossRef]
31. Weiss, M.; Baret, F. S2ToolBox Level 2 Products: LAI, FAPAR, FCOVER. Available online: http://step.esa.int/docs/extra/ATBD_S2ToolBox_L2B_V1.1.pdf (accessed on 29 July 2019).
32. Djamai, N.; Fernandes, R. Comparison of SNAP-derived Sentinel-2A L2A product to ESA product over Europe. *Remote Sens.* **2018**, *10*, 926. [CrossRef]
33. Pasqualotto, N.; Delegido, J.; Van Wittenberghe, S.; Rinaldi, M.; Moreno, J. Multi-crop green LAI estimation with a new simple Sentinel-2 LAI Index (SeLI). *Sensors* **2019**, *19*, 904. [CrossRef]
34. METEOBLUE Weather. Climate Caserta. Available online: https://www.meteoblue.com/en/weather/forecast/modelclimate/caserta_italy_3179866 (accessed on 15 May 2019).
35. METEOBLUE Weather. Climate Tarquinia. Available online: https://www.meteoblue.com/en/weather/forecast/modelclimate/tarquinia_italy_3165919 (accessed on 15 May 2019).
36. METEOBLUE Weather. Climate Bahía Blanca. Available online: https://www.meteoblue.com/en/weather/forecast/modelclimate/bahía-blanca_argentina_3865086 (accessed on 15 May 2019).
37. METEOBLUE Weather. Climate Valencia. Available online: https://www.meteoblue.com/en/weather/forecast/modelclimate/valencia_spain_2509954 (accessed on 15 May 2019).
38. VALERI. Land European Remote-Sensing Instruments Field Protocol. Available online: http://w3.avignon.inra.fr/valeri/ (accessed on 16 May 2019).
39. Casa, R.; Upreti, D.; Pelosi, F. Measurement and estimation of leaf area index (LAI) using commercial instruments and smartphone-based systems. *IOP Conf. Ser. Earth Environ. Sci.* **2019**, *275*, 012006. [CrossRef]
40. Parry, C.; Mark Blonquist, J.; Bugbee, B. In situ measurement of leaf chlorophyll concentration: Analysis of the optical/absolute relationship. *Plant. Cell Environ.* **2014**, *37*, 2508–2520. [CrossRef] [PubMed]

41. European Space Agency (ESA). *ESA's Optical High-Resolution Mission for GMES Operational Services*. Available online: https://sentinel.esa.int/documents/247904/349490/S2_SP-1322_2.pdf (accessed on 29 July 2019).
42. ESA server. Available online: https://scihub.copernicus.eu/ (accessed on 3 May 2019).
43. Louis, J.; Debaecker, V.; Pflug, B.; Main-Knorn, M.; Bieniarz, J.; Mueller-Wilm, U.; Cadau, E.; Gascon, F. Sentinel-2 SEN2COR: L2A processor for users. In Proceedings of the Living Planet Symposium, Prague, Czech Republic, 9–13 May 2016; pp. 1–8.
44. Jacquemoud, S.; Baret, F. PROSPECT: A model of leaf optical properties spectra. *Remote Sens. Environ.* **1990**, *34*, 75–91. [CrossRef]
45. Verhoef, W. Light scattering by leaf layers with application to canopy reflectance modeling: The SAIL model. *Remote Sens. Environ.* **1984**, *16*, 125–141. [CrossRef]
46. Baret, F.; Jacquemoud, S.; Hanocq, J.F. About the soil line concept in remote sensing. *Adv. Sp. Res.* **1993**, *13*, 281–284. [CrossRef]
47. Vuolo, F.; Dini, L.; D'Urso, G. Assessment of LAI retrieval accuracy by inverting a RT model and a simple empirical model with multiangular and hyperspectral CHRIS/PROBA data from SPARC. In Proceedings of the 3rd CHRIS/Proba Workshop, Frascati, Italy, 21–23 March 2005.
48. Akdim, N.; Alfieri, S.M.; Habib, A.; Choukri, A.; Cheruiyot, E.; Labbassi, K.; Menenti, M. Monitoring of irrigation schemes by remote sensing: Phenology versus retrieval of biophysical variables. *Remote Sens.* **2014**, *6*, 5815–5851. [CrossRef]
49. Fox, G.A.; Sabbagh, G.J.; Searcy, S.W.; Yang, C. An automated soil line identification routine for remotely sensed images. *Soil Sci. Soc. Am. J.* **2004**, *68*, 1326. [CrossRef]
50. Jordan, C.F. Derivation of leaf area index from quality of light on the forest floor. *Ecology* **1969**, *50*, 663–666. [CrossRef]
51. Rouse, J.W.; Hass, R.H.; Schell, J.A.; Deering, D.W. Monitoring vegetation systems in the great plains with ERTS. In Proceedings of the Third Earth Resources Technology Satellite (ERTS) Symposium, Washington, DC, USA, 10–14 December 1973; Volume 1, pp. 309–317.
52. Delegido, J.; Verrelst, J.; Alonso, L.; Moreno, J. Evaluation of sentinel-2 red-edge bands for empirical estimation of green LAI and chlorophyll content. *Sensors* **2011**, *11*, 7063–7081. [CrossRef]
53. Sharma, L.K.; Bu, H.; Denton, A.; Franzen, D.W. Active-optical sensors using red NDVI compared to red edge NDVI for prediction of corn grain yield in North Dakota, U.S.A. *Sensors* **2015**, *15*, 27832–27853. [CrossRef]
54. Vincini, M.; Frazzi, E.; D'Alessio, P. Comparison of narrow-band and broad-band vegetation indices for canopy chlorophyll density estimation in sugar beet. In Proceedings of the 6th European Conference on Precision Agriculture, Skiathos, Greece, 3–6 June 2007; pp. 189–196.
55. Frampton, W.J.; Dash, J.; Watmough, G.; Milton, E.J. Evaluating the capabilities of Sentinel-2 for quantitative estimation of biophysical variables in vegetation. *ISPRS J. Photogramm. Remote Sens.* **2013**, *82*, 83–92. [CrossRef]
56. Huete, A.; Didan, K.; Miura, T.; Rodriguez, E.P.; Gao, X.; Ferreira, L.G. Overview of the radiometric and biophysical performanceof the MODIS vegetation indices. *Remote Sens. Environ.* **2002**, *83*, 195–213. [CrossRef]
57. Gitelson, A.A.; Gritz, Y.; Merzlyak, M.N. Relationships between leaf chlorophyll content and spectral reflectance and algorithms for non-destructive chlorophyll assessment in higher plant leaves. *J. Plant Physiol.* **2003**, *160*, 271–282. [CrossRef] [PubMed]
58. Haboudane, D.; Miller, J.R.; Tremblay, N.; Zarco-Tejada, P.J.; Dextraze, L. Integrated narrow-band vegetation indices for prediction of crop chlorophyll content for application to precision agriculture. *Remote Sens. Environ.* **2002**, *81*, 416–426. [CrossRef]
59. Rondeaux, G.; Steven, M.; Baret, F. Optimization of soil-adjusted vegetation indices. *Remote Sens. Environ.* **1996**, *55*, 95–107. [CrossRef]
60. Dash, J.; Curran, P.J. The MERIS terrestrial chlorophyll index. *Int. J. Remote Sens.* **2004**, *2523*, 5403–5413. [CrossRef]
61. Gitelson, A.; Merzlyak, M.N. Spectral reflectance changes associated with autumn senescence of Aesculus hippocastanum L. and Acer platanoides L. leaves. Spectral features and relation to chlorophyll estimation. *J. Plant Physiol.* **1994**, *143*, 286–292. [CrossRef]

62. Barnes, E.M.; Clarke, T.R.; Richards, S.E.; Colaizzi, P.D.; Haberland, J.; Kostrzewski, M.; Waller, P.; Choi, C.; Riley, E.; Thompson, T.; et al. Coincident detection of crop water stress, nitrogen status and canopy density using ground-based multispectral data. In Proceedings of the Fifth International Conference on Precision Agriculture, Bloomington, MN, USA, 16–19 July 2000; Volume 1619.
63. Delegido, J.; Alonso, L.; González, G.; Moreno, J. Estimating chlorophyll content of crops from hyperspectral data using a normalized area over reflectance curve (NAOC). *Int. J. Appl. Earth Obs. Geoinf.* **2010**, *12*, 165–174. [CrossRef]
64. Vanino, S.; Nino, P.; De Michele, C.; Falanga, S.; Urso, G.D.; Di, C.; Pennelli, B.; Vuolo, F.; Farina, R.; Pulighe, G. Capability of Sentinel-2 data for estimating maximum evapotranspiration and irrigation requirements for tomato crop in Central Italy. *Remote Sens. Environ.* **2018**, *215*, 452–470. [CrossRef]
65. Menenti, M.; Bastiaanssen, W.G.M.; Van Eick, D. Determination of surface hemispherical reflectance with Thematic Mapper data. *Remote Sens. Environ.* **1989**, *28*, 327–337. [CrossRef]
66. D'Urso, G.; Calera Belmonte, A. Operative approaches to determine crop water requirements from Earth Observation data: Methodologies and applications. In *AIP Conference Proceedings*; American Institute of Physics: College Park, MD, USA, 2006; pp. 14–25.
67. Vuolo, F.; Zóltak, M.; Pipitone, C.; Zappa, L.; Wenng, H.; Immitzer, M.; Weiss, M.; Baret, F.; Atzberger, C. Data service platform for Sentinel-2 surface reflectance and value-added products: System use and examples. *Remote Sens.* **2016**, *8*, 938. [CrossRef]
68. Kira, O.; Nguy-Robertson, A.L.; Arkebauer, T.J.; Linker, R.; Gitelson, A.A. Toward generic models for green LAI estimation in maize and soybean: Satellite observations. *Remote Sens.* **2017**, *9*, 318. [CrossRef]
69. Darvishzadeh, R.; Skidmore, A.; Abdullah, H.; Cherenet, E.; Ali, A.; Wang, T.; Nieuwenhuis, W.; Heurich, M.; Vrieling, A.; O'Connor, B.; et al. Mapping leaf chlorophyll content from Sentinel-2 and RapidEye data in spruce stands using the invertible forest reflectance model. *Int. J. Appl. Earth Obs. Geoinf.* **2019**, *79*, 58–70. [CrossRef]
70. Pasqualotto, N.; Delegido, J.; Pezzola, A.; Winschel, C.; Moreno, J. Estimación del contenido de clorofila a nivel de cubierta (CCC) en cultivos: Comparativa de índices de vegetación y el producto de nivel 2A de Sentinel-2. In Proceedings of the XVIII Congreso de la Asociación Española de Teledetección, Valladolid, Spain, 24–27 September 2019.
71. Clevers, J.G.P.W.; Gitelson, A.A. Remote estimation of crop and grass chlorophyll and nitrogen content using red-edge bands on Sentinel-2 and -3. *Int. J. Appl. Earth Obs. Geoinf.* **2013**, *23*, 344–351. [CrossRef]
72. Vuolo, F.; Neugebauer, N.; Bolognesi, S.F.; Atzberger, C.; D'Urso, G. Estimation of leaf area index using DEIMOS-1 data: Application and transferability of a semi-empirical relationship between two agricultural areas. *Remote Sens.* **2013**, *5*, 1274–1291. [CrossRef]
73. Tarantino, E.; Novelli, A.; Laterza, M.; Gioia, A. Testing high spatial resolution WorldView-2 imagery for retrieving the leaf area index. In Proceedings of the Third International Conference on Remote Sensing and Geoinformation of the Environment, Paphos, Cyprus, 16–19 March 2015; p. 95351N.
74. Clevers, J.G.P.W.; Kooistra, L.; van den Brande, M.M.M. Using Sentinel-2 data for retrieving LAI and leaf and canopy chlorophyll content of a potato crop. *Remote Sens.* **2017**, *9*, 405. [CrossRef]
75. Peschechera, G.; Fratino, U. Calibration of CLAIR model by means of Sentinel-2 LAI data for analysing wheat crops through Landsat-8 surface reflectance data. In *International Conference on Computational Science and Its Applications*; Springer International Publishing: Melbourne, Australia, 2018; pp. 294–304.
76. Xie, Q.; Dash, J.; Huete, A.; Jiang, A.; Yin, G.; Ding, Y.; Peng, D.; Hall, C.C.; Brown, L.; Shi, Y.; et al. Retrieval of crop biophysical parameters from Sentinel-2 remote sensing imagery. *Int. J. Appl. Earth Obs. Geoinf.* **2019**, *80*, 187–195. [CrossRef]
77. Djamai, N.; Fernandes, R.; Weiss, M.; McNairn, H.; Goïta, K. Validation of the Sentinel Simplified Level 2 Product Prototype Processor (SL2P) for mapping cropland biophysical variables using Sentinel-2/MSI and Landsat-8/OLI data. *Remote Sens. Environ.* **2019**, *225*, 416–430. [CrossRef]
78. Delloye, C.; Weiss, M.; Defourny, P. Retrieval of the canopy chlorophyll content from Sentinel-2 spectral bands to estimate nitrogen uptake in intensive winter wheat cropping systems. *Remote Sens. Environ.* **2018**, *216*, 245–261. [CrossRef]
79. Chen, A.; Orlov-Levin, V.; Meron, M. Applying high-resolution visible-channel aerial imaging of crop canopy to precision irrigation management. *Agric. Water Manag.* **2019**, *216*, 196–205. [CrossRef]

80. Hssaine, B.A.; Merlin, O.; Rafi, Z.; Ezzahar, J.; Jarlan, L.; Khabba, S.; Er-Raki, S. Calibrating an evapotranspiration model using radiometric surface temperature, vegetation cover fraction and near-surface soil moisture data. *Agric. For. Meteorol.* **2018**, *256–257*, 104–115. [CrossRef]
81. Richter, K.; Vuolo, F.; D'Urso, G. Leaf area index and surface albedo estimation: Comparative analysis from vegetation indexes to radiative transfer models. *Int. Geosci. Remote Sens. Symp.* **2008**, *3*, III-736–III-739. [CrossRef]
82. Verrelst, J.; Muñoz, J.; Alonso, L.; Delegido, J.; Rivera, J.P.; Camps-Valls, G.; Moreno, J. Machine learning regression algorithms for biophysical parameter retrieval: Opportunities for Sentinel-2 and -3. *Remote Sens. Environ.* **2012**, *118*, 127–139. [CrossRef]
83. Confalonieri, R.; Francone, C.; Foi, M. The PocketLAI smartphone app: An alternative method for leaf area index estimation. In Proceedings of the International Environmental Modelling and Software Society (iEMSs), San Diego, CA, USA, 15–19 June 2014; p. 6.
84. Paleari, L.; Movedi, E.; Vesely, F.M.; Thoelke, W.; Tartarini, S.; Foi, M.; Boschetti, M.; Nutini, F.; Confalonieri, R. Estimating crop nutritional status using smart apps to support nitrogen fertilization. A case study on paddy rice. *Sensors* **2019**, *19*, 981. [CrossRef]
85. Campos-Taberner, M.; García-Haro, F.J.; Confalonieri, R.; Martínez, B.; Moreno, Á.; Sánchez-Ruiz, S.; Gilabert, M.A.; Camacho, F.; Boschetti, M.; Busetto, L. Multitemporal monitoring of plant area index in the valencia rice district with PocketLAI. *Remote Sens.* **2016**, *8*, 202. [CrossRef]
86. Orlando, F.; Movedi, E.; Coduto, D.; Parisi, S.; Brancadoro, L.; Pagani, V.; Guarneri, T.; Confalonieri, R. Estimating leaf area index (LAI) in vineyards using the PocketLAI smart-app. *Sensors* **2016**, *16*, 2004. [CrossRef]


VNIVERSITAT
DE VALÈNCIA